



Journal of INNOVATIVE SCIENCE and ENGINEERING

Volume	5
Issue	2
Year	2021

E-ISSN: 2602-4217

www.jise.btu.edu.tr

Transmit Antenna Selection for Spatial Modulation Based on Hexagonal Quadrature Amplitude Modulation

Fatih Cogen^{1,2} , Erdogan Aydın^{2*} 

¹ Turkish-German University, Istanbul, Turkey

^{2*} Istanbul Medeniyet University, Istanbul, Turkey

Abstract

There is a tremendous demand from various industries for next-generation 5G networks, which has dramatically increased the need for high data rates and energy efficiency. It is an indisputable fact that next-generation networks should be not only energy-efficient but also resource-efficient. Given the fact that 10% of the current energy consumption in the world is caused by Information and Communication Technology, it is evident that energy-efficiency has become the most crucial performance criteria in the next-generation communication techniques. Based on these needs, we previously suggested the hexagonal quadrature amplitude modulation (HQAM) aided spatial modulation (SM) technique (HQAM-SM) to the literature. In this study, we found it appropriate to do this research to further increase the performance of the HQAM-SM scheme through the antenna selection technique and to investigate the effects of antenna selection technique on HQAM-SM. Moving from this point, in this article, rational capacity-optimized antenna selection (COAS), SM, and energy-efficient HQAM techniques are combined, and a new system called COAS-HSM is presented. Hexagonal constellations are to optimize the constellation points to form a hexagonal constellation to minimize the Hamming distance between the constellation points. This layout not only offers better energy efficiency than traditional QAM constellations but also performs almost the same BER performance as QAM at high signal-to-noise ratio (SNR) values. On the other hand, antenna selection algorithms are one of the transmission schemes that have been frequently encountered in the literature in recent years, and that considerably increases the performance of various multiple-input multiple-output (MIMO) communication structures. In particular, the COAS transmission scheme is an intelligent method of selecting transmission antennas over the highest channel amplitudes. Performance analysis of the proposed COAS-HSM technique is carried out in Rayleigh fading channels.

Keywords: Spatial modulation (SM), hexagonal quadrature amplitude modulation (HQAM), capacity-optimized antenna selection (COAS), multiple-input multiple-output (MIMO) systems.

Cite this paper as:
Cogen, F., Aydın, E. (2021). *Transmit Antenna Selection for Spatial Modulation Based on Hexagonal Quadrature Amplitude Modulation*. Journal of Innovative Science and Engineering. 5(2): 76-90

*Corresponding author: Erdoğan Aydın
E-mail: erdogan.aydin@medeniyet.edu.tr

Received Date: 21/11/2020
Accepted Date: 10/01/2021
© Copyright 2021 by
Bursa Technical University. Available
online at <http://jise.btu.edu.tr/>



The works published in Journal of Innovative Science and Engineering (JISE) are licensed under a Creative Commons Attribution-NonCommercial 4.0 International License.

1. Introduction

In recent years, besides internet applications such as high data-rated internet usage, online gaming, high definition video broadcasting and watching; many internet of things (IoT) fields such as personal multimedia devices, smart home appliances, wearable devices, audiovisual devices, smart measurement, fleet management is developing day by day. The greatest need for these areas is undoubtedly high data-rates and energy-efficiency, which has become one of the most critical needs of our time. It is a fact that by 2025, the number of devices connected to the internet will reach nearly 80 million. From this point of view, it can be easily understood that the next-generation communication techniques should be energy-efficient as well as high data-rated [1–5].

Novel and high-speed communication structures use big constellations such as M -ary amplitude modulation (AM) or M -ary phase modulation (PM) constellation systems. Although they are easy to apply and theoretically explained, they cannot conjoin these symbols as energy-efficiently as possible. Due to its straightforwardness and convenience of use, especially quadrature amplitude modulation (QAM) constellations are included in many recent scientific publications. However, it is known that the constellations of QAM are not optimal for a given average transmitted symbol power; QAM constellations are called sub-optimal constellations. It is an indisputable fact that the next-generation communication techniques must be energy-efficient and therefore require the development of next-generation energy-efficient constellations. Moving from this point, this article deals with hexagonal-QAM (HQAM) constellations that minimize the transmitted power for a given average transmitted symbol power. Studies show that HQAM both performs similarly to traditional QAM constellations and is superior to QAM (sub-optimal, not optimal) in terms of energy efficiency [6–9].

Multiple-input multiple-output (MIMO) systems are judicious techniques developed to deal with multi-way fading and are shown as a competitive candidate for new generation communication techniques in many studies. In the structure of MIMO systems, both the transmitting and receiving terminals are equipped with multiple antennas. MIMO is an infrastructure developed for qualified communication, which can transmit data from various antennas as various signals at the same time and use a single signal channel for this. The data to be sent is divided into multiple data streams at the transmission point and recombined on the receiver side with the help of another MIMO module set with the same number of antennas. The receiver is designed to take into account time differences between the reception of each signal, added noise, interference, and loss signals [10–13].

One of the essential methods that belong to the MIMO systems family and constitute the core of this study is undoubtedly the spatial modulation (SM) technique. In the SM system, only one radio frequency (RF) chain is used during a transmission period between the transmitter and the receiver. While part of the communication in SM is provided with traditional modulating symbols, another part is provided through the antenna activated by SM. With this rational technique, inter-channel interference (ICI) is wholly eliminated, signal processing and circuit complexity are reduced, and energy efficiency is increased. Besides, SM does all these benefits with simple equipment, requiring a minimal additional cost [14–16].

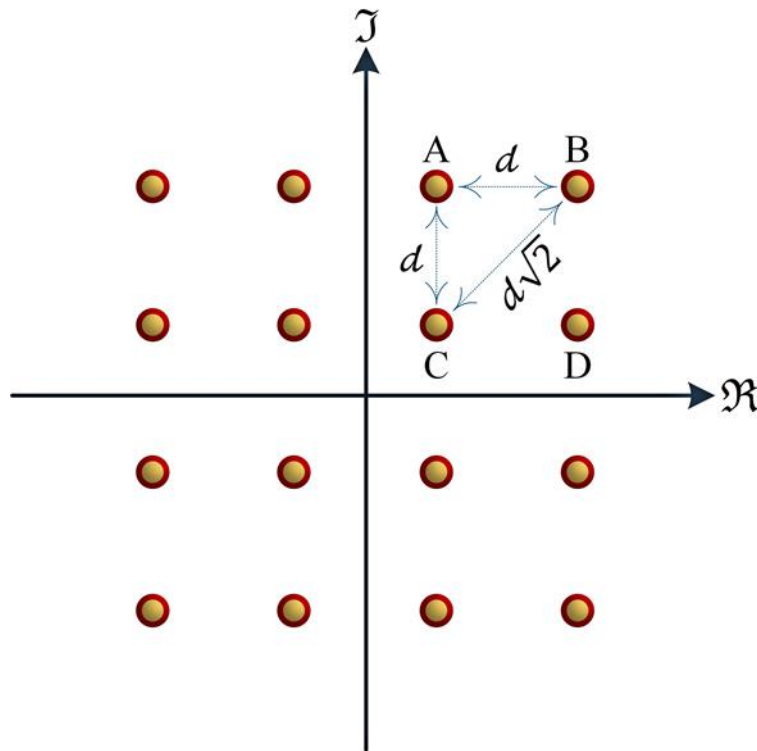


Figure 1. Conventional 16-QAM Constellation

In recent years, much research has been done on antenna selection for MIMO systems. These studies have shown that transmitter antenna selection techniques result in considerable increases in the performance of MIMO systems. Transmitter antenna selection (TAS) is an intelligent logic that emphasizes selecting a subset of antennas from within a particular set of antennas. Thanks to TAS, bit error rate (BER) and symbol error rate (SER) metrics improve, while hardware complexity, cost, and maintenance costs are reduced. Especially in this article, the capacity-optimized antenna selection (COAS) technique is emphasized. The COAS technique is an antenna selection method that shows improvements on the BER and has low complexity, which selects the antennas based on the highest channel amplitudes [12,17–19]. Besides, a technique called HQAM-SM by combining hexagonal constellations and rational SM technique has been proposed by the authors in [9], and this method shows similar BER performances with SM at high signal-to-noise ratio (SNR) values and is energy-efficient.

In this study, a novel capacity optimization antenna selection based HQAM-SM technique called COAS-HSM is proposed for next-generation communication systems. The proposed novel technique provides better performance compared to the SM, quadrature spatial modulation (QSM) and HQAM-SM techniques, provides nearly similar performance compared to the COAS-SM method, and has high energy efficiency compared to these methods. Performance analysis of the considered COAS-HSM technique is carried out in Rayleigh fading channels. Performance analysis of the considered COAS-HSM technique is carried out in Rayleigh fading channels.

The paper is organized as follows: In section 2, hexagonal constellations are introduced. In Section 3, COAS technique for the HQAM-SM scheme is presented. In Section 4, the system model of COAS-HSM is introduced. Performance Analysis for COAS-HSM is presented in Section 5. Finally, the simulation results and discussion are given in Section 6 and in Section 7 the paper is concluded.

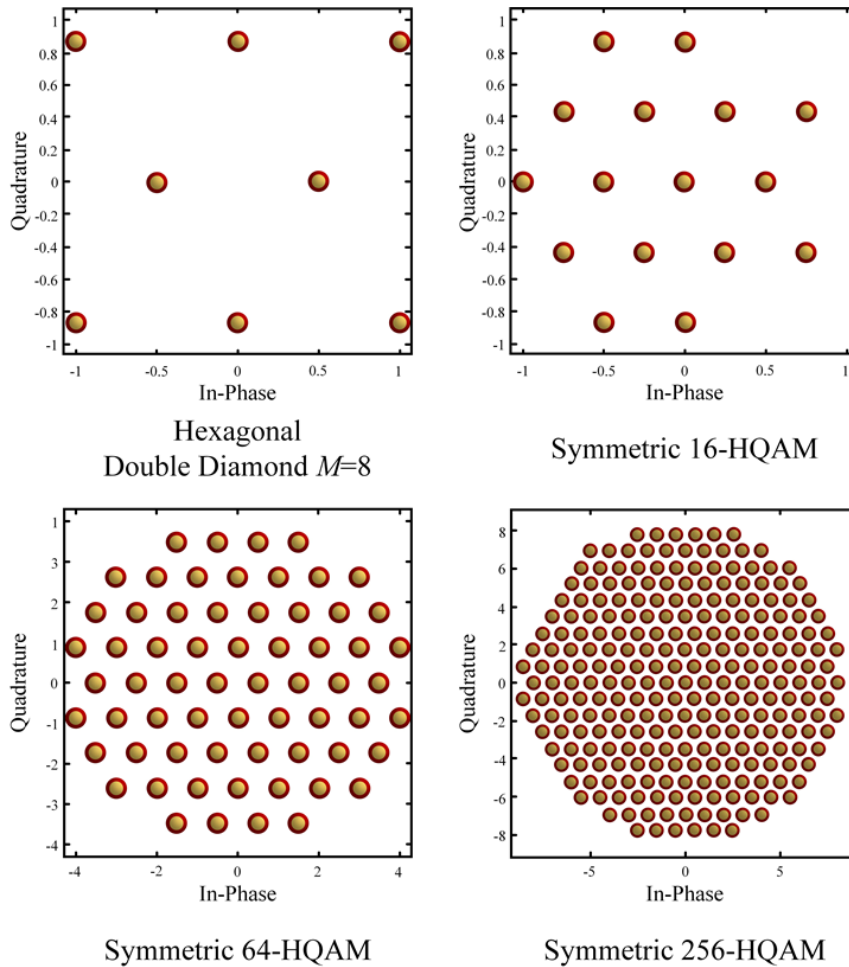


Figure 2. Various HQAM Constellations

Notation: The following notation is used throughout this paper. Bold lower/upper case symbols represent vectors/matrices; $(\cdot)^H$, $(\cdot)^T$, $\|\cdot\|_F$, and $|\cdot|$ denote Hermitian, transpose, Frobenius norm and absolute value operators, respectively, $\Re(\cdot)$ and $\Im(\cdot)$ are the real and imaginary parts of a complex-valued quantity.

2. Hexagonal Constellations

In this section, HQAM constellations will be explained in detail. Let us simply try to explain the superiority of HQAM constellation as follows. Consider a traditional 16-QAM structure as illustrated in Figure 1. Assume that the minimum distance between the two constellation points is d and the amplitude of the noise is $d/2$. The signal received by the receiver can be accurately detected if it is no more than $d/2$ away from the midpoint. However, considering the distance between \overline{BC} it can be straightforwardly seen that is $d/\sqrt{2}$. Thus, if the received signal is in the \overline{BC} range, the transmitted symbol can be obtained in the receiver correctly as long as the amplitude of the noise is less than $d\sqrt{2}/2$. From this point forth, there is no need to limit the noise amplitude of all signals received by the receiver to $d/2$ even if the amplitude of noise between \overline{BC} is equal to $d\sqrt{2}/2$ this signal could be received correctly in the receiver. If HQAM constellation is considered carefully, it is seen that there is no such inefficiency problem in HQAM constellation

Table 1. Constellation power measurement comparisons for a given unit minimum symbol separation [7]

Constellation Type	$P_{average}$	P_{peak}
64-QAM	10.5	24.5
64-HQAM	8.8125	16.75
128-QAM	20.5	42.5
128-HQAM	17.6366	34.519
256-QAM	42.5	112.5
256-HQAM	35.254	71.77
512-QAM	82.5	188.5
512-HQAM	70.53	143.43
1024-QAM	170.5	480.5
1024-HQAM	141.13	279.9

as in QAM constellation; because distances between constellation points in the HQAM structure are equal. In other words, under the same power assumption, HQAM constellation schemes are called optimal in the literature. Various HQAM constellation schemes such as hexagonal double diamond and symmetric HQAM with $M = 16, 64, 256$ are shown in Figure 2.

In order to show the superiority of HQAM constellations, we have also given a comparison through the Table 1. It can be clearly seen that HQAM constellations provide significant energy efficiency compared to conventional QAM constellations. Therefore, we are of the opinion that the use of these constellations in the next-generation communication systems will be of great benefit in today's world, where the energy problem and the carbon footprint are a huge problem. Here, the power measurements are *Watts/unit*² and for detailed information, please see the article [7], where $P_{average} = (M - 1)d^2 / 6$ for MQAM modulation, here $d^2 = 1$ for square constellations and $d^2 = 0.9685$ for rectangular constellations.

3. COAS Technique for HQAM-SM (COAS-HSM)

COAS scheme is an antenna selection technique that selects antennas with channel amplitudes from a sub-antenna group with the maximum absolute value of the channel amplitude among the total transmission antennas. In the proposed system, this choice will be made by selecting n antennas among N_T transmit antennas. The COAS technique both improves the performance of MIMO communication systems and offers a low complexity experience.

Under the assumption that the channel state information (CSI) and SNR are well-known at the transmitter terminal, the capacity of the antenna selection based MIMO scheme for N_T number of transmission antennas can be expressed as follows [20]:

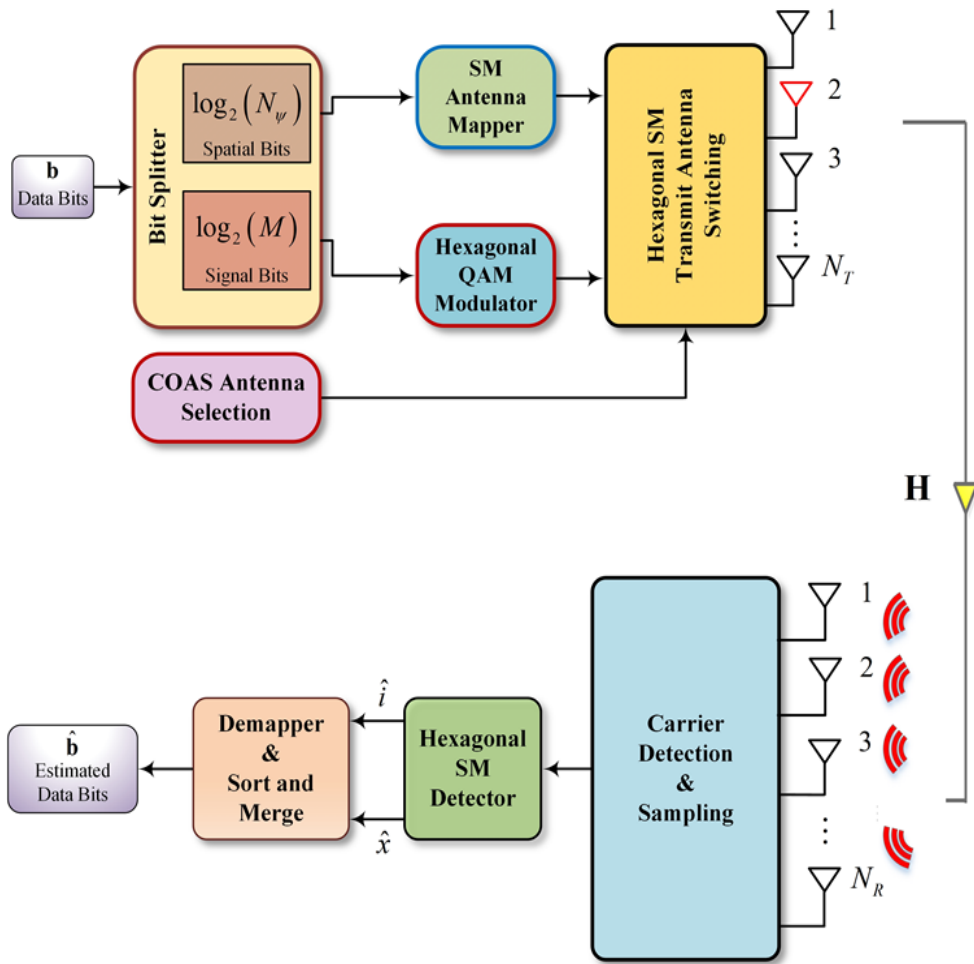


Figure 3. System Model of the COAS-HSM scheme

$$C \leq C_{HSM} \leq C + \log_2(N_{\psi}), \tag{1}$$

where; C_{HSM} depicts the capacity of hexagonal SM system, C can be written as $C = \frac{1}{N_{\psi}} \sum_{i=1}^{N_{\psi}} \log_2(1 + \gamma \|\mathbf{h}_i\|^2)$, and γ depicts the SNR value.

In order to maximize the capacity of MIMO system, the C value must be maximized. Therefore, C must be maximized by selecting N_{ψ} antennas corresponding to the largest channel norms. On the receiver side, N_{ψ} sub-antenna groups are calculated from N_T antennas and feedback is given to the transmitter. Based on all these described, COAS based antenna set can be easily found as follows [21]:

$$C_{COAS} = \{\alpha_1, \alpha_2, \dots, \alpha_{N_{\psi}}\}, \tag{2}$$

Here, $\alpha_1, \alpha_2, \dots, \alpha_{N_{\psi}}$ represents the index information of the channel vectors in order of magnitude of the norm. These values can be obtained as follows steps.

During the generation of the C_{COAS} set, the following steps are followed:

1. With $C_{COAS} \in \{1, 2, \dots, N_T\}$, the Frobenius norm of each column vector in the \mathbf{H} wireless channel matrix is calculated:

$$\|\mathbf{h}_{\alpha_i}\|_F^2, \tag{3}$$

2. The Frobenius norm of each channel vector should be arranged in descending order.

$$\|\mathbf{h}_{\alpha_1}\|_F^2 > \|\mathbf{h}_{\alpha_2}\|_F^2 > \dots > \|\mathbf{h}_{\alpha_{N_\psi}}\|_F^2 > \|\mathbf{h}_{\alpha_{N_\psi+1}}\|_F^2 > \dots > \|\mathbf{h}_{\alpha_{N_T}}\|_F^2, \tag{4}$$

3. Select the highest N_ψ channel gain vectors to create wireless channel channel vector \mathbf{H}_{COAS} 's $N_R \times N_\psi$ channel Matrix expressed as follows: expressed as follows: $\mathbf{H}_{COAS} = [\mathbf{h}_{\alpha_1}, \mathbf{h}_{\alpha_2}, \dots, \mathbf{h}_{\alpha_{N_\psi}}]$, where \mathbf{H}_{COAS} is the sub-matrix of \mathbf{H} .

After the best antenna set C_{COAS} has been successfully acquired, the hexagonal SM technique is carried out with this set.

4. System Model of COAS-HSM

In this section, COAS-HSM scheme will be mentioned. The system model of the COAS-HSM system is given in Figure 3. In the COAS technique, as mentioned before, a sub-antenna group that gives the highest channel amplitudes among a certain antenna group is selected and the transmission is carried out through these selected antennas. In the proposed COAS-HSM system, among the N_T transmission antennas, N_ψ COAS sub-antenna groups are selected and the transmission is accomplished through these selected antennas. As in the traditional SM system, there are N_R receiver antennas in the COAS-HSM system. In the proposed system, similar to the traditional SM system, active antenna indices are selected over N_ψ transmission antennas and these active antenna indices are used to transmit information with little additional hardware costs. However, unlike the traditional SM technique, in the HSM technique, traditional M -QAM constellations are not used to transmit data, but hexagonal constellations are used.

If the COAS-HSM scheme is examined carefully, it is seen that vector \mathbf{b} with the size of $1 \times k$ is the data vector to be transmitted to the receiver terminal. At the transmitter terminal, \mathbf{b} is divided into sub vectors \mathbf{b}_1 with the size of $1 \times k_1$ and \mathbf{b}_2 with the size of $1 \times k_2$, where $k_1 = \log_2(N_\psi)$ and $k_2 = \log_2(M)$, and communication is provided over \mathbf{b}_1 and \mathbf{b}_2 .

If the COAS-HSM scheme is examined carefully, it is seen that vector \mathbf{b} with the size of $1 \times k$ is the data vector to be transmitted to the receiver terminal. At the transmitter terminal, \mathbf{b} is divided into sub vectors \mathbf{b}_1 with the size of $1 \times k_1$ and \mathbf{b}_2 with the size of $1 \times k_2$, where $k_1 = \log_2(N_\psi)$ and $k_2 = \log_2(M)$, and communication is provided over \mathbf{b}_1 and \mathbf{b}_2 .

The received faded signal with added noise is given as:

$$\mathbf{r} = \sqrt{g} \mathbf{x}_{ip} \mathbf{H}_{\text{COAS}} + \mathbf{w}, \tag{5}$$

here; g expresses the average SNR, \mathbf{x}_{ip} is the spatial modulated HQAM symbol vector, \mathbf{H}_{COAS} expresses the communication channel matrix with the size $N_R \times N_\psi$ and follows the Rayleigh distribution. Also, \mathbf{H}_{COAS} is the sub-matrix of \mathbf{H} with the size of $N_R \times N_T$. \mathbf{w} is the complex Gaussian random process with size of N_R , zero mean and variance of N_0 , i.e., $\mathbf{w} \sim (0, N_0)$.

As it is well-known, SM uses the antenna indices as an extra dimension to transmit information bits. Thereon, a vector using SM mapper is created which is given as follows:

$$\mathbf{x}_{ip} = \begin{bmatrix} 0 & \cdots & 0 & \underset{\substack{\uparrow \\ i^{\text{th}} \text{ position}}}{x_p} & 0 & \cdots & 0 \end{bmatrix}^T, \tag{6}$$

here, x_p shows the p^{th} symbol of M -ary HQAM and $p = 1, 2, 3, \dots, M$; i shows the active antenna index and $i = 1, 2, 3, \dots, N_\psi$. Here, only the i^{th} antenna will remain active during the transmission of the corresponding symbol.

If the x_p symbol is transmitted by the i^{th} antenna, the channel output in (5) can be rewritten as follows:

$$\mathbf{r} = \sqrt{g} x_p \mathbf{h}_i + \mathbf{w}, \tag{7}$$

here, \mathbf{h}_i is the i^{th} column of the wireless communication channel \mathbf{H}_{COAS} .

Under the assumption that the channel inputs of SM are approximately equal according to the SM optimal receiver principle, the indices of COAS-HSM system can be obtained according to the maximum-likelihood (ML) principle as follows [21]:

$$\begin{aligned}
 [\hat{i}, \hat{p}] &= \arg \max_{i,p} p_r \{ \mathbf{r} | x_{ip}, \mathbf{H}_{\text{COAS}} \} \\
 &= \arg \min_{i,p} \left\{ \|\mathbf{r} - \mathbf{h}_i x_i\|_F^2 \right\} \\
 &= \sqrt{g} \|\mathbf{A}_{ip}\|_F^2 - 2\text{Re} \{ \mathbf{r}^H \mathbf{A}_{ip} \},
 \end{aligned} \tag{8}$$

here; $1 \leq i \leq N_\psi$, $1 \leq p \leq M$, and \mathbf{A}_{ip} is in the form of $\mathbf{A}_{ip} = \mathbf{h}_i x_p$. Also,

$p_r \{ \mathbf{r} | x_{ip}, \mathbf{H}_{\text{COAS}} \} = \pi^{-N_R} \exp \left(-\|\mathbf{r} - \mathbf{H}_{\text{COAS}} x_{ip}\|_F^2 \right)$ is the conditional probability density function according to x_{ip} and \mathbf{H}_{COAS} .

5. Performance Analysis for COAS-HSM System

The performance of the COAS-HSM method can be straightforwardly calculated using the union bound technique. From this point on, the average BER expression of the COAS-HSM system can be given as follows [22]:

$$\begin{aligned}
 P_{\text{COAS-HSM}} &\leq E_x \left\{ \sum_{i,\hat{p}} n(p, \hat{p}) P(x_{ip} \rightarrow x_{i\hat{p}}) \right\} \\
 &= \sum_{i=1}^{N_\psi} \sum_{p=1}^M \sum_{\hat{i}=1}^{N_\psi} \sum_{\hat{p}=1}^M \frac{n(p, \hat{p}) P(x_{ip} \rightarrow x_{i\hat{p}})}{N_\psi M},
 \end{aligned} \tag{9}$$

where; $n(p, \hat{p})$ is the number of bits in error between the symbol x_p and $x_{\hat{p}}$. In other words, the number of erroneous bits that occur when x_p is transmitted and $x_{\hat{p}}$ is received is expressed as $n(p, \hat{p})$. $P(x_{ip} \rightarrow x_{i\hat{p}})$ is the pairwise error probability (PEP) of deciding on the constellation vector $x_{i\hat{p}}$ while x_{ip} is transmitted. By the help of (8), the PEP conditioned on \mathbf{H}_{COAS} (CPEP) can be written as [23]:

$$\begin{aligned}
 P(x_{ip} \rightarrow x_{i\hat{p}} | \mathbf{H}_{\text{COAS}}) &= P \left(\sqrt{g} \|\mathbf{A}_{ip}\|_F^2 - 2\text{Re} \{ \mathbf{r}^H \mathbf{A}_{ip} \} > \sqrt{g} \|\mathbf{A}_{i\hat{p}}\|_F^2 - 2\text{Re} \{ \mathbf{r}^H \mathbf{A}_{i\hat{p}} \} \right) \\
 &= Q \left(\sqrt{\frac{g}{2}} \|\mathbf{A}_{ip} - \mathbf{A}_{i\hat{p}}\|_F \right),
 \end{aligned} \tag{10}$$

where, $Q(\cdot)$ stands for Q function.

As shown in (4), in order to minimize the error rate in (10), the N_ψ is highest normed of the channel matrix \mathbf{H} columns are selected to generate \mathbf{H}_{COAS} matrix. Thus, the antenna group that reaches the highest SNR in the receiver is selected.

As a result, the CPEP expression in (10) is minimized. To the best of the authors' knowledge, the closed form expression of the CPEP expression in (10) does not exist.

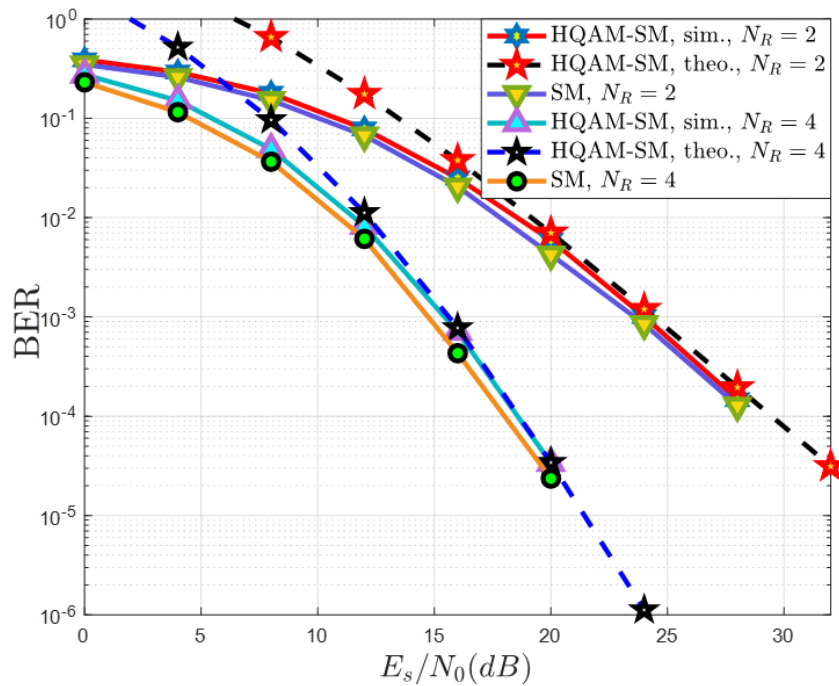


Figure 4. Performance comparisons of SM and HQAM-SM schemes where $M = 16$, $N_T = 4$ and $N_R = 2, 4$

On the other hand, for HQAM-SM system unconditional PEP can be written as follows [9]:

$$P(x_{ip} \rightarrow x_{i\hat{p}}) = \zeta_\alpha^{N_R} \sum_{k=0}^{N_R-1} \binom{N_R-1+k}{k} [1-\zeta_\alpha]^k, \tag{11}$$

where, $\zeta_\alpha = \frac{1}{2} \left(1 - \sqrt{\frac{\nu_\alpha^2}{1+\nu_\alpha^2}} \right)$ and $\nu_\alpha^2 = \frac{g(|x_p|^2 + |x_{\hat{p}}|^2)}{4}$. Using (11) in (9), average BER of the HQAM-SM technique

is given as follows [9]:

$$P_{HQAM-SM} \leq \frac{\sum_{p=1}^M \sum_{\hat{p}=1}^M N_T n(p, \hat{p}) \zeta_\alpha^{N_R} \sum_{k=0}^{N_R-1} \binom{N_R-1+k}{k} [1-\zeta_\alpha]^k}{M}. \tag{12}$$

6. Simulation Results

In this section, simulation results are given for COAS-HSM, HQAM-SM, QAM-SM and QSM techniques on Rayleigh fading channels. While obtaining the simulation results, the Monte Carlo simulation technique is used. 10^{-5} BER value is used to compare SNR performance gains of the techniques with each other. Also, in all performance comparisons, SNR is given as $SNR(dB) = 10 \log_{10}(E_s/N_0)$, where E_s represents the average symbol energy. It is also assumed that

CSI is perfectly known at the receiver. Subsequently, the ML detector is used to estimate the transmitted symbols and indices.

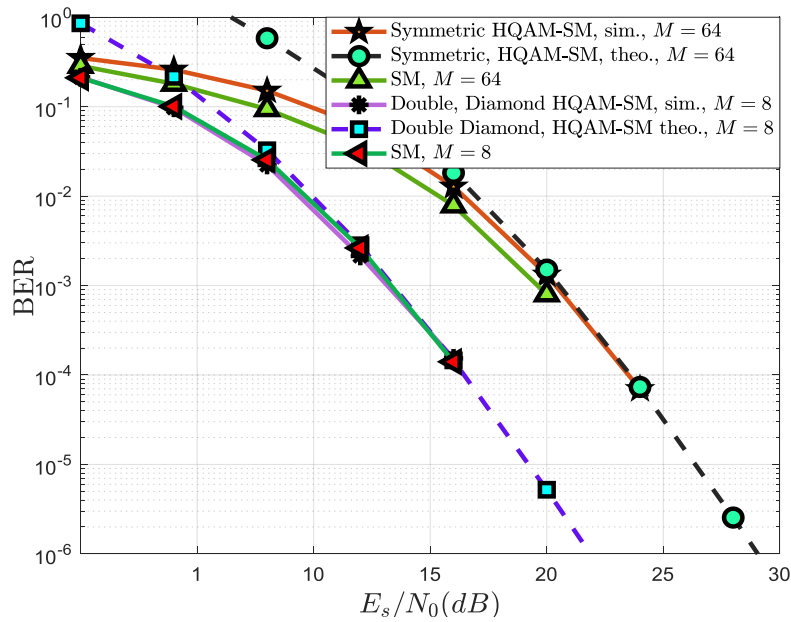


Figure 5. Performance comparisons of SM and HQAM-SM schemes where $N_T = 4$, $M = 8, 64$ and $N_R = 4$

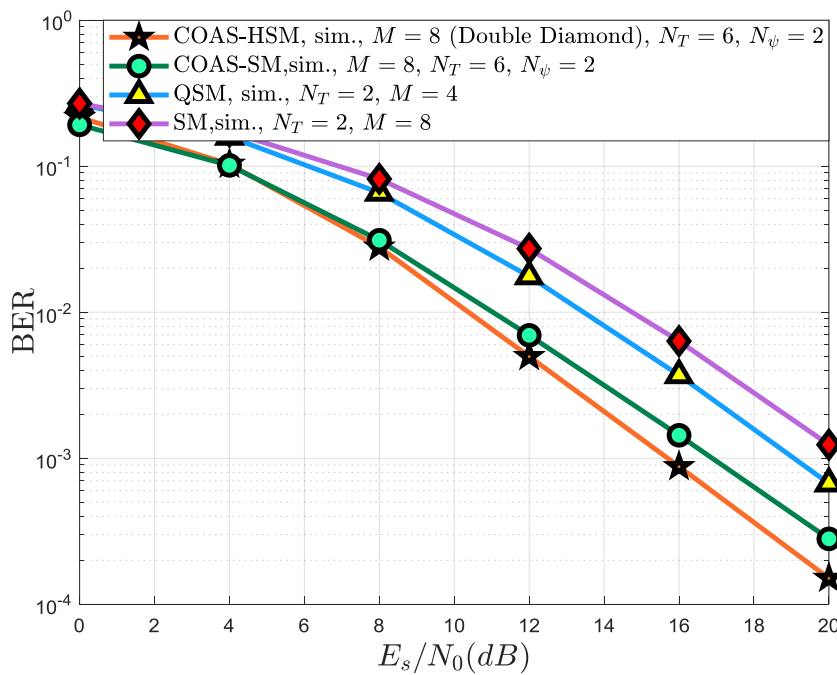


Figure 6. Performance comparisons of COAS-HSM, COAS-SM, SM and QSM systems where $N_T = 6$, $N_\psi = 2$, $N_R = 2$

In Figure 4, both theoretical and simulated performance comparisons of HQAM-SM system with QAM-SM system are given. In these comparisons, $N_T = 4$ and $M = 16$, and the receiver antenna numbers are chosen as $N_R = 2$ and $N_R = 4$. In this comparison, the QAM-SM and HQAM-SM comparisons transmit a total of $k = 6$ bits; 2 bits by antenna index, and 4 bits by 16-QAM/16-HQAM symbol.

In Figure 5, both theoretical and simulated performance comparisons of HQAM-SM system with QAM-SM system are presented. However, in these comparisons $N_T = 4$ and $N_R = 4$, and the modulation degree is chosen as $M = 8$ or $M = 64$. In systems, when $M = 8$ is selected, $k = 5$ bits are transmitted; and when $M = 64$ is selected, $k = 8$ bits are transmitted. If Figure 4 and Figure 5 are examined together, it can be seen that HQAM-SM and traditional QAM-SM

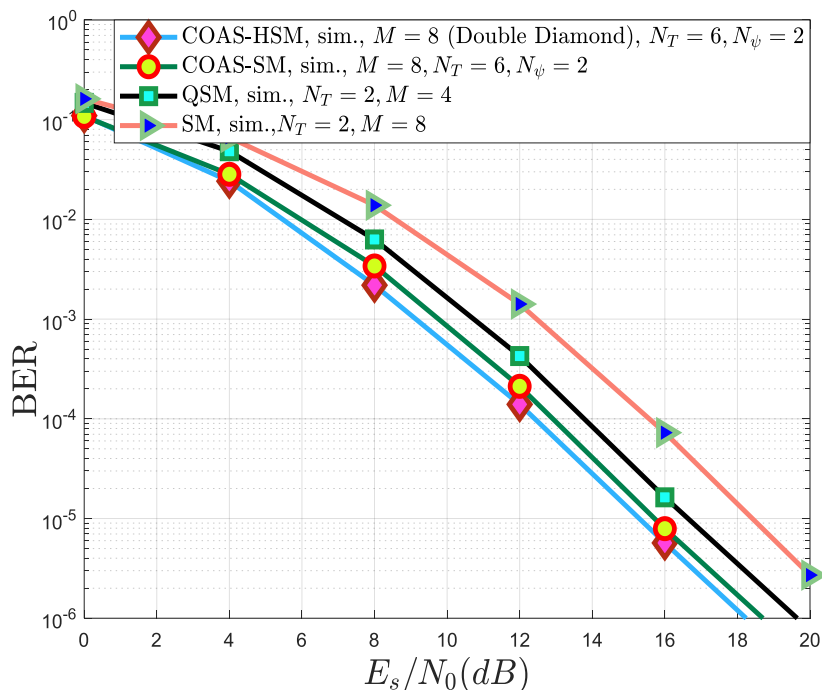


Figure 7. Performance comparisons of COAS-HSM, COAS-SM, SM and QSM systems where $N_T = 6$, $N_\psi = 2$,

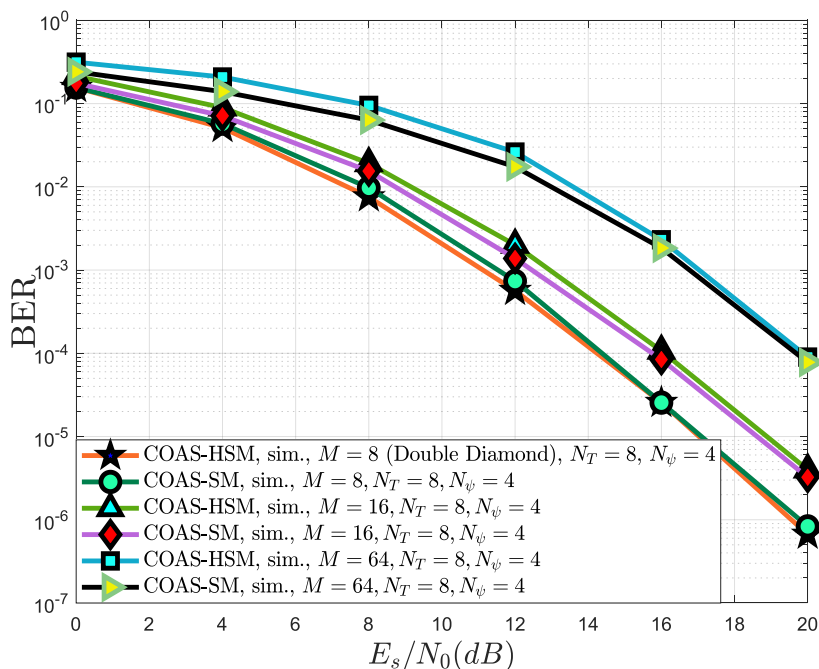


Figure 8. Performance comparisons of COAS-HSM and COAS-SM when $N_T = 8$, $N_\psi = 4$, $M = 8, 16, 64$, $N_R = 4$

techniques show similar performances, especially in high SNR. Besides, the HQAM-SM system is optimal in terms of energy efficiency.

In Figure 6, performance analyzes of COAS-HSM, COAS-SM, SM and QSM systems were performed for $k = 4$. In COAS-HSM and COAS-SM techniques, $N_T = 6$ and $N_{\psi} = 2$ are selected, and in all techniques, the number of receiver antennas as $N_R = 2$ is selected. As can be seen from the figure, the COAS-HSM technique provides approximately 1.3 dB gain compared to COAS-SM technique, 3.4 dB gain compared to QSM technique and 5.1 dB gain compared to the SM technique. Especially in these simulations, it has been observed that “the double diamond $M = 8$ ” scheme provides better performance in the COAS technique compared to other HQAM schemes, because the double diamond HQAM constellation can separate symbols from each other more accurate.

For other constellation schemes, as mentioned before, HQAM provides almost equivalent performances and is energy efficient. In Figure 7, precisely the systems in Figure 6 are compared. The only difference is that the number of receiver antennas is $N_R = 4$. Besides, the COAS-HSM technique provides a gain of about 0.55 dB compared to COAS-SM technique, a gain of 1.5 dB compared to QSM technique and a gain of 3.16 dB compared to the SM technique.

Finally, in Figure 8, performance comparisons for $M = 8, 16$, and 64 are given when COAS-HSM and COAS-SM systems have $N_T = 8$ and $N_{\psi} = 4$. As can be seen from the figure, COAS-HSM and COAS-SM techniques show similar BER performances at high SNR region. In addition, the COAS-HSM technique is an energy efficient next-generation communication technique.

7. Conclusion

In this study, a high data rated and energy-efficient communication technique called COAS-HSM is proposed. Considered method is obtained by adapting HQAM and SM techniques together with COAS based antenna selection scheme. The proposed new technique provides remarkable SNR gains compared to traditional SM, QSM and HQAM-SM techniques, while it offers similar SNR gains compared to the COAS-SM technique. However, the simulation results obtained also prove that the COAS-HSM system consumes less transmission energy, and on the other hand, has the error performance nearly equivalent to the COAS-SM technique. In addition to all these, when hexagonal constellations are used, energy efficiencies of up to 20% are obtained as given in Table 1, and they are potential candidates for next-generation energy-efficient communication systems.

References

- [1] Buzzi, S., Chih-Lin, I., Klein, T.E., Poor, H.V., Yang, C., and Zappone, A. (2016) A survey of energy-efficient techniques for 5G networks and challenges ahead. *IEEE J. Sel. Areas Commun.*, 34 (4): 697–709.
- [2] Sharma, S.K., Woungang, I., Anpalagan, A., and Chatzinotas, S. (2020) Towards tactile internet in beyond 5G era: recent advances, current issues and future directions. *IEEE Access*, 1–1.

- [3] Navarro-Ortiz, J., Romero-Diaz, P., Sendra, S., Ameigeiras, P., Ramos-Munoz, J.J., and Lopez-Soler, J.M. (2020) A survey on 5G usage scenarios and traffic models. *IEEE Commun. Surv. Tutorials*, 1–1.
- [4] Chen, X., Ng, D.W.K., Yu, W., Larsson, E.G., Al-Dhahir, N., and Schober, R. (2020) Massive access for 5G and beyond.
- [5] Aydin, E., Cogen, F., and Basar, E. (2019) Code-index modulation aided quadrature spatial modulation for high-rate MIMO systems. *IEEE Trans. Veh. Technol.*, 68 (10), 10257–10261.
- [6] Gunduz, Rugini, L. (2016) Symbol error probability of hexagonal QAM. *IEEE Commun. Lett.* 20 (8): 1523–1526.
- [7] Murphy, C.D. (2000) High-order optimum hexagonal constellations. *IEEE Int. Symp. Pers. Indoor Mob. Radio Commun. PIMRC*, 1: 143–146.
- [8] Gao Xingxin, Lu Mingquan, and Feng Zhenming (2002) Asymmetric hexagonal QAM based OFDM system. *IEEE 2002 Int. Conf. Commun. Circuits Syst. West Sino Expo.*, 1:299–302.
- [9] Cogen, F., and Aydin, E. (2019) Hexagonal quadrature amplitude modulation aided spatial modulation. 2019 11th Int. Conf. Electr. Electron. Eng., 730–733.
- [10] Huang, H., Papadias, C.B., and Venkatesan, S. (2012) *MIMO communication for cellular networks*, Springer US, Boston, MA.
- [11] Hampton, J.R. (2013) *Introduction to MIMO communications*, Cambridge University Press, Cambridge.
- [12] Kumbhani, B., and Kshetrimayum, R.S. (2017) *MIMO wireless communications over generalized fading channels*, CRC Press.
- [13] Heath Jr, R.W., and Lozano, A. (2018) *Foundations of MIMO communication*, Cambridge University Press.
- [14] Mesleh, R.Y., Haas, H., Sinanović, S., Ahn, C.W., and Yun, S. (2008) Spatial modulation. *IEEE Trans. Veh. Technol.*, 57 (4): 2228–2241.
- [15] Mesleh, R., and Alhasssi, A. (2018) *Space modulation techniques*, John Wiley & Sons, Inc, Hoboken, NJ, USA.
- [16] Cogen, F., Aydin, E., Kabaoglu, N., Basar, E., and Ilhan, H. (2020) Generalized code index modulation and spatial modulation for high rate and energy-efficient MIMO systems on rayleigh block-fading channel. *IEEE Syst. J.*, 1–8.
- [17] Pillay, N., and Xu, H. (2017) Improved generalized spatial modulation via antenna selection. *Int. J. Commun. Syst.*, 30 (10): e3236.
- [18] Asaati, B., and Abu-Hudrouss, A. (2020) Transmit antenna selection schemes for STBC-SM. *TURKISH J. Electr. Eng. Comput. Sci.*, 28 (4): 2077–2087.
- [19] Aydin, E. (2019) EDAS/COAS based antenna selection for code index modulation aided spatial modulation. *Electrica*, 19 (2): 113–119.
- [20] Rajashekar, R., Hari, K.V.S., and Hanzo, L. (2013) Antenna selection in spatial modulation systems. *IEEE Commun. Lett.*, 17 (3): 521–524.
- [21] Cogen, F., and Aydin, E. (2020) Cooperative quadrature spatial modulation with euclidean distance and capacity optimized antenna selection. *Int. J. Commun. Syst.*
- [22] Proakis, J., and Salehi, M. (2008) *Fifth edition: digital communications*.

- [23] Jeganathan, J., Ghrayeb, A., and Szczecinski, L. (2008) Spatial modulation: optimal detection and performance analysis. *IEEE Commun. Lett.*, 12 (8):545–547.

Low-Cost Android Based Telemonitoring System for Body Temperature Measurement

Ahmet Remzi Ozcan¹ , Ahmet Mert^{1*} 

^{1*} Bursa Technical University, Bursa, Turkey

Abstract

The increasing number of pandemic issues require to pay attention to health conditions and social distance. The explicit sign of COVID-19 is body fever. It is a simple and affordable detection method when compared to other blood tests. However, it is required to be physically close to a visitor to measure body temperature. For this reason, we have designed and developed a low-cost microprocessor measurement system with an infrared non-contact temperature sensor, and a Bluetooth for sending to long distance. Android application has been developed to read and set the alarm function using a smart telephone or a tablet far from the visitors. With the help of these circuit and application designs, body temperatures can be checked from long distance considering the pandemic situations. The printed circuit of the microcontroller, Bluetooth, sensor, and light-dependent resistor (LDR) triggering are manufactured, and the software of the controller and the application are integrated and tested successfully.

Keywords: Temperature sensor, Telemonitoring, Body temperature, Measurement, Android application.

Cite this paper as:

Ozcan, R. A., Mert, A. (2021). *Low-Cost Android Based Telemonitoring System for Body Temperature Measurement*. Journal of Innovative Science and Engineering, 5(2): 91-100

*Corresponding author: Ahmet Mert
E-mail: ahmet.mert@btu.edu.tr

Received Date: 06/12/2020
Accepted Date: 06/02/2021
© Copyright 2021 by
Bursa Technical University. Available
online at <http://jise.btu.edu.tr/>



The works published in Journal of Innovative Science and Engineering (JISE) are licensed under a Creative Commons Attribution-NonCommercial 4.0 International License.

1. Introduction

The increasing number of pandemic issues and chronic illness of the elderly require to pay attention to the health condition. The monitoring physiological values of chronic patients were one of the popular topics in biomedical engineering. With the help of the advanced medical sensor technologies, telemonitoring of medical parameters of the patient is a useful tool for healthcare specialists. Heart rate monitoring based on photoplethysmography (PPG) or electrocardiography (ECG) [1] is the most studied electronic system the telemonitoring system due to being a vital indicator [2]. Blood pressure, electroencephalography (EEG), and blood glucose are also used for long-term monitoring, especially for telemedicine [3,4].

Body temperature is the most applied measurement for the diagnosis of an illness. For this reason, various types of devices have been designed. NTC type thermistor, and contactless IR sensor-based devices are the most common types. Due to fast response and being contactless, IR temperature circuit is preferred [5]. There is an increasing demand for contactless temperature sensor after SARS-CoV-2 pandemic. The fever is the most general symptom, so researchers focus on contactless temperature telemonitoring due to prevent the spread of COVID-19. A wearable device, and measurement from wrist were applied to patients in hospitals to investigate the effects on COVID-19 pandemic [6,7]. Biotelemetry is interdisciplinary engineering to transfer and monitor various vital signs of ambulatory patients [8]. Saturated O₂ (SpO₂), ECG, body temperature can be connected to the microcontroller and wireless communication systems. Thus, these physiological signals can be traced from long distance or internet [9]. Telemedicine or telemonitoring systems can be categorized depending on measured signal(s) /sign(s), a total number of the channels (mono or multi), communication protocol, and the user interface [10]. After signal amplification, it was applied to the microcontroller for processing and sent via Bluetooth, ZigBee, and Wi-Fi networks [12-14]. Wireless body area networks (WBANs) also combine multi- sensor signal processing and transmitting them via multiple communication systems depending signals health priority [15-17]. Thus, the health status of the patients can be detected, and doctors can track them without visiting the hospital [15]. In [18], GPS was integrated into the measurement system to track the patient. In addition, there are some commercial devices and applications to monitor some physiological signals (e.g, smartwatches), which are listed in [19].

In this study, we designed an IR contactless temperature monitoring circuit and application in accordance with pandemic conditions. The temperature measurement circuit is designed using an IR sensor, microcontroller, and Bluetooth. An Android application is developed to monitor and warn after receiving Bluetooth signals. Thus, body temperature can be checked from a long distance without disturbing isolation in SARS-CoV-2 pandemic. This developed system can be adapted to continuous temperature device in the range of Bluetooth. The remainder of the paper is organized as follows: Section Material and Methods provides the description of the used components, the designed circuit and the application. In Section Results and Discussion designed system and application software are examined, and the conclusions are drawn in Section Conclusion.

2. Material and Methods

2.1. Non-Contact Temperature Sensor

Thermopile IR sensors are based on the detection of IR energy from an object from a distance. The more energy means a higher temperature level. We have used the medical version of the MLX90615 IR sensor [20]. It consists of the sensor, a 16-bit ADC, and a microcontroller with SMBus (similar to I2C) protocol. The block diagram of the sensor is given in Figure 1.

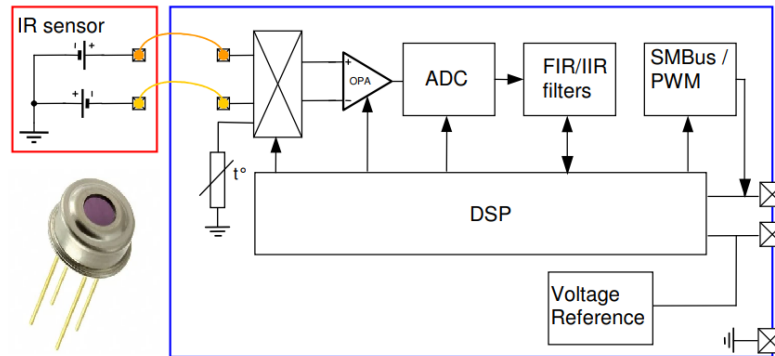


Figure 1. The block diagram of the non-contact temperature sensor, MLX90615 [20].

This sensor has a fast response of measurement with error rate $\pm 0.2^{\circ}\text{C}$ in the medical range shown in Figure 2.

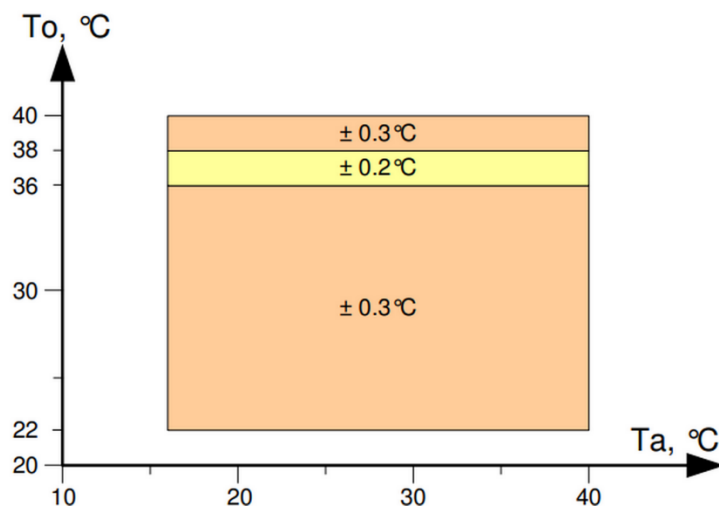


Figure 2. Accuracy of the sensor for medical applications [20].

MLX90615DAA has self-calibrating property depending on ambient temperature (T_a) measured by the internal sensor. The detected temperature of the object (T_o) can be read from the memory of 0xB7 using two-wire SMBus.

2.2. Design of Microcontroller Based Measurement Device

A circuit consisting of a microcontroller, Bluetooth, LED, light-dependent resistor (LDR), and MLX 90615 IR temperature sensor has been designed in this study. For temperature measurement MLX 90615 is connected to low energy microcontroller, PIC12LF1822 [21] via I2C I/O pins. The measurement starts with the trigger signal from the LDR pin, and then the temperature in the 0xB7 using I2C is processed to convert it to Celsius degree. Finally, the value is sent using Bluetooth to an Android application, and the status LED is turned on. The block diagram of the designed circuit is shown in Figure 3.

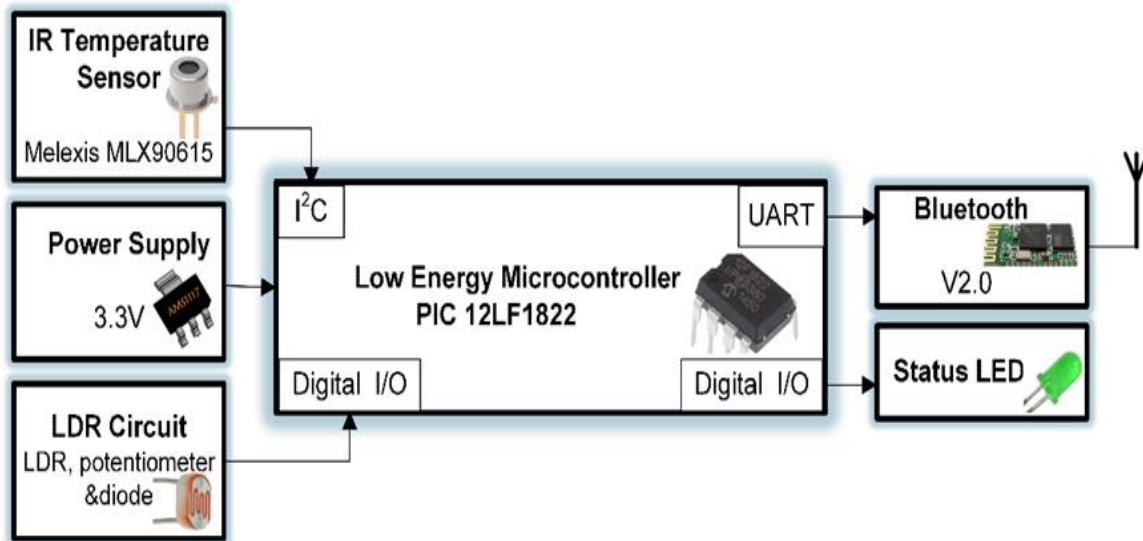


Figure 3. The block diagram of the designed microcontroller-based measurement device.

The LDR circuit is to detect the wrist is placed or not. After detection, the trigger digital level exists, and the measurement starts via I2C. The value in 0xB7 is then converted by

$$T(^{\circ}C) = 0xB7 \times 0.02 - 273.15 \quad (1)$$

The temperature is transferred writing it to UART port of the controller, and then it is received by the paired Bluetooth module of the Android device. An algorithm is also developed for PIC12LF1822 microcontroller, and the pseudocode is given in Algorithm 1.

Algorithm 1: The Pseudo-Code of The Microcontroller.

<p>Program starts Initialize Configuration, Initialize UART module at 9600bps, Initialize I²C module at 100kHz. Start Main Loop Start Loop1 Send ID via UART IF Sent ID==Received ID Then Break End Loop1 IF LDR Pin==True Then WakeUp MLX90615</p>	<p>Start I²C, write 0xB6, write 0x27 Repeated start, write 0xB7 Read LSB &MSB Convert temperature (T) to °C Compute averaged T(°C) Write temperature to UART Status LED =True Delay 500ms End IF Status LED =False End Main Loop</p>
--	--

In this algorithm, the temperature value is measured 3-times to make a simple moving average filtering, and the filtered value $T(^{\circ}C) = (T_1 + T_2 + T_3) / 3$ is sent to a smart phone or tablet.

2.3. Android Based Monitoring Application

An Android-based monitoring application has been developed to monitor the temperature data in the system and to control the measurement devices. The main objective of the application is to monitor the temperature values measured in real-time by the measuring device and to warn the user when a temperature above the determined threshold value is detected. Furthermore, the application has functionalities such as measurement device selection, threshold temperature value configuration and temperature calibration. Data communication between the application and the measurement device is provided via Bluetooth, which is a communication protocol that stands out with its low power consumption and widespread use. The flowchart of the monitoring application is outlined in Figure 4.

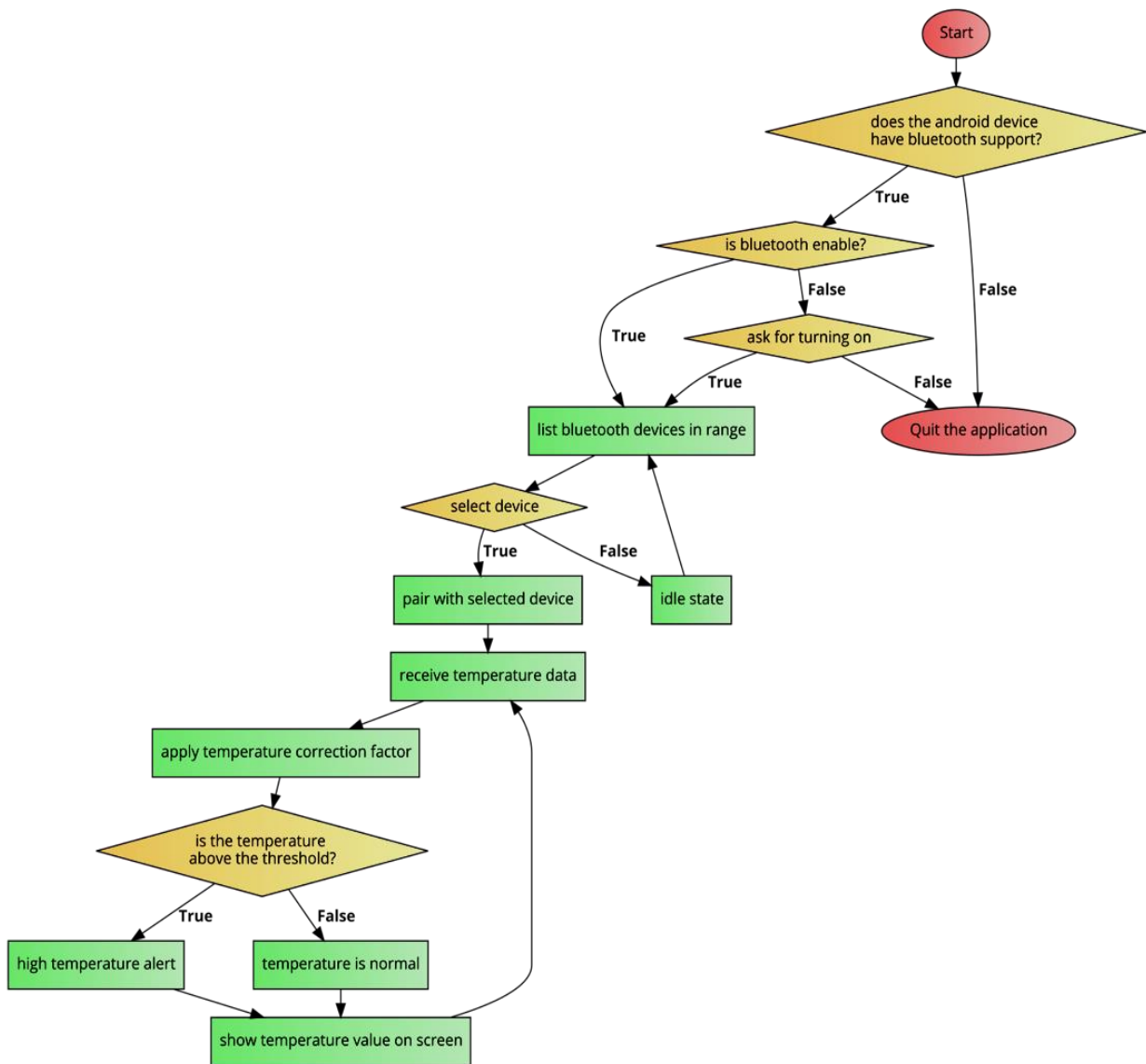


Figure 4. The flowchart for Android-based monitoring application

When the application is opened, it first scans the Bluetooth devices in range and presents the list of available devices to the user for selection. After the device selection, a virtual serial port interface is established over Bluetooth to be used for data transfer. With the start command sent from the application, the measuring device starts to send the measured temperature data in the specified period. In the temperature data, the threshold evaluation process is started after the temperature correction determined in accordance with the region where the temperature is measured. Temperature correction value can be modified with the "Calibration" option in the application settings. If the obtained temperature value is above the determined maximum value, the high-temperature phrase appears on the application screen and the user is warned audibly. Otherwise, only the temperature value on the application screen is updated. Using the application settings menu, the threshold value for the maximum temperature can be modified, and the warning function can be activated for cases where the threshold value is exceeded. As long as the application is open, the temperature evaluation process continues cyclically.

3. Results and Discussion

First, we have designed an electronic circuit to measure and transmit temperature value. The PIC12LF1822 microcontroller, HC-05 Bluetooth v2, and MLX 90615 IR non-contact temperature sensor-based circuit has been integrated, and LDR triggering is adopted to its algorithm. After the wrist is closed to the device, contactless measurement starts, and the temperature value is sent to an Android device. The schematic of the circuit is shown in Figure 5.

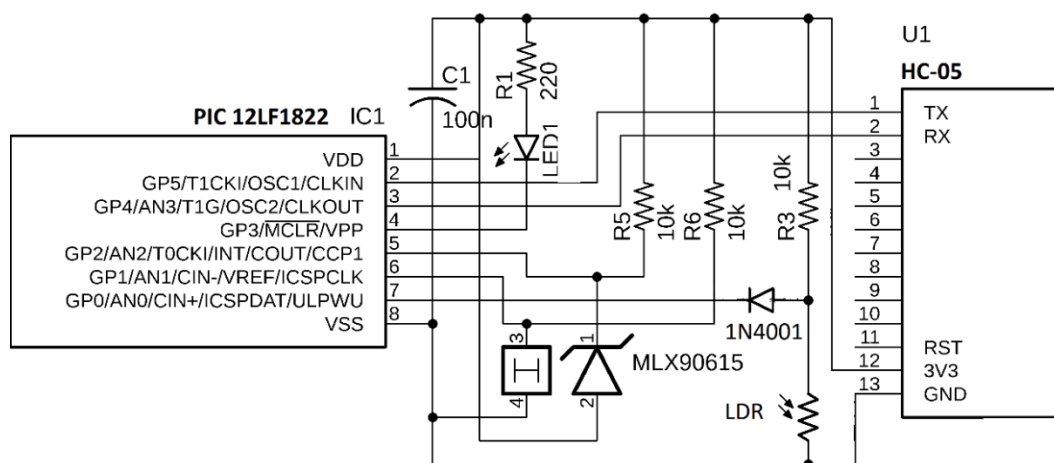


Figure 5. The schematic view of the microcontroller-based circuit.

C language-based approximately 2kB code is developed for this device. SMBus (I2C) and UART protocols, and the conversions are embedded. For user-friendly usage of the device, the 3-D model of the chassis is designed. This model and the position of the temperature measurement from the wrist are shown in Figure 6.

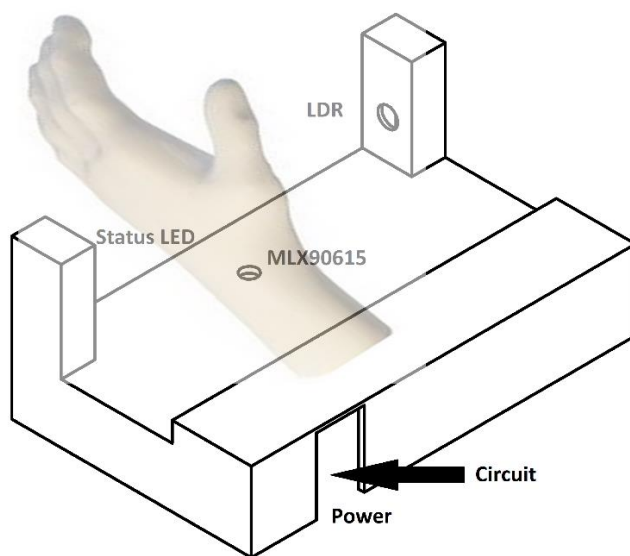


Figure 6. 3-D chassis model and the scheme of the measurement from the wrist.

3D model is then constructed using a 3D printer, and the circuit is mounted in it. After the user puts the wrist to closer to LDR, at the same time, closer to MLX90615 sensor, it is measured and sent to the application in on a smartphone from long distance. The Android application can be seen in Figure 7.

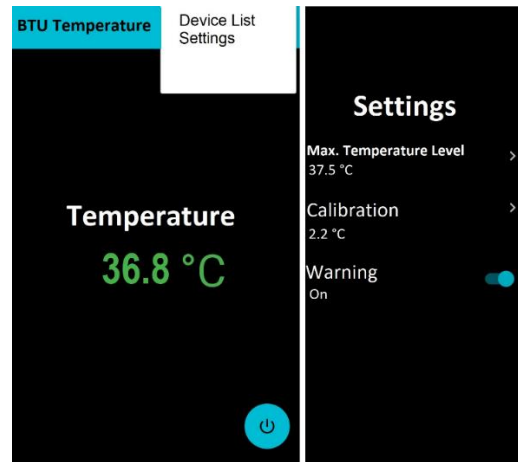


Figure 7. The view of the Android application.

The transferred measurement data to the application is in object mode temperature. In other words, it should be arranged to body temperature considering measurement from the wrist. For this reason, we measured the temperature of the wrist at object mode, and then body mode at least 10 times using a calibrated device. The mean difference between object and body mode (2.2 °C) is added to the calibration panel on the application. This can be also re-adjusted if any deviation exists.

With the help of the designed device and application, body temperature in the entrance of the university or mall can be detected from long distance in accordance with isolation in a pandemic situation. In case of fever, audible and visual alarms can be set.

This is a low-cost design for checking body temperature without getting closer, however, it has limitations of the range and voice. To compare the study to previous designs, their technologies are summarized in Table 1.

Table 1: The Comparison of Body Temperature Measurement Devices in the Literature.

Study	Technology
Kuzu and Tulum [4]	Atmega, SpO2, blood pressure, temperature (only measurement)
Şakar and Öviz [5]	PIC18F4620, DS18B20, MLX90614 (Contact/non-contact sensor)
Gülenç & Kartal [8]	Atmega328P, Max30100, MLX90614, MPU6050, ESP8266, WEB
Korkmaz et al. [10]	PIC16F877A, LabVIEW, Nonin 800A, DS18B20, RF UFM-M11
Wijaya et al [12]	Atmega16, LM35, Heart rate (only measurement)
Gupta et al. [13]	Arduino, Heart Rate, NTC, LCD
Mert et al. [14]	PIC18F4550, LCD, MLX90615, HIH6006, DBM01, Wi-Fi.
Hasan [16]	MAX30205, ESP8266 MCU, SR-04, RFID (RC522), ThingSpeak, IoT
Karthi & Jayakumar [18]	NodeMCU ESP8266, AWS IoT,RFID, DT11, GPS
This study	MLX90615, PIC12LF1822, LDR, HC-05, Android application.

This design in this paper is an effective and low-cost solution considering the pandemic issues. HC-05 Bluetooth v2.0 has a wider range (up to 10m) when compared to Bluetooth 4.0 low energy modules, but it might be insufficient for some places. Moreover, PIC12LF1822 is suitable to re-design it using battery due to low power consumption, but it has 2kB flash program memory, which disables us to add voice command option and speaker. For further designs, these considerations can be re-designed.

4. Conclusion

In this study, we have designed a low-cost microcontroller-based body temperature measurement circuit with an Android application. Infrared non-contact temperature sensor is connected to microcontroller using I2C protocol, and Bluetooth module at the UART pins is used to transfer body temperature. With the help of developed Android application, the received data from a smart telephone or tablet can be shown, checked, and audible or visual alarms can be set in case of fever. Thus, long-distance measurement circuit with its microcontroller and application codes are developed considering the COVID-19 pandemic conditions. At the entrance of a building such as a university or a mall, the fever of the visitors can be detected safely, without contacting physically.

Acknowledgement

This work is supported by the Research Fund of Bursa Technical University, Project Number: 200COVID05.

References

- [1] Hanilçi, A., & Gürkan, H. (2019). ECG biometric identification method based on parallel 2-D convolutional neural networks. *Journal of Innovative Science and Engineering (JISE)*, 3(1), 11-22.
- [2] Verma, S., & Gupta, N. (2012). Microcontroller-based Wireless Heart Rate Telemonitor for Home Care. *IOSR J Eng (IOSRJEN)*, 2(7), 25-31.
- [3] Castaneda, D., Esparza, A., Ghamari, M., Soltanpur, C., & Nazeran, H. (2018). A review on wearable photoplethysmography sensors and their potential future applications in health care. *International journal of biosensors & bioelectronics*, 4(4), 195.
- [4] Kuzu, M., Taş, O., & Tulum, G. (2017). Uzaktan İzlenebilir Hasta Parametreleri Sistemi. 2. Ulusal Biyomedikal Cihaz Tasarımı ve Üretimi Sempozyumu, 16 Mayıs 2017.
- [5] Özgören, M., Şakar, M., & Öviz, A. (2010,). Contact/non-contact sensor mesh for body temperature monitoring. In 2010 15th National Biomedical Engineering Meeting (pp. 1-4). IEEE.
- [6] Chung, Y. T., Yeh, C. Y., Shu, Y. C., Chuang, K. T., Chen, C. C., Kao, H. Y., Ko, W. C., Chen, P. L., & Ko, N. Y. (2020). Continuous temperature monitoring by a wearable device for early detection of febrile events in the SARS-CoV-2 outbreak in Taiwan, 2020. *Journal of microbiology, immunology, and infection* 53(3), 503–504. <https://doi.org/10.1016/j.jmii.2020.04.005>

- [7] Holt, S. G., Yo, J. H., Karschimkus, C., Volpato, F., Christov, S., Smith, E. R., ... & Champion De Crespigny, P. (2020). Monitoring skin temperature at the wrist in hospitalised patients may assist in the detection of infection. *Internal Medicine Journal*.
- [8] Gülenç, N. G., & Kartal, M. (2020, November). Noninvasive Measurement of Baby's Vital Data and Mobile Monitoring-Analysis System Design. In *2020 Medical Technologies Congress (TIPTEKNO)* (pp. 1-4). IEEE.
- [9] Duman, Ü., & Aydın, E. (2020, September). IOT Based Baby Cradle System with Real Time Data Tracking. In *2020 5th International Conference on Computer Science and Engineering (UBMK)* (pp. 274-279). IEEE.
- [10] Fidan, U., & Güler, N. F. (2007). 4 Kanallı Biyotelemetri Cihazı Tasarımı. *Journal of the Faculty of Engineering & Architecture of Gazi University*, 22(1).
- [11] Eriş, Ö., Korkmaz, H., Toker, K., & Buldu, A. (2010). İnternet Üzerinden Hasta Takibi Amaçlı PIC Mikrodenetleyici Tabanlı Kablosuz Pals-Oksimetre Ölçme Sistemi Tasarımı ve LabVIEW Uygulaması. *TURKMIA*, 10, 16-25.
- [12] Wijaya, N. H., Fauzi, F. A., Helmy, E. T., Nguyen, P. T., & Atmoko, R. A. (2020). The Design of Heart Rate Detector and Body Temperature Measurement Device Using ATMega16. *Journal of Robotics and Control (JRC)*, 1(2), 40-43.
- [13] Gupta, S., Talwariya, A., & Singh, P. (2020). Development of Arduino-Based Compact Heart Pulse and Body Temperature Monitoring Embedded System for Better Performance. In *Performance Management of Integrated Systems and its Applications in Software Engineering* (pp. 189-197). Springer, Singapore.
- [14] Mert, A., Seçgin, Ö., & Akan, A. Sürekli Vucut Sıcaklığı Ölçümü İçin Biyotelemetri Cihaz Tasarımı Tıp Teknolojileri Ulusal Kongresi, TIPTEKNO'14 (pp.312-315). Nevşehir, Turkey
- [15] Kim, Y., Lee, S., & Lee, S. (2015). Coexistence of ZigBee-based WBAN and WiFi for health telemonitoring systems. *IEEE journal of biomedical and health informatics*, 20(1), 222-230.
- [16] Hasan, M. W. (2021). Covid-19 fever symptom detection based on IoT cloud. *International Journal of Electrical & Computer Engineering*, 11(2), 1823-1829.
- [17] Akleyek, S, Kılıç, E, Söylemez, B, Aruk, E, Aksaç, C. (2020). Nesnelerin İnterneti Tabanlı Sağlık İzleme Sistemleri Üzerine Bir Çalışma. *Mühendislik Bilimleri ve Tasarım Dergisi, Special Issue: International Conference on Artificial Intelligence and Applied Mathematics in Engineering (ICAIAME 2020)*, 80-89.
- [18] Karthi, P., Jayakumar, M. (2020). Smart Integrating Digital Contact Tracing with IoMT for COVID-19 using RFID and GPS. *Journal of Xi'an Shiyou University, Natural Science Edition*, 16(12), 38-43.
- [19] Costin, H., & Rotariu, C. (2018). Vital Signs Telemonitoring by Using Smart Body Area Networks, Mobile Devices and Advanced Signal Processing. In *Advances in Biomedical Informatics* (pp. 219-246). Springer, Cham.
- [20] Melexis MLX 90615 temperature sensor datasheet, <https://www.melexis.com/-/media/files/documents/datasheets/mlx90615-datasheet-melexis.pdf>, 30.11.2020.
- [21] PIC12LF1822 microcontroller datasheet, <http://ww1.microchip.com/downloads/en/devicedoc/40001413e.pdf>, 30.11. 2020.

Communication Network Simulation for Smart Metering Applications: A Review

Folasade Dahunsi ^{1*} , Sunday Olayanju ² , Akinlolu Ponnle ¹ , Oluwafemi Sarumi ¹ 

^{1*} *Department of Electrical and Electronics Engineering, Federal University of Technology Akure, Akure, Ondo State, Nigeria.*

² *Department of Electrical Engineering, University of Ilorin, Ilorin, Kwara, Nigeria.*

Abstract

Many countries are witnessing the deployment of millions of smart meters, as they strive to upgrade their traditional grid to the smart grid already prominent in the developed parts of the world. Communication networks that can offer high-speed communication will be required for transmission of the copious amount of data resulting from the numerous smart meters and other intelligent electronic devices (IEDs) in the distribution network substation. Therefore, there is a need to critically assess the available communication infrastructure for eventual upgrade and deployment. In this paper, a survey of the communication network and networks simulation software used for this purpose was carried out, with specific emphasis on smart metering applications. Some critical requirements identified are security, quality of service (QoS) and optimal cost for system operation. Also discussed are methods employed in the works of literature to handle the critical issues raised. For data transmission between the meters and data concentrators; power line communication (PLC) was mostly cost-effective and hence, mostly deployed. In the wireless category, ZigBee (802.15.4), Wi-Fi (802.11), and WiMAX (802.16) among others are suitable and have been successfully deployed. OPNET, NS-3, NS-2, and OMNET++ have been successfully employed for communication network simulations in smart metering applications.

Keywords: Communication Network, Simulation, Smart Meter, Data Transmission, Advanced Metering Infrastructure.

Cite this paper as:

Dahunsi, F., Olayanju, S., Ponnle, A., Sarumi, O. (2021). *Communication Network Simulation for Smart Metering Applications: A Review*. Journal of Innovative Science and Engineering. 5(2): 101-128

*Corresponding author: Folasade Dahunsi
E-mail: futa.edu.ng

Received Date: 04/12/2020
Accepted Date: 11/03/2021
© Copyright 2021 by
Bursa Technical University. Available
online at <http://jise.btu.edu.tr/>



The works published in Journal of Innovative Science and Engineering (JISE) are licensed under a Creative Commons Attribution-NonCommercial 4.0 International License.

1. Introduction

Electrical energy usage is not optimized when consumers are not aware of their consumption patterns and financial implications. With smart meters, via a home display, consumers see exactly when and how much electrical energy they are using. With advanced metering infrastructure (AMI), smart meters have the capability of performing and reporting continuous measurement of customer's energy consumption rate in real-time. It captures the voltage, current, phase angle, and frequency of the supply. Besides, it can communicate with the consumers and the utility provider, in a mutual relationship for energy management and optimization. The installation of smart meters in buildings is the foundation and bridge to the construction of smart grids. A smart grid can be described as an electrical grid that is characterized by smart energy measurements, smart operations and control by including smart meters, smart appliances, smart devices, renewable energy and energy-efficient resources. Smart meters allow the interconnection and operation of all entities that make up the smart grid. Hence, the functionality of the smart grid relies heavily on the accuracy and effectiveness of its meters [1]; [2]. Smart grid concepts could be verified experimentally or through simulations [3].

Smart metering is regarded as a major component of the smart grid whose functionality drives its performance, and as new communication and information systems and technologies emerge, selection of the best communication technology for successful application of smart meter becomes an issue of interest. New technology can enhance the reliability and availability of information from such meters. However, effective simulation of the performance of the selected technology before deployment is very important. Performance analysis of an electric network will be enhanced by the selection of the appropriate simulator for the analysis, and this will eventually guide the selection of adequate infrastructure for metering applications.

[1] discussed smart grid architecture highlighting issues that are related to obtaining higher performance. Focusing on smart metering applications and the requirement for effective communications, the survey explores the flexibility of operation, reliability, and cost-effectiveness. In [4], common techniques for simulation of smart grid communication was surveyed, with emphasis on the framework for co-simulation and their enabling technologies.

In [5], three types of simulators in a smart grid environment were considered: power system, communication network, and co-simulators for simultaneous simulations of both communication and power networks. The research work focused on distinct simulators following the intended use cases, extent and detail of the simulation model, and architecture. The work by [6] focuses on smart grids and the required communication systems applicable for smart grid operations. The key areas are infrastructure for smart grid operation, which include smart measurement and metering, technologies for smart grid communication, and security concerns as related to successful smart grid operation. However, the survey does not consider simulators applicable for analysing the performance of the communication networks. [7] presented a review of simulation tools in communication networks. In their work, ten commonly used network simulators were reviewed, the strength and weaknesses of the said simulators were highlighted. A classification and comparison which consider the type, as well as the deployment mode including

network defects and protocol supported, were also carried out, including the methods of simulation, techniques employed for evaluation and acceptability of simulation studies and outcomes. The review only considers general network simulators without any specific reference to smart metering applications. [3] carried out a survey of twenty-six smart grid co-simulators based on peculiarities such as simulators used, research themes, open-source availability and synchronisation mechanism for used simulators. In [8] a survey on basic principles of real-time as well as co-simulators for the improvement of electric power system protection, control and monitoring applications were presented. Several applications were also introduced for the same purpose. Besides, testing environments for smart grid predicated on real-time and co-simulators were presented.

Building on previous reviews, the interest of this work is in the review of the simulation of the communication networks for applications in smart metering. The aim is to survey and identify the communication networks for smart grids and the simulation tools that are employed in studying their performance with specific emphasis on smart metering applications.

1.1. Bibliometric Analysis

To provide an overview of the previous relevant work on communication network simulation for smart metering applications, a bibliometric analysis based on the IEEE Explore, Science Direct, Springer Link and ACM digital databases was carried out on 25th July 2020. The said analysis was carried out using the search syntax: (“Communication network simulation” OR “Communication network simulator” OR “Network simulation”) AND (“Smart metering applications” OR “smart meters” OR “Smart grid”). An initial result of 2093 journal articles was returned after the search of all the digital databases. An inclusion/exclusion criterion was set for the selection of the most relevant articles, and articles considered were between 2010 – 2020 with a focus on communication network simulation for smart metering applications in a smart grid network. Only 45 articles made the final list of articles eventually considered for the review in this paper. Figure 1 shows the percentage of journal articles selected in each of the digital repositories. As can be seen from Figure 1, IEEE Explore is a traditional digital repository for smart meters and smart grid-related paper. Others are Science Direct and Springer Link.

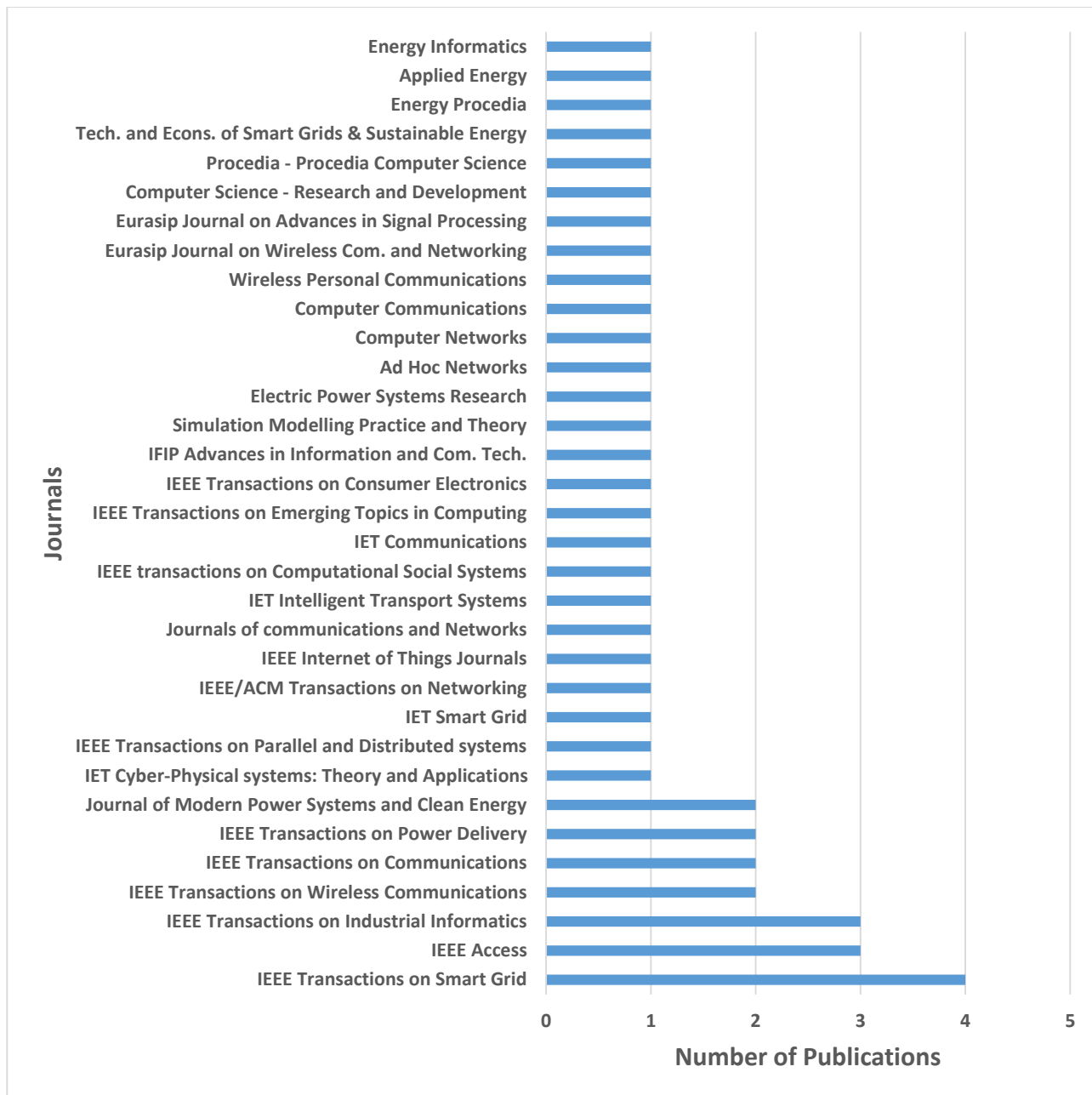


Figure 1. Percentage of journal articles selected per database.

12. Relevant Review Articles

Smart grid revolution is not possible without the advanced metering infrastructure (AMI). For AMI to be successfully implemented, a two-way communication scheme is a basic requirement. Several review works have been carried out to determine the veracity of the communication network. A comprehensive review of wireless communication technologies for smart grid applications was the focus of the review in [9]. The comparison of communication technologies for AMI applications including AMI network structures reviewed in [10] was based on privacy and security, cost of deployment, reliability and communication coverage, while the comparison of commonly deployed wired and wireless communication technologies in customer premises network was carried out in [11]. Adaptability to home area networks, protocol, coverage range and data rate were the elements of comparison. [12] reviewed energy policies for the implementation of smart metering infrastructures in Spain, Europe and the rest of the world. State of the art of communication technologies for smart grid applications was reviewed in [13]. A special focus was given to

telecommunication technologies for smart metering applications and monitoring. Key elements of a smart metering system as well as a compilation of mostly deployed technologies together with their main features were the objectives of the review by [14].

Varying uses of metering data in a smart grid following privacy policies were reviewed in [15]. While [16] conducted a review on data analytics in retail markets, load forecasting applications, intrusion detection, demand response management and segmentation of consumers were also considered in the review work. Tools applicable in smart grid research, simulators for power system and communication systems simulations were reviewed by [5]. Besides, classification and comparison of communication network simulators were carried out in [7]. The work intends to aid researchers in selecting appropriate tools that will give reliable conclusions while using simulations to evaluate performances of designs before realistic implementation.

This review seeks to provide a comprehensive report on communication networks used for smart metering applications in the AMI network, and common simulators employed for their evaluation in the literature. Specific attention is given to the critical issues raised in different kinds of literature published in the immediate past decade. The paper is arranged as follows: Section II introduces the concept of smart grid, its basic components and also give an overview of the communications networks available for smart metering applications; section III discusses major network simulation software packages. Critical issues of simulation of a communication network for smart metering applications are raised and discussed in section IV. The findings of the research are analysed and discussed in section V while the conclusion of the review is given in section VI.

2. Smart Grid Concept and Smart Metering

The traditional electric power grid, an enormous interconnection of infrastructure for conveying electricity from generating plants to points of consumption, does not have the capabilities of the smart grid. The smart grid (SG) incorporates advanced two-way communications and computing capabilities [15] [17].

To monitor, analyse, control and communicate with the energy delivery chain, the smart meter is required. It helps enhance efficiency, optimization of energy consumption, lower cost and increase transparency and dependability of the energy supply chain [18]. The application of advancement in digital technology to systems and devices has enabled the smart grid to achieve its current status.

The grid will become smarter as new technology emerges for applications and devices closely related to the smart grid. New devices and systems allow for advanced sensing and control of grid elements, extensive information sharing and communication, more powerful computing, and better control. Declining costs of digital technology is another driver of the advancement being witnessed. The trend in digital networks will eventually result in greater levels of information exchange between utilities and their customers. The emergence of other infrastructures such as smart buildings and cities, transportation, and telecommunications can only be on the increase as the smart grid develops [19]. Figure 2 shows various units connected to and controlled by the smart grid. Data from each of the units are shared via the communication network with the aid of smart meters.

2.1. Major Components of a Smart Grid

The smart grid major components include the advanced metering infrastructure (AMI), the communication infrastructure and the control unit.

Automated meter reading (AMR) is equipped with one-way communication systems. However, the modern smart grid is well furnished with advanced metering infrastructure (AMI), making it capable of effective monitoring, measurement and control of consumer power consumption in real-time. Electricity monitoring and control is enabled by AMI. It also promotes applications that include management of outages in the network, energy billing, pricing, detection of faults, forecasting and demand response, thereby encouraging consumer participation in energy optimization [20].

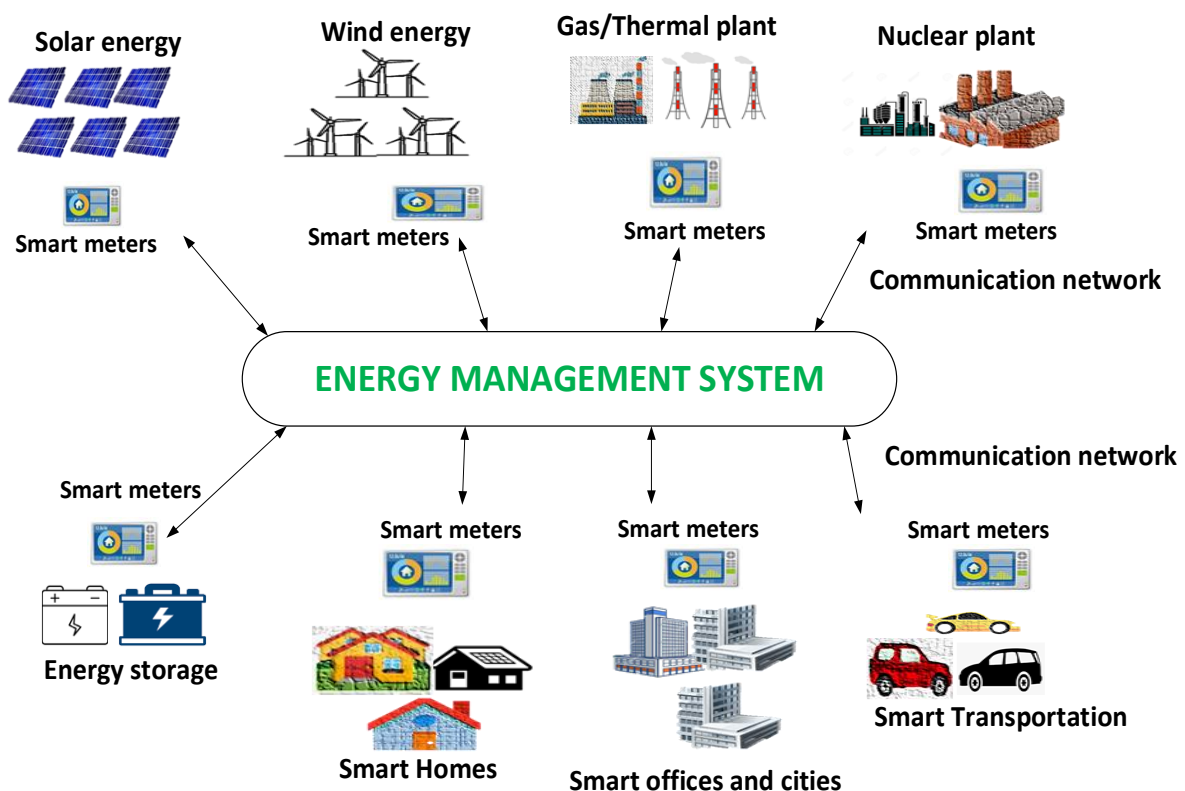


Figure 2. Concept of the Smart Grid applications

Smart grid communication infrastructure fundamentally has three networks frames: Home Area Network (HAN)/Building Area Network (BAN), Neighbourhood Area Network (NAN)/ Field Area Network (FAN), and Wide Area Network (WAN) [20, 25].

The performance of the three smart grid communication infrastructure is compared in Table 1 based on their data rate, coverage area, the technology used, and application domain. All smart grid components and communication infrastructure, including renewable energy sources, transmission, distribution, control, and monitoring it is built on WAN.

Table 1. Comparison of the smart grid communication infrastructure [20, 25, 1]

	Data Rate	Coverage Range	Implementation Technologies	Typical Applications
HAN	1 – 100kbps	1-100m	ZigBee, Wi-Fi, Bluetooth, PLC, Ethernet.	Home automation, building automation
NAN	100kbps 10Mbps	– 100m – 10km	ZigBee mesh networks, Wi-Fi mesh networks, PLC, WiMAX, Cellular, Digital Subscriber Line, and Coaxial Cable	Smart metering, demand response and distribution automation
WAN	10Mbps 1Gbps	– 10 – 100km	Optical Fibre, Cellular, WiMAX and Satellite communications	Wide-area control, monitoring and protection.

The harmonious interaction of the different components of the SG is made achievable by the control centre. The smart grid control centre or data management system (DMS) handles the collection and saving of the metering information data for the eventual purpose of processing and analysis. Besides, the control centre handles the consumer applications, system for weather forecasting, load management, control and geographic information systems applications. With the availability of information technology infrastructure and intelligent electronic devices (IEDs), smart grid control has evolved to a more sophisticated system capable of taking instructions, make decisions and managing the whole system while in operation [21].

Measurement data generated in the smart grid network while in operation is invaluable to energy companies. With such data, it is possible to make a myriad of predictions such as availability of energy, the likelihood of power failures, and forecasts of customers' behaviour or pattern of consumption with the aid of predictive analysis. This empowers energy companies to take dynamic actions instead of responding to events late and when only corrective actions can be taken after the damage has been done.

The smart meter is the core device of advanced metering infrastructure (AMI) [22, [22]. Its functions include observation of home appliances status and usage of power, collection of power usage information, and transmitting the same through the communication network to the management system, and in-home energy display [23]. It supports the tariff system based on time, this includes peak and off-peak pricing, operation-time, and pricing system in real-time [24, 9]. Besides, additional capabilities concerning the infrastructure such as anticipation and control of the load, and observation and monitoring of the quality of power can be provided.

2.2 Overview of Communication Technology for Smart Metering Applications

These are the wireless and wireline communication technologies for smart metering applications and they have varying coverage areas, bandwidth and energy consumption constraint. Table 2 summarises the available communication network commonly deployed for smart metering applications.

a. Cellular Technologies: GSM/GPRS/3G-4G/LTE

Taking the coverage area into consideration, the cellular network is among the most appropriate technologies for smart metering applications when the link for communication spans between the data aggregator and the energy company's server. Operating at 900 and 1800 MHz bands, the global system for mobile communications (GSM) and general packet radio service (GPRS) are good examples of a cellular network with existing network infrastructures, making them attractive to utilities for smart metering applications [23]. Network operators now provide SIM cards meant to be used

with data modem devices of GSM, they came with provisions for data only services and offering tariff packages meant for such usage [24];[25].

Table 2. Summary of some common communication technology in smart metering applications.

Technology		Data Rate	Frequency Bands	Range
Wireless				
Cellular	3G-4G	60–240 kbps	824–894 MHz, 1900 MHz	about 50 km
	GSM	≥ 14.4 kbps.	900–1800 MHz	1–10 km
	GPRS	≥ 170 kbps.	900–1800 MHz	1–10 km
IEEE 802.15 Group	ZigBee	20-250 kbps	868 MHz/915 MHz/2.4 GHz	10-1000m
	6LoWPAN			
IEEE 802.11 Group	Bluetooth	721 kbps	2.4–2.4835 GHz	1-100m
	Wi-Fi	≥ 54 Mbps.	2.4 GHz/5.8GHz	1-100m
	Enhanced Wi-Fi	≥ 54 Mbps.	2.4 GHz	1-100m
IEEE 802.16	IEEE 802.11 n	≥ 600 Mbps.	2.4 GHz	1-100m
Satellite	WiMAX	70 Mbps	1.8–3.65 GHz	50 km
	Satellite Internet	1 Mbps	1-40 GHz	100–6000 km
Wired				
NB-PLC	PRIME G3-PLC	up to 500 kbps	3–500 kHz	Several km
BB-PLC	HD-PLC	Up to several hundred Mbps	1.8–250 MHz	Several km
DSL	ADSL	800 kbps Upstream and 8Mbps Downstream	25 kHz-1 MHz	5 km
	HDSL	2 Mbps		3.6 km
	VHDSL	15-100 Mbps		1.5 km

2.2.1. Wireless Technologies

b. IEEE 802.15 Group

i. ZigBee

The media access control (MAC) layer and the physical (PHY) layer of ZigBee a wireless technology is established on the IEEE 802.15.4 standard. Operating in the 2.4 GHz band and spanning between 10 and 100m is preferred in smart metering applications for information handling encompassing the smart meter and the data aggregator units, instead of handling information sharing in the link between the data aggregator and the utility server [22]. ZigBee is suitable for wireless control and monitoring. It performed excellently when the requirement of the application for optimum operations are low data rates and low power utilisation [26];[25].

In [27], a smart meter interfaced with ZigBee was designed and applied for Wireless Sensor Home Area Network. [28] analyses the effectiveness of ZigBee considering throughput, a ratio of packet delivery, delay average, and average energy used in different three-dimensional environments of a smart grid. The simulation results based on QualNet, reveals that IEEE 802.15.4 built on ZigBee is most appropriate for applications in a smart grid that require low reliability.

ii. 6LoWPAN

The IPv6 over Low power Wireless Personal Area Networks (6LoWPAN) technology was designed to define mechanisms for header compression for sending packets of IPv6 to and from, networks based on IEEE 802.15. The basic concept of the internet of things (IoT) could be realised by 6LoWPAN since all devices, including sensors and actuators, can be assigned with an IP address. In [29], a NAN architecture built on 6LoWPAN for the operation of all the smart

electric meters in the coverage area of NAN was designed. The system is to sustain the requirements for Quality of Service (QoS) of the various applications in the NANs coverage area.

An analysis of the effectiveness of a radio mesh network built on 6LoWPAN was carried out using the OPNET network modelling package for simulation. The potential of merging sensory devices of the modern smart meter with application logic using a technology built on 6LoWPAN over an event-driven Internet infrastructure was investigated in [30]. An experimental setup was used to monitor power quality, and initial results indicate that the smart metering infrastructure if combined with appropriate ICT tools, is capable of offering ingenious enhanced services. A cluster-tree based 6LoWPAN network for the NAN applications was investigated in [31]. To increase the throughput and reduce the latency of packet in the NAN, a simulation model built in OPNET was developed to analyse the effectiveness of demand management and data communications of a smart meter in a NAN. Results from the simulations carried out revealed that the performance of a NAN can be notably improved by using the staggered link design approach combined with a technique of aggregation of packet employed in the research.

iii. Bluetooth

Bluetooth is a wireless communication technology that was built on the IEEE 802.15.1 standard. It is an open wireless protocol designed to provide personal area networks (PANs). Bluetooth low energy (BLE) is an advancement in Bluetooth technology. The technology is capable of exchanging data within short distances from either fixed or mobile devices. Originally, the idea was to create an alternative wireless data link against the wireline data cables [32]. Even though Bluetooth technology has a low power consumption capability, its deployment in smart metering applications is very limited because of the short coverage area. [33].

c. IEEE 802.11 Group (Wi-Fi/Enhanced Wi-Fi/ IEEE.802.11n)

The wireless standards allow devices on the network to communicate with each other wirelessly. There are different standards of wireless technology, 802.11a which supports a bandwidth of up to 54 Mbps and signals in a regulated frequency spectrum of 2.4 GHz and 5 GHz. The 802.11b supports a maximum bandwidth of 11Mbps and signals in the unregulated frequency of 2.4 GHz. The 802.11g combines the good attributes of 802.11a and 802.11b, which supports the bandwidth up to 54 Mbps and a frequency of 2.4 GHz. The 802.11n is the newest of all and is designed to support multiple wireless signals and antennas. It supports a maximum of 100 Mbps of data rate.

d. IEEE 802.16 (WiMAX)

The Worldwide Inter-operability for Microwave Access (WiMAX) was built on IEEE 802.16 standard. It is broadband access wireless technology. It can support a speed of up to 70 Mbit/s bi-directional for transmission and capable of either a network topology that is point-to-point or point-to-multi-point [34]; [35]. WiMAX is suitable for joining the back-haul energy company system with data aggregators in a smart grid network. It is regarded many times as an alternative to cellular technologies such as GSM and CDMA. A possible drawback of this technology is that its bandwidth has to be shared among other users.

[34] presented a work that analyses the performance of a smart grid with the communication layer built on WiMAX technology. OPNET simulation software package was used to simulate the application traffic. The MAC and PHY layers of the WiMAX standard form the basis on which a wireless network architecture presented by [36] was built. The design

was meant to serve smart grid divers metering applications and the smart meters connected to the network. The analysis of the size of the cell, models of terrain, the capacity of the channel, packet delay and losses, and transmission power were carried out with the aid of OPNET simulation models. Simulation results of their research support the applicability of WiMAX for smart metering applications.

e. Long-range (LoRa)/Long Range Wide Area Network (LoRaWAN)

Long Range (LoRa) is the physical layer that generates the long-range communication link while Long Range Wide Area Network (LoRaWAN) is the communication protocol and system architecture for the network. LoRa operates on the unlicensed radio frequency bands, it enables long-range transmissions with low power consumption [37]. The application of LoRa and LoRaWAN as a wireless communication standard for smart devices is seeing consistent growth in the last few years. Attributes such as long-range, low power and low cost are the main reasons why this technology is becoming more important. LoRa has found applications in smart metering devices that require low data rates and long-range communication [38]. [39] successfully use LoRa technology for transmission of data from smart meters to utility servers. In Slabicki *et al.*, (2018), OMNeT++ was used for LoRa simulation to study the adaptive configuration of LoRa when deployed in handling dense internet of things (IoT). To improve system security, an improved session key management was employed by [41] to secure the meter reading system based on LoRa technology. In similar research, [42] used a symmetric cryptography method for the protection of end-to-end communication established between the substation automation system and smart meters based on LoRa technology. The evaluation of the method used shows the possibility of practical implementation in real-world scenarios.

2.2.2 Wireline Technologies

a. NB-PLC

The transmission of data is done through a narrow band of frequency and at a low bit rate in Narrowband PLC (NB-PLC) technology. Technologies built on NB-PLC were designed for smart grid applications and automation in buildings and homes. For instance, in an earlier work conducted by [43], OMNET++ was used to implement a G3-PLC cross-platform simulator. In [44], PLC links were employed to evaluate the time of transmission between smart meters and local aggregators for different sizes of data. OPNET simulator was used in the assessment of infrastructure for smart metering applications built on PLC. The study engages several smart meters. By varying the size of smart meters and concentrators connected to the PLC medium, bandwidth limitations were investigated. To confirm data delivery by meters to the concentrators, a successful transmission rate within a specified time was also evaluated.

b. BB-PLC

Operating at a frequency band between 2 and 30 MHz and up to hundreds of Mbps data rates, Broadband PLC (BB-PLC) was introduced to be able to provide applications for internet access. The initial concept was to apply BB-PLC for the network applications around the home and also for last-mile communication. Like the NB-PLC, procurement of new infrastructure is not needed. BB-PLC has been deployed in smart homes, but, extensive use in the smart metering application is yet to be seen.

c. Digital Subscriber Line (DSL)

The DSL operates at a frequency range of 25 kHz– to 1 MHz and covers a range between 1.5 km - 5 km. It utilises the old phone lines for the transmission of data and has been used to offer smart metering applications. It is capable of providing a backhaul for the transmission of smart grid data from residential buildings to energy companies. DSL infrastructure already exists, making it a low-cost solution. A drawback of this technology lies in the fact that subscriber distance from utilities is proportional to its throughput.

2.3. Data Quality Challenges in Smart Meters

The energy data obtained from smart meters is used for analysis such as billing. Thus, for operational effectiveness, the quality of such data must be maintained. Data quality directly affects the operation and readiness of an electric power supply. The security, quality, and reliability of the electric power system lean heavily on the integrity of its data. As a result, data quality has been considered a prominent issue in the smart grid[45]. Data derivable from the smart grid are mainly categorized into three: measurement data, business data, and external data. Measurement data are data from smart meters whereas data from the consumers of electricity are business data. An example of external data is weather data [46].

Indices of low-quality data were reported in a study conducted by [47]: Data is regarded as missing data of low quality when data recording is missing for some time. The missing data could have serious effects on research outputs because relying on such incomplete data will eventually lead to a wrong conclusion. Another factor is the zero record periods; a situation where data is available but recorded as zeros [46]. To understand a record of this kind becomes very difficult, for one wonders whether the said records were altogether missing, sent, or were not recorded in the first place.

When values that are taken over a particular range of time are outrageously large or low as compared to the mean value of data recorded, they are termed out-of-range.

Error from measurement may be a result of a failure in communication, outages of equipment, data loss, and interruptions in power source among others. Other indices include unreliable data points which could come via premeditated cyber-attacks on the smart grid infrastructure. Attacks of this nature could involve false data injection via fake data-points. Unreliable data-points could result in the manipulation of the overall operations of the smart grid leading to operation failure. Also, when data that are time-stamped arrive out of the expected time, the quality of the data may be compromised. Delay experienced by the data could be a result of the communication network deployed for data transmission.

3. Simulation of the Communication Infrastructure

In the past and recent years, several simulation software was developed and utilised to assess the performance of the communication network infrastructures of smart metering systems. It is, therefore, necessary to take a deep look at some of the simulation tools in this regard. In communication network simulations, researchers seek to improve system performance (such as delays and throughput), reduce expenditures, and increase confidence that performance objectives are realised before the purchase or lease of equipment. Bottleneck recognition and pinpoint before the implementation of the system and reduction in development time for the system are further reasons why communication network simulation is embarked upon [48].

3.1. Simulation Software

An overview of the most common network simulators used for modelling the communication infrastructure for automated metering infrastructure is presented.

3.1.1. Network Simulator 2 (NS-2) and Network Simulator 3 (NS-3)

Network Simulator version 2 (NS-2) is an object-oriented discrete-event simulator. It has gained wide acceptance and uses among researchers today. It was developed in 1995 at Lawrence Berkeley Laboratory, University of California, Berkeley. It gives support for TCP simulation, routing, and multicast protocols over wireline and wireless networks. C++ is the programming language and for interface configuration and command OTcl was used. It is suitable for both distributed and parallel simulations. NS-2, though an open-source software, does not support the vivid graphical presentation of simulation output data.

Network Simulator version 3 (NS-3) is also an open-sourced discrete-event network simulator. Started in 2006 and written in C++, the simulator is fashioned as a library and capable of either statistical or dynamical link with a C++ programme. The commencement of simulation and its topology is defined by these libraries. Users of the simulation software package can setup simulations of communication networks. Analysis and simulations of traffic models, generators, TCP/IP protocols and the likes, channels such as Wi-Fi, and devices can be carried out with a simulator.

3.1.2. Optimized Network Engineering Tool (OPNET)

OPNET was developed at the Massachusetts Institute of Technology (MIT), as commercial software that gives a development environment that is comprehensive for aiding modelling of distributed systems and data communication networks. Simulation scenarios such as change of parameter after an elapsed time set, and update of topology, are often implemented by writing C or C++ code. With an easily understandable model library, a modular development, extensive modelling detail, an interactive GUI, and adaptable simulations results from the exhibition, OPNET stands out as advantageous over many other simulators. However, OPNET parameter categorization is not very transparent and the software package is very expensive. A simulation of 6LoWPAN based radio mesh network was designed to supply smart meters in a NAN network [29].

3.1.3. Objective Modular Network Testbed in C++ (OMNET++)

OMNET++ is a component-based, modular, and open-architecture discrete event simulator framework most commonly employed for the simulation of computer networks. More so, it has found applications in queuing network simulations among others [49]. Written in C++, the class library of OMNET++ has a simulation kernel, and for random generation of numbers, collection of statistics, and discovery of topology it uses the utility classes. There are two types of OMNET++ modules: the simple and compound modules. The algorithm definition is done through simple modules. They are active components of the simulator in which the occurrence of events takes place and the manners of the model, creation of events and response on events is defined. To form a compound module, a group of simple modules which are interacting together is required. The power of OMNET++ includes its GUI, object examiners that allow for zooming into the component level and the ability to display the state of each component during the simulation. Its modular architecture and abstraction, configurability, and comprehensive modules implementation and protocols are added

advantages of the simulator under discussion. However, OMNET++ could be a bit slow due to its long simulation run and high memory consumption.

3.2. Comparative Analysis of Network Simulation Software Packages

Presented in Table 3 are the network simulators that are commonly used in designing AMIs. The comparison is based on their availability, the network protocol supported and the operating system supported among others.

Table 3. General comparison of simulation software packages for network simulation

Simulator	Availability	Language	Network protocol supported	Current Version	Date of release	Operating System
NS-2	Open-source	C++ and Python	TCP/IP, Multicast routing, TCP protocols over wired and wireless networks.	ns-2.35	Nov. 4 2011.	Linux, FreeBSD, macOS
NS-3	Open-source	C++	TCP/IP, Multicast routing, TCP protocols over wired and wireless networks.	Ns-3.30	Aug. 21 2019	Linux, FreeBSD, macOS
OPNET	Commercial	C and C++	ATM, TCP, Fibre distributed data interface (FDDI), IP, Ethernet, Frame Relay, 802.11, and support for wireless	Version 18.8.0	Feb. 4 2019	Linux and Windows
OMNeT++	Open-source	C++	Wireless networks	version 5.5.1	Jun. 13 2019	Linux, macOS, Windows

4. Critical Issues of Communication Network Simulation for Smart Metering Applications in Literature

In this section, a breakdown of major issues raised in the 45 journal articles from the IEEE Explore, Science Direct, Springer Link and ACM digital databases is presented. Three major issues were addressed by different authors using different methods. The major issues discussed in the reviewed papers are on: security of smart meters and the corresponding communication networks, quality of service obtainable from the operation of the smart grid and, optimal cost achievement in the smart grid operation.

4.1. Security of Smart Meters and Communication Network

Generally, attacks on AMI seek to compromise the confidentiality, integrity and availability of power and associated data [20]. If the right steps are not taken, the malicious attacks could result in power theft, loss of privacy and denial or disruption of power supply. Presented in Table 4 are some pieces of literature with a specific focus on the security of smart meters and the communication networks that provide metering applications. To effectively operate the smart grid, the issue of security of the entire network take a front stage in designers' considerations. A cyberattack could be mitigated with the careful design of the communication network supporting the grid. Methods highlighted in Table 4 have been successfully employed by the authors in the works referenced. The issues to tackle and the corresponding constraints are presented in the first and second column respectively, also presented are the communication networks employed as well as the simulation tools used.

4.1.1. Intrusion Detection System (IDS)

Unauthorised access to a network, data or information is regarded as an intrusion. Such attacks could render legitimate users stranded and make the system unresponsive to them. Therefore, an IDS seeks to identify and single out such an attack for stoppage and prevention of loss it could cause for the entire system for both the utility and consumers alike. For effective intrusion detection in the reviewed papers, [50] used two stages; an algorithm based on support vector machine (SVM) was used to detect intrusion in smart meters, while in the second stage, attack route generation was handled with temporal failure propagation graph (TFPG). The pattern recognition algorithm proposed, is employed to determine the similarity index between predefined cyber-attack and unexpected events. The high similarity index is an indication that a smart meter is being attacked. NS-3 simulation results reveal that the test scenarios were properly recognised by the intrusion detection unit. Meter data tampering algorithm was used for energy theft detection and mitigation in [51]. In [52] distributed Hash Trees (DHTs) was used to reduce the space requirement of a certificate revocation list (CRL) in smart meter operation while in [53] a scheme to ensure meter data privacy was employed considering smart meters, electricity utilities and trustful anchors. In [54] analysis of energy theft via cyber-attack is first carried out then, a detection method based on partially observable Markov decision process and Bollinger bands were used. To enhance the detection accuracy, a belief state reduction based adaptive dynamic programming, which is a probabilistic approach was employed. Simulations were carried out using the MATLAB software package.

4.1.2. Data and Information Protection

Protecting information and meter data during collection, while in transit or when stored is a significant step that is not taken lightly in the implementation of the smart grid. Smart meter data and the information they carried are used for control, monitoring and billing purposes. Attackers who are intent in deriving undue advantages from such resources seek to tamper with them. In pieces of literature, many authors have given methods to ensure the anonymity of consumers and protect information related to electric power systems. In [55] electric vehicle to grid (EV2G) communication was enabled using smart meters. The idea of distributed CRL management was introduced to achieve EV2G secure exchange of communication. Attack simulations have been conducted on a realistic electrical grid topology in [56]. The simulated network consisted of smart meters, a power plant and a utility server. In [57] differential privacy was applied to real smart metering consumption data. [58] presented a Protocol that decentralizes the certificate of authority (using split certification key and distribution key) and Hop-by-hop authentication was used to prevent a single point failure and minimise denial of service problem respectively. The method was able to transmit metering data safely and remotely using PLC. In [59] Laplace Distribution base time perturbation was employed in transmitting data from smart meters to utility servers and also to ensure protection while in storage. According to the work carried out by [60], a cluster of smart meters with a likelihood of sharing information within the AMI network is formed to impede delay, conserve bandwidth and storage. Therefore, the certificate revocation list will be local to the group. Two grouping algorithms: one based on routes between smart meters and the gateway using a bottom-up approach assuming the use of the shortest path and the other, considering the minimum spanning tree of the network uses a top-down approach for the grouping. The approach was implemented using NS-3 simulation software that runs a version of IEEE802.11s. The results established that the method achieves stability, comparing the size of the certificate revocation list and the size of signatures generated by certification authorities while ensuring the privacy of the communication network.

Table 4. Summary of the pieces of literature on the security of smart meters and Communication network

Critical Issues Considered	Constraint	Communication Technology	Simulation Tool/Method	References
Intrusion Detection for Cybersecurity of Smart Meters	Reduced vulnerability under malicious attack	IEEE 802.15.4	NS-3	[50]
Detection of energy theft cyber-attack	Reduced vulnerability under malicious attack	ZigBee, Bluetooth, WiMAX and LTE.	MATLAB	[54]
Remote meter reading security requirements	Preventing certification key exposure	PLC	-	[58]
Security of communications between smart meters	Reduction in delay, bandwidth and storage conservation	IEEE 802.11s	NS-3	[60]
Maintaining the privacy of the user	Allowing state estimation access	IEEE 802.11s wireless mesh standard	NS-3	[61]
Simultaneous detection of meter manipulation and bypassing	Time-efficient and detection accuracy	PLC and Wi-Fi are applicable		[62]
Security of smart meter data for Electric Vehicle (EV) Charging	Secure and efficient EV communications	IEEE 802.11s, IEEE 802.11p and LTE	NS-3	[55]
Security against distributed denial of service (DDoS)	Large-scale DDoS	wireless network	NeSSi ²	[56]
Differential privacy on real smart metering data	Large dataset required		MATLAB	[57]
Meter data security	CRL distribution and storage effectiveness	IEEE 802.11s	NS-3	[52]
Meter data privacy	Consumer data protection	IEEE802.11ah	NS-3	[53]

[61] employed vectors for obscurity which are separated among multiple gateways to reduce vulnerability. A partial vector for obfuscation is sent from each gateway handling sets of smart meters to other gateways. If the obfuscation vector for a gateway is compromised, the attacker can only have access to that section of the grid and the damage will be limited. Advanced encryption standard (AES) was employed for hiding while elliptic curve cryptography (ECC) gave authentication to the obfuscation values dispatched within the AMI network. The implementation of the proposed approach was carried out in NS-3. Simulation results revealed overheads on both meters and communication network is insignificant. Intermediate monitor meter (IMM)-based power distribution was analysed in [62]. The NAN was broken into the smallest unit networks forming segments, to detect non-technical loss (NTL). The intermediate monitor meter power distribution network model was used. A timely and 95% detection accuracy was achieved via simulations.

4.2 Operational Cost and Energy Usage Optimization

Huge data transmission is involved in an effective smart grid. Efficient collection and communication of data in a smart grid for monitoring, control and billing purposes could place the financial burden on both the utilities and the consumers. However, careful design of the network can reduce this challenge. Table 5 illustrates critical issues to address, communication networks that have been deployed and methods that have been simulated to achieve cost-effective operation of the smart grid.

A routing mechanism that embraces minimization of energy consumption and elongation of the lifetime of the network is appropriate to cut both the deployment and operational cost of smart meters in the AMI network. Reviewed research papers with a specific interest in the said area are presented in this section. A routing mechanism that is both energy and congestion aware for smart meters network was proposed by [63]. The technique, an adaptive selection of parent nodes that take into considerations the remaining energy of surrounding nodes and queue utilization was utilized. Cooja simulation software 3.0 was used to evaluate the scheme proposed and the results indicate reduced average power consumption and an improved packet delivery ratio. Cost minimization for meter data collection (CMM) problem was formulated by [64] to resolve the issues of channel selection and scheduling. Two power pricing model were employed: linear pricing (a mixed-integer linear programming problem) and nonlinear pricing (a nonconvex mixed-integer nonlinear programming problem) models and three-layer network model: home area network, neighbourhood area network and wide area network were also employed. In [65] an optimization framework to determine the extent needed for data aggregation was designed for a multi-level data concentrator unit topology. Then, an algorithm for managing the volume of AMI data traffic was proposed which doubles in ensuring QoS in a situation of congestion. NS-3 simulator was used for evaluating different network congestion for different scenarios of data traffic. The results showed that the approach can handle latencies during congestion in AMI networks.

In [19] data traffic in the AMI are grouped as either random or scheduled, a soft MAC protocol (SMAC) has an alternate operational mode given the type of data to be collected. SDMAC is used to collect scheduled data while OTRA-THS is employed for random data collection. The changes in mode translate to a reduction in latency due to data collection and control overheads. As a result of the said reduction, more meters can be served by a base station. This reduces the number of base stations required for data transmission and hence the required bandwidth. The overall capital and operational cost will be reduced. The proposed approach was simulated and analysed using a Markov chain. The result demonstrated the capability to reduce both capital and operational expenditure.

The communication connection that can experience failure in a broken network, communication topologies and questions related to access networks were first examined in [66]. Then, the proposed solution was evaluated and optimised to maintain a robust and reliable communication architecture while still minimising the deployment cost of the communication network. Simulation results show that the reliability of a single communication falls with the number of redundancies. [67] and [68] treated household separately and a forecast for 24 hours was done using SVM and neural network-based methods. The reasonable forecast was achieved through the technique applied. Also, the demands of consumers with and without smart meters were handled using a hybrid demand modelling technique in [69].

4.3. Quality of Service (QoS)

The efficiency and continued reliability of the smart grid rest so much with the quality of service integrated into its communication infrastructures, automated control, metering technologies and energy management techniques. Various issues critical to achieving QoS of the grid are highlighted in Tables 6 and 7. Issues ranging from mitigating impulsive noise, handling congestion and traffic in the network data collection and improving packet delivery ratio.

Table 5. Summary of works of literature on specific cost-driven constraint

Critical Issues Considered	Constraint	Communication Technology	Simulation Tool/Method	References
Energy usage minimization and prolong a network lifetime	Low energy usage and low processing power	IEEE 802.15.4g, IEEE 802.15.4e, and IEEE 802.11 standards	Cooja simulation software 3.0	[63]
Meter data collection	The optimal overall cost for both power and communication	Secondary spectrum in cellular networks	-	[64]
Data congestion and traffic.	Zero investment in infrastructures	PLC and low power wireless network are applicable	NS-3 simulator	[65]
Latency reduction and control overhead in smart meter data collection	Reduction in the capital and operational expenditure.	3G Cellular	Markov chain	[19]
Reliability and resilience of the access network in AMI	Minimization of communication deployment cost	A mesh-based NAN	-	[66]

4.3.1. Network Reliability

For AMI, low bandwidth and high latency is a requirement for smooth operation. The- different aspect reliability encompasses to meet the need of unfettered AMI operations includes the provision of redundant communication paths, approximated latency of the network, message loss probability and jitters. In the reviewed papers, several methods have been employed to ensure network reliability which includes:

Reinforcement learning algorithms were applied in [70] to mitigate the latency of AMI communications in Low power wide area networks (LPWANs). The analysis of the effects of a collision on different frequency access schemes was carried out. A new communication framework called Adaptive Forwarding Area Routing (AFAR) was proposed by [71] for smart grid communication. The said communication framework mitigate delay in smart meter communication in the smart grid. To minimise the network traffic associated with proactive and reactive, on-demand protocols was used in [72], the proposed application layer approach was employed. Two smart polling algorithms proposed are the routing protocol for low-power and lossy networks (RPLL) and the lightweight on-demand Ad hoc distance-vector routing (LOADng). Upon a polling request from the data concentrator, a query for search path is broadcasted to the whole network to identify a feasible route which is delivered using relay nodes to the specific smart meter via the MAC. Smart meter response is similarly transmitted to the data concentration unit in the uplink direction. Simulations were carried out using OMNET++. To enable AMI communications, a two-level frequency hop (FH) sequence set was proposed in the network design by [73]. For data traffic, the proposed two-level sequence set used a general Poisson model, in terms of error probability of FH based AMI communication network, average bit rate was used to determine the QoS metrics. Results show the method can give QoS to power consumers [74]. Based on the interference limitations, smart meters' best configuration was calculated for each smart meter in the network by spectrum engineering advanced Monte Carlo analysis tool (SEAMCAT), a software tool formed on the Monte-Carlos simulation method. The proposed scheme uses the TV band spectrum. The simulation results indicate that smart meters and digital television can simultaneously operate without negative effects on other wireless networks.

Attenuation, delay spread, and coherence bandwidth were taken into consideration while analysing the channel response [75]. To achieve monitoring, a support vector machine was used in research conducted by [76] to segregate power disturbance from regular values. In a pilot project carried out in Spain, current communication technology suitability for

AMI applications was evaluated by [77]. [78] used smart meter information and outage area identification technique to determine the impact of communication performance of AMI on outage management. Application of smart meters data was used by [79] for distribution network observation and monitoring. A new simulation framework was proposed for achieving a detailed large-scale RF-mesh AMI system in [80].

4.3.2 Impulsive Noise Mitigation

Voltage variation and spike, short-duration irregular pulses and intermittent occurrence of energy spikes all describe impulsive noise which greatly degrades signal quality and could reduce significantly the QoS of a system. Mitigating impulsive noise has seen much attention from several authors, and the methods used in the papers reviewed are presented here.

[81] proposed a Polling procedure for AMR and used neighbour relay polling and clustered polling in their research. Simulation results reveal that using smaller packets before the transmission will reduce significantly the effects of impulsive noise in the AMR system. The technique of blanking/clipping for impulsive noise mitigation in a narrowband OFDM PLC system was used in [82]. The impulsive noise was simulated using Middleton's class A model. The PLC bit error rate (BER) performance was simulated in MATLAB. The results show that the BER of the communication network was slightly improved with the method used. Noises and signal attenuations were modelled using MATLAB software package while Network topology and related processes were modelled using OMNET++ by [83]. The output of the MATLAB simulations was applied as the input for the network model. The communication layer stack was completed using the device language message specification (DLMS). Simulation results show that the required time to reading the meters increase notably in the presence of impulsive noise.

Table 6. Summary of literature on QoS of network reliability and Impulsive noise mitigation

Critical Issues Considered	Constraint	Communication Technology	Simulation Tool/Method	References
Acquisition of data and automatic meter reading	Minimization of Network traffic	PLC	OMNET++	[72]
Network security and Quality of services (QoS)	Malicious attacks on the network	ZigBee, Bluetooth, WiMAX and LTE.	-	[73]
Optimization of data transmission	Minimization of interference to the digital television system and SMs	TV white space	Spectrum Engineering Advanced Monte Carlo Analysis Tool (SEAMCAT)	[74]
Data collection delay and throughput	Impulsive noise interference mitigation	PLC	-	[81]
Feasibility of using PLC infrastructure for data communication	Impulsive noise interference mitigation	PLC	Middleton's class A model and MATLAB	[82]
Data communication	Impulsive noise, channel attenuation and multi-path effects	PLC_PRIME	OMNET++ and MATLAB	[83]
Reduction of latency in AMI communication	LoRaWAN AMI backhaul	LoRaWAN	MATLAB	[70]
Performance of NB-PLC for metering communications	Consideration for channel noise	NB-PLC		[75]

In [84] time taken to read the meters; the number of registered nodes were defined as performance key indicators for the performance of the communication network. MATLAB was used to implement the physical layer and the mode of communication while OMNET++ event simulation software was employed for the simulation of the upper layer with its logical effects. The results show that the process of registration impact performance.

4.3.3. Data Collection Technique

Smart meters in AMI can achieve two-way communication of data and power system sensitive information for system control and billing processes. A few methods employed for data collection between the consumers who usually houses the smart meters and the utilities which provide the electric energy are explored in this review paper. Table 7 gives a summary of some of the methods used. [85] proposed a data collection mechanism for wireless automatic meters reading (WAMR) based on IEEE 802.11p and using public transportation buses enabled with wireless communication capability. The smart meters transmit data to the bus stop while the data were transmitted to the passing bus for onward transmission to the server of the utility. Ad-hoc on-demand distance vector (AODV) and Dynamic Source Routing (DSR) protocols were simulated using an NS-2 simulator to obtain an end-to-end delay and the ratio of delivery. Results of simulations indicate a better delivery ratio and an end-to-end delay while using DSR. In the model presented by [86] concentrators were allowed to determine communication links. A stochastic reinforcement learning algorithm was designed for the alternative probabilistic route. This is to avoid possible information interchange among meters. The approach maintains QoS under internal faults and external attack as shown by simulation results. A genetic algorithm is used to perform the optimization process when transmitting data between smart meters and data concentrator units.

Table 7. Summary of literature on QoS of data collection methods

Critical Issues Considered	Constraint	Communication Technology	Simulation Tool/Method	References
Data collection from smart meters using vehicular ad hoc networks	End to end delay reduction and high delivery ratio.	IEEE 802.11p	NS-2 Simulator	[85]
Resilient and Reliable meter data collection	Strict data transmission latency	ZigBee, Bluetooth, WiMAX and LTE.	-	[86]
Scalability and Replicability performance of PLC-PRIME	Integration of both physical and upper layer	PLC	OMNET++ and MATLAB	[84]
Outage Management system	Smart meter information-dependent	NB-PLC and BB-PLC	-	[78]

4.3.4. Latency and Throughput

Latency is a function of the time required for a packet to be transferred across a network, and it could be taken as a one-way or two-way (round) trip. Throughput describes the quality of the data being transmitted and received over the communication network within a time unit. Applications in smart grid require varying latencies and throughput to ensure QoS. Presented in Table 8 are various methods employed in the review paper for the reduction of end-to-end latency and throughput enhancement techniques.

A scheduling algorithm where all the meter nodes follow distinct paths to each gateway in a mesh network architecture that is multi-gate in nature was developed by [87]. The stability region of the network was quantified for the application of the scheduling algorithm. The simulation results show that the approach was able to achieve reduced latency upon implementation. A communication network for high-rise building was developed by [88]. The network has two parts: the backbone network and a floor network, each of which represents frequency channels used. A multi-interface management framework was both clarified and designed for the coordination of multiple interfaces operations. The network is applicable in divers smart meter management functions as the demand side management for smart grid utilization. Both experimental results and simulations carried out using OPNET software revealed a significant improvement in latency at the application layer of the backbone and floor networks.

In the work by [89], measurement was performed to get initial data to formulate objectives functions for large scale optimal solution. Then, a model to mitigate interference was developed before Non-Dominated Genetic Algorithm-II customization for design development. Evaluation of large-scale analysis was implemented using the OPNET simulation software package. According to [90], IEC 61850 standard was used to model smart home system and smart meters to bring about its integration to a power grid while striving to ensure interoperability of the different devices. Riverbed Modeler simulation evaluations were carried out using various wired and wireless communication technologies. End to end delay performance and packet delivery rate were improved by the proposed approach.

Table 8. Summary of works of literature on Quality of service under various constraints

Critical Issues Considered	Constraint	Communication Technology	Simulation Tool/Method	References
Network reliability Delay reduction	Varying outage conditions	IEEE 802.11	-	[87]
High traffic communications	Intra and inter-floor communications.	Multi-interface ZigBee building area network	OPNET	[88]
High traffic smart metering	Interference mitigation capability	ZigBee-based	OPNET	[89]
Interoperability among smart home systems and smart meters	Interaction between the microgrid and the main grid	LAN, Wi-Fi (IEEE 802.11n/g) and WiMAX.	Riverbed Modeler Simulator	[90]
Evaluation of radiofrequency mesh network performance	Large scale network	RF-Mesh	-	[91]
Timely and reliable smart meter communications	Preamble congestion	long term evolution (LTE) network	OPNET	[92]
Establishing paths with minimum end to end delay and packet loss ratio	Using the shortest distance between SM and DCU	IEEE 802.11s	OPNET	[93]
Network performance evaluation	Operate in a large geographical area	RF-mesh		[80]
Delay mitigation	Smart grid application	AFAR	OPNET	[71]

Based on computational delay the performance evaluation of a large-scale radio frequency mesh was established by [91]. Frequency hopping spread spectrum-based time-slotted ALOHA was used. Based on Markov modulated modelling, an analytic formulation for the delay was derived. Simulation results established the feasibility of the approach. [92] used an approach that employs a combination of contention and non-contention random access procedure in smart grid data communication. Access mechanism uses periodic time communication that is fixed. Although LTE

was designed for human-to-human communication, the proposed model which combined several preamble signatures shows effectiveness when tested for machine-to-machine communication. The simulation results carried out using OPNET software shows improvement in latency, a smart meter packet scenario was used for the simulations. However, packet loss was not estimated in the work. Using the enhanced hybrid wireless mesh routing protocol (HWMP) routing technique, each node is chosen to ensure a minimum end to end delay and packet loss ratio. The proposed method chooses the shortest path between the smart meters and data concentrators leveraging on the relative position of the node selected and signal strength. To have more ranges for hop selection, the sector is divided into ranges. OPNET modeller simulations reveal shorter routing paths were selected by the proposed methods compared with existing methods [93].

5. Findings and Discussions

In the previous sections, some research papers were reviewed with an emphasis on smart metering applications. Considering Tables 4-7, which gives a summary of the literature on security, quality of service and optimum operating cost of the smart grid in the core domain of the review, the following points were observed:

The critical issues that attract the attention of most of the authors in the kinds of literature are the quality of service, smart meters and communication network security and optimum cost operation of the smart metering applications in the AMI network. QoS requirement has some constraints to take into account while designing the system such as interference mitigation, varying outage conditions, congestion, impulsive noise mitigation end to end delay mitigation, and outage probability determination. Various types of information exchange demand varying QoS. An enhanced routing protocol such as the routing protocol for low-power and lossy networks (RPL), the lightweight on-demand Ad hoc distance-vector routing (LOADng), Ad-hoc on-demand distance vector (AODV) and Dynamic Source Routing (DSR) protocols were successfully used in the articles reviewed. Polling algorithm like neighbour relay polling and clustered polling were also successfully deployed.

The designs in several of the literature use methods such as Advanced Encryption Standard (AES) and elliptic curve cryptography (ECC) to protect the privacy of users. Intrusion detection and prevention were also successfully done. To fend off a cyber-attack that was carried out with the intent to manipulate data for economic gain, an algorithm based on a support vector machine (SVM) was used to detect intrusion in smart meters. The objectives of the methods and designs employed in the reviewed literature seek to improve the financial implications of operating the smart grid.

5.1. Communication Network Simulators

Considering Figure 3 and Table 4-7, it was evident that NS-2, NS-3, OPNET and OMNET++ are popular among researchers for the simulation of communication networks. NS-2, NS-3 and OMNET++, which is an open source software, have been widely used. The simulators could be used to study the performance of smart meters over various communications networks. Metering applications generally is a current area undergoing steady development over the years.

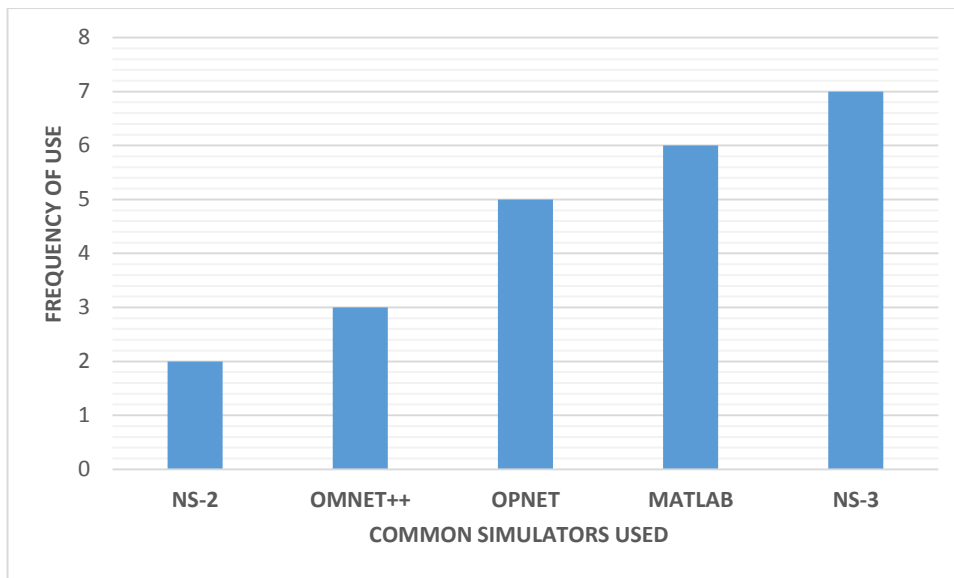


Figure 3. Common simulator deployed in the reviewed journal articles

5.2 Communication Network

Power line communication (PLC) is suitable for smart metering deployment. Power line Communications use the existing AC wired infrastructure. Therefore, no extra cost is needed for cabling purposes before the deployment of the technology. While it is not as fast as actual Ethernet cables, PLC speeds are often fast enough to deliver most consumer-based content. In the wireless category, ZigBee, Wi-Fi, Bluetooth, and WiMAX among others are suitable for deployment, and they have been successfully deployed. LTE network originally configured for human-to-human communication has been tested for adaptability for machine-to-machine communication in applications such as smart metering. The simulation results show a great deal of applicability.

ZigBee is more suitable when accuracy is not a major concern. It is suitable for smart electric grid applications with fewer reliability demands, which requires low energy. Wi-Fi networks could also fit into use for data communication between the data concentration unit and the meter. The Wi-Fi network can operate adequately in a Local Area Network (LAN). WiMAX and cellular network are deployable for metering activities between the data aggregation unit and the utility server. WiMAX was designed particularly for metropolitan area networks (MAN) communications as it provides very high transmission rates at a range unequalled by other wireless protocols.

6. Conclusion

In this paper, a comprehensive review of communication networks and simulators for smart metering applications has been provided. This includes communication networks applicable for smart metering applications details of common simulation software for communication networks, and the critical issues of considerations while installing smart meters in an AMI network. The current issues raised have been discussed. The issue of security, quality of service and optimum operational cost remains paramount in smart grid implementation. A review of this kind in the future could look closely into the simulators and networks employed at each category of the smart grid communication infrastructure; the HAN, NAN and WAN. Also, analysis and methods of improving energy data quality from smart meters based on the packet lost during transmission in the communication channel should be focused upon in similar review in the future.

Acknowledgements

This research was funded by TETFund Research Fund Grant 2020.

References

- [1] V. C. Gungor et al., "A Survey on Smart Grid Potential Applications and Communication Requirements," *IEEE Trans. Ind. Informatics*, vol. 9, no. 1, pp. 28–42, 2013, doi: 10.1109/TII.2012.2218253.
- [2] Y. Wang, Q. Chen, T. Hong, C. Kang, and C. Y. Mar, "Review of Smart Meter Data Analytics : Applications, Methodologies, and Challenges," no. June, pp. 1–24, 2017.
- [3] M. Vogt, F. Marten, and M. Braun, "A Survey And Statistical Analysis of Smart Grid Co-Simulations," *Applied Energy*, vol. 222, no. September 2017. Elsevier, pp. 67–78, 2018, doi: 10.1016/j.apenergy.2018.03.123.
- [4] W. Li and X. Zhang, "Simulation of the Smart Grid Communications: Challenges, Techniques, and Future Trends," *Comput. Electr. Eng.*, vol. 40, no. 1, pp. 270–288, 2014, doi: 10.1016/j.compeleceng.2013.11.022.
- [5] K. Mets, J. A. Ojea, and C. Develder, "Combining Power and Communication Network Simulation For Cost-Effective Smart Grid Analysis," *IEEE Commun. Surv. Tutorials*, vol. 16, no. 3, pp. 1771–1796, 2014, doi: 10.1109/SURV.2014.021414.00116.
- [6] Y. Kabalci, "A Survey on Smart Metering and Smart Grid Communication," *Renewable and Sustainable Energy Reviews*, vol. 57. Elsevier, pp. 302–318, 2016, doi: 10.1016/j.rser.2015.12.114.
- [7] N. I. Sarkar, S. Member, and S. A. Halim, "A Review of Simulation of Telecommunication Networks: Simulators, Classification, Comparison, Methodologies, and Recommendations," *J. Sel. Areas Telecommun.*, no. January 2011, 2014.
- [8] C. Rehtanz and X. Guillaud, "Real-time and Co-Simulations For The Development of Power System Monitoring, Control and Protection," in *19th Power Systems Computation Conference, PSCC 2016*, 2016, doi: 10.1109/PSCC.2016.7541030.
- [9] A. Mahmood, N. Javaid, and S. Razzaq, "A Review of Wireless Communications for Smart Grid," *Renew. Sustain. Energy Rev.*, vol. 41, pp. 248–260, 2015, doi: 10.1016/j.rser.2014.08.036.
- [10] D. Bian, M. Kuzlu, M. Pipattanasomporn, and S. Rahman, "Analysis of Communication Schemes for Advanced Metering Infrastructure (AMI)," in *IEEE Power and Energy Society General Meeting, 2014*, vol. 2014-Octob, no. October, doi: 10.1109/PESGM.2014.6939562.
- [11] M. Kuzlu, M. Pipattanasomporn, and S. Rahman, "Review of Communication Technologies for Smart Homes/Building Applications," in *Proceedings of the 2015 IEEE Innovative Smart Grid Technologies - Asia, ISGT ASIA 2015*, 2016, pp. 1–6, doi: 10.1109/ISGT-Asia.2015.7437036.
- [12] J. Leiva, A. Palacios, and J. A. Aguado, "Smart Metering Trends, Implications and Necessities : A Policy Review," *Renew. Sustain. Energy Rev.*, vol. 55, pp. 227–233, 2016, doi: 10.1016/j.rser.2015.11.002.
- [13] M. C. Falvo, L. Martirano, D. Sbordone, and E. Bocci, "Technologies for Smart Grids: A Brief Review," in *12th International Conference on Environment and Electrical Engineering, EEEIC 2013*, 2013, pp. 369–375, doi: 10.1109/EEEIC.2013.6549544.
- [14] N. Uribe-Pérez, L. Hernández, D. de la Vega, and I. Angulo, "State of the Art and Trends Review of Smart Metering in Electricity Grids," *Appl. Sci.*, vol. 6, no. 3, pp. 1–24, 2016, doi: 10.3390/app6030068.
- [15] M. R. Asghar, G. Dán, D. Miorandi, and I. Chlamtac, "Smart Meter Data Privacy: A Survey," *IEEE Commun. Surv. Tutorials*, vol. 19, no. 4, pp. 2820–2835, 2017, doi: 10.1109/COMST.2017.2720195.
- [16] Y. Wang, Q. Chen, T. Hong, and C. Kang, "Review of Smart Meter Data Analytics: Applications, Methodologies, and Challenges," *IEEE Trans. Smart Grid*, vol. 10, no. 3, pp. 3125–3148, 2019, doi: 10.1109/TSG.2018.2818167.

- [17] Y. Yan, Y. Qian, H. Sharif, and D. Tipper, "A Survey on Smart Grid Communication Infrastructures: Motivations, Requirements And Challenges," *IEEE Communications Surveys and Tutorials*, vol. 15, no. 1, pp. 5–20, 2013, doi: 10.1109/SURV.2012.021312.00034.
- [18] R. Deng, Z. Yang, M. Y. Chow, and J. Chen, "A Survey on Demand Response in Smart Grids: Mathematical Models And Approaches," *IEEE Trans. Ind. Informatics*, vol. 11, no. 3, pp. 570–582, 2015, doi: 10.1109/TII.2015.2414719.
- [19] S. Garlapati, T. Kuruganti, M. R. Buehrer, and J. H. Reed, "SMAC: A Soft MAC to Reduce Control Overhead and Latency in CDMA-Based AMI Networks," *IEEE/ACM Trans. Netw.*, vol. 24, no. 5, pp. 2648–2662, 2016, doi: 10.1109/TNET.2015.2481718.
- [20] A. Kondoro, I. Ben Dhaou, D. Rwegasira, A. Kelati, H. Tenhunen, and N. Mvungi, "A Simulation Model for the Analysis of Security Attacks in Advanced Metering Infrastructure," in *2018 IEEE PES/IAS PowerAfrica, PowerAfrica 2018*, 2018, pp. 533–538, doi: 10.1109/PowerAfrica.2018.8521089.
- [21] F. G. Gonzalez, "An Intelligent Controller for The Smart Grid," in *Procedia Computer Science*, 2013, vol. 16, pp. 776–785, doi: 10.1016/j.procs.2013.01.081.
- [22] N. Andreadou, M. O. Guardiola, and G. Fulli, "Telecommunication Technologies For Smart Grid Projects With Focus on Smart Metering Applications," *Energies*, vol. 9, no. 5, 2016, doi: 10.3390/en9050375.
- [23] M. Kuzlu, M. Pipattanasomporn, and S. Rahman, "Communication Network Requirements For Major Smart Grid Applications in HAN, NAN and WAN," *Computer Networks*, vol. 67, Elsevier B.V., pp. 74–88, 2014, doi: 10.1016/j.comnet.2014.03.029.
- [24] M. F. Khan, A. Jain, V. Arunachalam, and A. Paventhan, "Communication Technologies for Smart Metering Infrastructure," in *2014 IEEE Students' Conference on Electrical, Electronics and Computer Science, SCEECS 2014*, 2014, doi: 10.1109/SCEECS.2014.6804427.
- [25] Z. Lipošćak and M. Bošković, "Survey of Smart Metering Communication Technologies," in *IEEE EuroCon 2013*, 2013, no. November 2015, pp. 1391–1400, doi: 10.1109/EUROCON.2013.6625160.
- [26] D. Baimel, S. Tapuchi, and N. Baimel, "Smart Grid Communication Technologies- Overview, Research Challenges and Opportunities," in *2016 International Symposium on Power Electronics, Electrical Drives, Automation and Motion, SPEEDAM 2016*, 2016, pp. 116–120, doi: 10.1109/SPEEDAM.2016.7526014.
- [27] M. Burunkaya and T. Pars, "A Smart Meter Design and Implementation Using ZigBee Based Wireless Sensor Network in Smart Grid," in *2017 4th International Conference on Electrical and Electronics Engineering, ICEEE 2017*, 2017, pp. 158–162, doi: 10.1109/ICEEE2.2017.7935812.
- [28] R. S. Chauhan, J. Sharma, M. K. Jha, and J. V Desai, "Simulation-Based Performance Analysis Of Zigbee in Three-Dimensional Smart Grid Environments," in *International Conference on Communication and Signal Processing, ICCSP 2016*, 2016, pp. 1546–1550, doi: 10.1109/ICCSP.2016.7754418.
- [29] D. Chen, J. Brown, and J. Y. Khan, "6LoWPAN Based Neighborhood Area Network For a Smart Grid Communication Infrastructure," in *International Conference on Ubiquitous and Future Networks, ICUFN*, 2013, pp. 576–581, doi: 10.1109/ICUFN.2013.6614885.
- [30] J. Hoglund, D. Ilic, S. Karnouskos, R. Sauter, and P. Goncalves Da Silva, "Using a 6LoWPAN Smart Meter Mesh Network for Event-Driven Monitoring of Power Quality," in *2012 IEEE 3rd International Conference on Smart Grid Communications, SmartGridComm 2012*, 2012, no. November, pp. 448–453, doi: 10.1109/SmartGridComm.2012.6486025.
- [31] D. Chen, J. Brown, and J. Y. Khan, "Performance Analysis of a Distributed 6LoWPAN Network for the Smart Grid Applications," in *IEEE ISSNIP 2014 - 2014 IEEE 9th International Conference on Intelligent Sensors, Sensor Networks and Information Processing, Conference Proceedings*, 2014, no. April, pp. 21–24, doi: 10.1109/ISSNIP.2014.6827646.
- [32] A. Yarali and S. Rahman, "Smart grid networks: Promises and challenges," *J. Commun.*, vol. 7, no. 6 *SPECL. ISSUE*, pp. 409–417, 2012, doi: 10.4304/jcm.7.6.409-417.
- [33] M. Collotta and G. Pau, "A solution based on Bluetooth Low Energy for Smart Home Energy Management," *Energies*, vol. 8, no. 10, pp. 11916–11938, 2015, doi: 10.3390/en81011916.




- [34] O. Neagu and W. Hamouda, "Performance of WiMAX for Smart Grid Applications," in 2016 International Conference on Selected Topics in Mobile and Wireless Networking, MoWNeT 2016, 2016, doi: 10.1109/MoWNeT.2016.7496613.
- [35] L. Štastný, L. Franek, and P. Fiedler, "Wireless Communications in Smart Metering," in IFAC Proceedings Volumes (IFAC-PapersOnline), 2013, vol. 12, no. PART 1, pp. 330–335, doi: 10.3182/20130925-3-CZ-3023.00035.
- [36] G. D. Castellanos and J. Y. Khan, "Performance Analysis of WiMAX Polling Service For Smart Grid Meter Reading Applications," in 2012 IEEE Colombian Communications Conference, COLCOM 2012 - Conference Proceedings, 2012, no. May, doi: 10.1109/ColComCon.2012.6233661.
- [37] Y. Kabalci, E. Kabalci, S. Padmanaban, J. B. Holm-Nielsen, and F. Blaabjerg, "Internet of Things Applications as Energy Internet in Smart Grids And Smart Environments," *Electron.*, vol. 8, no. 9, pp. 1–16, 2019, doi: 10.3390/electronics8090972.
- [38] C. Paolini, H. Adigal, and M. Sarkar, "Upper Bound on LoRa Smart Metering Uplink Rate," in 2020 IEEE 17th Annual Consumer Communications and Networking Conference, CCNC 2020, 2020, pp. 1–4, doi: 10.1109/CCNC46108.2020.9045439.
- [39] F. Helder, P. S. Dester, E. M. G. Stancanelli, and P. Cardieri, "Feasibility of Alarm Events Upon Smart Metering in LoRa Networks," in Proceedings of the International Symposium on Wireless Communication Systems, 2019, vol. 2019-August, no. August, pp. 480–484, doi: 10.1109/ISWCS.2019.8877346.
- [40] M. Slabicki, G. Premsankar, and M. Di Francesco, "Adaptive Configuration of LoRa Networks for Dense IoT deployments," *IEEE/IFIP Netw. Oper. Manag. Symp. Cogn. Manag. a Cyber World, NOMS 2018*, pp. 1–9, 2018, doi: 10.1109/NOMS.2018.8406255.
- [41] Z. Xia, H. Zhou, K. Gu, B. Yin, Y. Zeng, and M. Xu, "Secure Session Key Management Scheme For A Meter-Reading System Based on LoRa Technology," *IEEE Access*, vol. 6, pp. 75015–75024, 2018, doi: 10.1109/ACCESS.2018.2883657.
- [42] Y. Cheng, H. Saputra, L. M. Goh, and Y. Wu, "Secure Smart Metering Based on LoRa Technology," 2018 IEEE 4th Int. Conf. Identity, Secur. Behav. Anal. ISBA 2018, vol. 2018-January, pp. 1–8, 2018, doi: 10.1109/ISBA.2018.8311466.
- [43] L. Di Bert, S. D'Alessandro, and A. M. Tonello, "A G3-PLC Simulator for Access Networks," in IEEE ISPLC 2014 - 18th IEEE International Symposium on Power Line Communications and Its Applications, 2014, pp. 99–104, doi: 10.1109/ISPLC.2014.6812329.
- [44] S. Panchadcharam, G. A. Taylor, Q. Ni, I. Pisica, and S. Fateri, "Performance Evaluation of Smart Metering Infrastructure using Simulation Tool," pp. 1–6, 2020.
- [45] W. Chen, K. Zhou, S. Yang, and C. Wu, "Data Quality of Electricity Consumption Data in a Smart Grid Environment," *Renewable and Sustainable Energy Reviews*, vol. 75, no. October 2016. Elsevier Ltd, pp. 98–105, 2017, doi: 10.1016/j.rser.2016.10.054.
- [46] M. Ge, S. Chren, B. Rossi, and T. Pitner, "Data Quality Management Framework for Smart Grid Systems," in *Lecture Notes in Business Information Processing*, 2019, vol. 354, no. March, pp. 299–310, doi: 10.1007/978-3-030-20482-2_24.
- [47] J. Shishido and E. U. Solutions, "Smart Meter Data Quality Insights," *ACEEE Summer Study Energy Effic. Build.*, pp. 277–288, 2012.
- [48] A. Razaq, B. Pranggono, H. Tianfield, and H. Yue, "Simulating Smart Grid: Co-Simulation Of Power and Communication Network," in Proceedings of the Universities Power Engineering Conference, 2015, vol. 2015-Novem, no. September, pp. 1–4, doi: 10.1109/UPEC.2015.7339763.
- [49] S. Saba, K. Ajay, and R.-B. Gupta, "Network Simulation Tools Survey," *Int. J. Adv. Res. Comput. Commun. Eng. Vol.*, vol. 1, no. 4, pp. 201–210, 2012.
- [50] C. Sun, S. Member, D. J. Sebastian, and S. Member, "Intrusion Detection for Cybersecurity of Smart Meters," *EEE Trans. Smart Grid*, vol. 3053, no. c, pp. 1–11, 2019, doi: 10.1109/TSG.2020.3010230.

- [51] P. Ganguly, M. Nasipuri, and S. Dutta, "A Novel Approach for Detecting and Mitigating the Energy Theft Issues in the Smart Metering Infrastructure," *Technol. Econ. Smart Grids Sustain. Energy*, vol. 3, no. 1, pp. 1–11, 2018, doi: 10.1007/s40866-018-0053-x.
- [52] M. Cebe and K. Akkaya, "Efficient Certificate Revocation Management Schemes for IoT-Based Advanced Metering Infrastructures in Smart Cities," *Ad Hoc Networks*, vol. 92, pp. 1–47, 2019, doi: 10.1016/j.adhoc.2018.10.027.
- [53] F. Wu, X. Li, L. Xu, and S. Kumari, "A privacy-preserving scheme with identity traceable property for smart grid," *Comput. Commun.*, vol. 157, no. April, pp. 38–44, 2020, doi: 10.1016/j.comcom.2020.03.047.
- [54] Y. Liu and S. Hu, "Cyber threat analysis and detection for energy theft in social networking of smart homes," *IEEE Trans. Comput. Soc. Syst.*, vol. 2, no. 4, pp. 148–158, 2015, doi: 10.1109/TCSS.2016.2519506.
- [55] M. Cebe and K. Akkaya, "Utilizing advanced metering infrastructure to build a public key infrastructure for electric vehicles," in *DIVANet 2017 - Proceedings of the 6th ACM Symposium on Development and Analysis of Intelligent Vehicular Networks and Applications, Co-located with MSWiM 2017*, 2017, pp. 91–98, doi: 10.1145/3132340.3132359.
- [56] S. Asri and B. Pranggono, "Impact of Distributed Denial-of-Service Attack on Advanced Metering Infrastructure," *Wirel. Pers. Commun.*, vol. 83, no. 3, pp. 2211–2223, 2015, doi: 10.1007/s11277-015-2510-3.
- [57] G. Eibl and D. Engel, "Differential privacy for real smart metering data," *Comput. Sci. - Res. Dev.*, vol. 32, no. 1–2, pp. 173–182, 2017, doi: 10.1007/s00450-016-0310-y.
- [58] S. Kim et al., "A secure smart-metering protocol over power-line communication," *IEEE Trans. Power Deliv.*, vol. 26, no. 4, pp. 2370–2379, 2011, doi: 10.1109/TPWRD.2011.2158671.
- [59] D. Mert, M. U. Şimşek, and S. Özdemir, "Privacy-Preserving Metering Protocol in Smart Grids," *IFIP Adv. Inf. Commun. Technol.*, vol. 458, no. AIAI 2015, pp. 467–477, 2015, doi: 10.1007/978-3-319-23868-5_34.
- [60] K. Akkaya, K. Rabieh, M. Mahmoud, and S. Tonyali, "Customized Certificate Revocation Lists for IEEE 802.11s-Based Smart Grid AMI Networks," *IEEE Trans. Smart Grid*, vol. 6, no. 5, pp. 2366–2374, 2015, doi: 10.1109/TSG.2015.2390131.
- [61] S. Tonyali, O. Cakmak, K. Akkaya, M. M. E. A. Mahmoud, and I. Guvenc, "Secure Data Obfuscation Scheme to Enable Privacy-Preserving State Estimation in Smart Grid AMI Networks," *IEEE Internet Things J.*, vol. 3, no. 5, pp. 709–719, 2016, doi: 10.1109/JIOT.2015.2510504.
- [62] J. Y. Kim, Y. M. Hwang, Y. G. Sun, I. Sim, D. I. Kim, and X. Wang, "Detection for Non-Technical Loss by Smart Energy Theft with Intermediate Monitor Meter in Smart Grid," *IEEE Access*, vol. 7, pp. 129043–129053, 2019, doi: 10.1109/ACCESS.2019.2940443.
- [63] R. Ullah, Y. Faheem, and B. S. Kim, "Energy and Congestion-Aware Routing Metric For Smart Grid AMI Networks in Smart City," *IEEE Access*, vol. 5, pp. 13799–13810, 2017, doi: 10.1109/ACCESS.2017.2728623.
- [64] P. Li, S. Guo, and Z. Cheng, "Joint Optimization of Electricity And Communication Cost For Meter Data Collection in Smart Grid," *IEEE Trans. Emerg. Top. Comput.*, vol. 1, no. 2, pp. 297–306, 2013, doi: 10.1109/TETC.2013.2273890.
- [65] U. Das and V. Namboodiri, "A Quality-Aware Multi-Level Data Aggregation Approach to Manage Smart Grid AMI Traffic," *IEEE Trans. Parallel Distrib. Syst.*, vol. 30, no. 2, pp. 245–256, 2019, doi: 10.1109/TPDS.2018.2865937.
- [66] S. Xu, Y. Qian, and R. Q. Hu, "Reliable and Resilient Access Network Design For Advanced Metering Infrastructures In Smart Grid," *IET Smart Grid*, vol. 1, no. 1, pp. 24–30, 2018, doi: 10.1049/iet-stg.2018.0008.
- [67] K. Gajowniczek and T. Ząbkowski, "Short Term Electricity Forecasting Using Individual Smart Meter Data," *Procedia - Procedia Comput. Sci.*, vol. 35, no. 2014, pp. 589–597, 2014, doi: 10.1016/j.procs.2014.08.140.

- [68] O. Valgaev, F. Kupzog, and H. Schmeck, "Adequacy Of Neural Networks For Wide-Scale Day-Ahead Load Forecasts On Buildings and Distribution Systems Using Smart Meter Data," *Energy Informatics*, vol. 3, no. 1, pp. 1–17, 2020, doi: 10.1186/s42162-020-00132-6.
- [69] Q. Ma, F. Meng, and X. J. Zeng, "Optimal Dynamic Pricing For Smart Grid Having Mixed Customers With and Without Smart Meters," *J. Mod. Power Syst. Clean Energy*, vol. 6, no. 6, pp. 1244–1254, 2018, doi: 10.1007/s40565-018-0389-1.
- [70] R. Bonnefoi, C. Moy, and J. Palicot, "Improvement of the LPWAN AMI Backhaul's Latency Thanks To Reinforcement Learning Algorithms," *Eurasip J. Wirel. Commun. Netw.*, vol. 2018, no. 1, pp. 1–18, 2018, doi: 10.1186/s13638-018-1044-2. Frequency-Hopping Based Communication Network With Multi-Level QoS in Smart Grid: Code Design And Performance Analysis,
- [71] K. Kim, H. Kim, J. Jung, and H. Kim, "AFAR : A Robust and Delay-Constrained Communication Framework for Smart Grid Applications," *Comput. Networks*, vol. 91, no. 2015, pp. 1–25, 2015, doi: 10.1016/j.comnet.2015.08.001.
- [72] Y. Ben-Shimol, S. Greenberg, and K. Danilchenko, "Application-Layer Approach for Efficient Smart Meter Reading in Low-Voltage PLC Networks," *IEEE Trans. Commun.*, vol. 66, no. 9, pp. 4249–4258, 2018, doi: 10.1109/TCOMM.2018.2828849.
- [73] Q. Zeng, H. Li, and D. Peng, "Frequency-Hopping Based Communication Network With Multi-Level QoS in Smart Grid: Code Design and Performance Analysis" *IEEE Trans. Smart Grid*, vol. 3, no. 4, pp. 1841–1852, 2012, doi: 10.1109/TSG.2012.2214067.
- [74] C. K. Huynh and W. C. Lee, "An Efficient Channel Selection And Power Allocation Scheme for TVWS based on Interference Analysis In Smart Metering Infrastructure," *J. Commun. Networks*, vol. 18, no. 1, pp. 50–64, 2016, doi: 10.1109/JCN.2016.000008.
- [75] J. A. Cortés, A. Sanz, P. Estopiñán, and J. I. García, "Analysis of Narrowband Power Line Communication Channels for Advanced Metering Infrastructure," *EURASIP J. Adv. Signal Process.*, vol. 2015, no. 1, 2015, doi: 10.1186/s13634-015-0211-4.
- [76] I. Parvez, M. Aghili, A. I. Sarwat, S. Rahman, and F. Alam, "Online Power Quality Disturbance Detection by Support Vector Machine in Smart Meter," *J. Mod. Power Syst. Clean Energy*, vol. 7, no. 5, pp. 1328–1339, 2019, doi: 10.1007/s40565-018-0488-z.
- [77] G. López, J. I. Moreno, H. Amarís, and F. Salazar, "Metering Infrastructures," *Electr. Power Syst. Res.*, 2014, doi: 10.1016/j.epsr.2014.05.006.
- [78] Y. He, N. Jenkins, and J. Wu, "Smart Metering for Outage Management of Electric Power Distribution Networks," *Energy Procedia*, vol. 103, no. April, pp. 159–164, 2016, doi: 10.1016/j.egypro.2016.11.266.
- [79] A. Al-Wakeel, J. Wu, and N. Jenkins, "State Estimation of Medium Voltage Distribution Networks Using Smart Meter Measurements," *Appl. Energy*, vol. 184, pp. 207–218, 2016, doi: 10.1016/j.apenergy.2016.10.010.
- [80] F. Malandra and B. Sansò, "A Simulation Framework for Network Performance Evaluation Of Large-Scale RF-Mesh AMIs," *Simul. Model. Pract. Theory*, vol. 75, no. 2017, pp. 165–181, 2017, doi: 10.1016/j.simpat.2017.04.004.
- [81] B. Sivaneasan, E. Gunawan, and P. L. So, "Modeling and Performance Analysis Of Automatic Meter-Reading Systems using PLC Under Impulsive Noise Interference," *IEEE Trans. Power Deliv.*, vol. 25, no. 3, pp. 1465–1475, 2010, doi: 10.1109/TPWRD.2010.2041257.
- [82] M. Korki, N. Hosseinzadeh, and T. Moazzeni, "Performance Evaluation of a Narrowband Power Line Communication For Smart Grid With Noise Reduction Technique," *IEEE Trans. Consum. Electron.*, vol. 57, no. 4, pp. 1598–1606, 2011, doi: 10.1109/TCE.2011.6131131.
- [83] J. Matanza, S. Alexandres, and C. Rodríguez-Morcillo, "Advanced Metering Infrastructure Performance Using European Low-Voltage Power Line Communication Networks," *IET Commun.*, vol. 8, no. 7, pp. 1041–1047, 2014, doi: 10.1049/iet-com.2013.0793.

- [84] L. González-Sotres, C. Mateo, P. Frías, C. Rodríguez-Morcillo, and J. Matanza, "Replicability Analysis of PLC PRIME Networks for Smart Metering Applications," *IEEE Trans. Smart Grid*, vol. 9, no. 2, pp. 827–835, 2018, doi: 10.1109/TSG.2016.2569487.
- [85] B. E. Bilgin, S. Baktir, and V. C. Gungor, "Collecting Smart Meter Data Via Public Transportation Buses," *IET Intell. Transp. Syst.*, vol. 10, no. 8, pp. 515–523, 2016, doi: 10.1049/iet-its.2015.0058.
- [86] Y. Cao, D. Duan, X. Cheng, L. Yang, and J. Wei, "QoS-oriented Wireless Routing For Smart Meter Data Collection: Stochastic Learning on Graph," *IEEE Trans. Wirel. Commun.*, vol. 13, no. 8, pp. 4470–4482, 2014, doi: 10.1109/TWC.2014.2314121.
- [87] H. Gharavi and C. Xu, "Traffic Scheduling Technique or Smart Grid Advanced Metering Applications," *IEEE Trans. Commun.*, vol. 60, no. 6, pp. 1646–1658, 2012, doi: 10.1109/TCOMM.2012.12.100620.
- [88] H. Y. Tung et al., "The Generic Design of a High-Traffic Advanced Metering Infrastructure Using ZigBee," *IEEE Trans. Ind. Informatics*, vol. 10, no. 1, pp. 836–844, 2014, doi: 10.1109/TII.2013.2280084.
- [89] H. R. Chi, K. F. Tsang, K. T. Chui, H. S. H. Chung, B. W. K. Ling, and L. L. Lai, "Interference-Mitigated ZigBee-Based Advanced Metering Infrastructure," *IEEE Trans. Ind. Informatics*, vol. 12, no. 2, pp. 672–684, 2016, doi: 10.1109/TII.2016.2527618.
- [90] S. M. S. Hussain, A. Tak, T. S. Ustun, and I. Ali, "Communication Modeling of Solar Home System and Smart Meter in Smart Grids," *IEEE Access*, vol. 6, pp. 16985–16996, 2018, doi: 10.1109/ACCESS.2018.2800279.
- [91] F. Malandra and B. Sanso, "A Markov-Modulated End-to-End Delay Analysis of Large-Scale RF Mesh Networks with Time-Slotted ALOHA and FHSS for Smart Grid Applications," *IEEE Trans. Wirel. Commun.*, vol. 17, no. 11, pp. 7116–7127, 2018, doi: 10.1109/TWC.2018.2860965.
- [92] C. Karupongsiri, K. S. Munasinghe, and A. Jamalipour, "A Novel Random Access Mechanism for Timely Reliable Communications for Smart Meters," *IEEE Trans. Ind. Informatics*, vol. 13, no. 6, pp. 3256–3264, 2017, doi: 10.1109/TII.2017.2706754.
- [93] A. Robert Singh, D. Devaraj, and R. Narmatha Banu, "Geographic HWMP (Geo-HWMP) Routing Method for AMI network with lossless packet forwarding," *IET Cyber-Physical Syst. Theory Appl.*, vol. 4, no. 1, pp. 68–78, 2019, doi: 10.1049/iet-cps.2017.0115.

A PID-Controlled High DC Voltage Gain Switched-Inductor&Capacitor-Based DC-DC Power Buck-Boost Converter applicable for PV utilizations

Hatice Kurnaz Araz¹, Davut Ertekin^{1*}, Musa Aydın¹

¹Department of Electrical and Electronics Engineering, Bursa, Turkey

Abstract

DC-DC converters are widely applied in different industrials such the Renewable Energy Sources (RESs) utilizations, Electrical Vehicle (EV) applications and power transmission technologies. Different topologies are presented for these converters including the modified Buck, Boost or Buck-Boost converters, switched-inductors and switched-capacitor-based structures and circuits with transformers. A DC-DC converter is needed to transmit and make the voltage applicable to the grid or home applications to use the different levels of the generated voltage by different voltage sources. In this study, a switched-inductor-based converter is presented to operate in low or high-power utilizations. One application of the proposed converter is aiming to supply the necessary voltages to the devices requiring low voltage, such as mobile phones and computers, and transmit the obtained voltage to the electricity grids that can be categorized at the high-voltage applications. Based on the load voltages level, there is a need to obtain a high-gain converter, which can operate as a buck and boost converter. Since electrical energy must be transmitted as lossless as possible, the converter must be highly efficient. In the proposed converter, the number of the components are optimized and only one power switch is used. The main advantage of the converter is that it can be controlled simply since it contains only one power switch. Also, three diodes are used in the proposed structure that only one of them is activated at the time intervals that the switch is on ON-state and the other two diodes are activated for the OFF-state of the switch. All these features can help for obtaining smaller dynamic and switching losses through the power transmission process. Both inductors are charged in the ON-state and discharged in the OFF-state operational modes that can guarantee a Continuous Conduction Mode (CCM) working conditions for the converter. Also, a capacitor is used to transfer the voltage between the input and output sides during the switching process.

Keywords: SEPIC Converter, High voltage gain, Switched-capacitor, Switched-inductor, PID controller.

Cite this paper as:

Ertekin, D.,Kurnaz Araz,H., Aydın,M. (2021). *Industry 4.0 – A PID-Controlled High DC Voltage Gain Switched-Inductor&Capacitor-Based DC-DC Power Buck-Boost Converter applicable for PV utilizations* Journal of Innovative Science and Engineering. 5(2): 129-142

*Corresponding author: Davut Ertekin
E-mail: davood.ghaderi@btu.edu.tr

Received Date: 07/10/2020
Accepted Date: 23/03/2021
© Copyright 2021 by
Bursa Technical University. Available
online at <http://jise.btu.edu.tr/>



The works published in Journal of Innovative Science and Engineering (JISE) are licensed under a Creative Commons Attribution-NonCommercial 4.0 International License.

1. Introduction

Power electronics circuits allow electrical power to be transmitted through electronic components. DC-DC converters convert direct voltage (DC) to direct voltage (DC) with higher or lower voltage magnitudes, usually in positive polarity. These converters can be isolated from each other by separating the grounds of the input and output voltages if desired [1]. Solar arrays with around 100W power typically generate voltages between 24 VDC and 36VDC under suitable temperatures and irradiances. The electrical energy received from solar panels where solar energy is converted into electrical energy is obtained with a DC-DC converter to help. More than one power electronic circuit is required to transmit the single-phase power grid's obtained electrical energy. Since the single phase of the network is an alternating voltage (AC) with a 220 V amplitude, the DC voltage with around 300 V is required. The direct voltage that is increased with a DC-DC converter is converted to alternative voltage with a converter's help. It is then filtered and delivered to the grid [2-12]. The solar panel is considered to consist of many serially connected cells. Therefore, the panel's nominal voltage is calculated as 24V, and the maximum voltage as 36V. It is planned to use two panels, which are connected in series. For this purpose, many of the configurations like conventional buck-boost, SEPIC, CUK, switched-capacitor, and switched-inductor-based converters are presented in the literature. The main disadvantages of the conventional buck-boost converters are their efficiencies and low voltage gains. For example, all the classical buck-boost, SEPIC, and CUK converters generate a voltage four times greater than the input voltage at 80 percent of the duty cycles. This level of the duty ratio makes the power switches to be activated a longer time. It increases the converter's dynamic losses, especially in high power applications, and decreases efficiency.

Quasi-active inductance switching converters with coupled inductor blocks are suggested in [13-14]. Such circuits are capable of generating high voltage gain along with low voltage stress on active switches using small coupled inductors. In these circuits, two additional capacitors and two diodes have been added to the circuit to reduce the voltage stress on the semiconductor switches and increase the voltage gain. This circuit has one capacitor and one diode less than the improved circuit of the active network, while all its other features are preserved. A combined method in order to increase the gain of the converter voltage has been proposed in [15]. In fact, by substituting two switching inductor circuits instead of two normal active network inductors, a higher voltage gain is achieved than a simple active network. Using this method has increased the number of diodes, which has reduced the efficiency of the converter compared to the efficiency of a conventional DC-DC converter. The converter proposed in [16] consists of a series connection of conventional Boost converters and a voltage multiplier that places a coupler inductor with two windings in its circuit. In this converter, only one active switch is used and no large duty cycle is required to achieve high voltage gain. Also, the energy stored in the coupled inductor is directed to the load instead of wasted, so the converter losses are reduced and the converter efficiency is increased.

In [17] a hybrid converter is proposed. This converter has been designed based on the active network converter. In order to achieve higher voltage gain, based on a conventional active network converter and a type of switched capacitor circuit including two capacitors and three diodes that are connected in series with the active network converter have been used. In [18], a transformerless active network converter that uses coupled inductors is proposed to solve problems

such as a large volume of conventional boost converters, the high voltage stress on active switches, and voltage gain limitations. In this converter, in addition to using the voltage balancing capacitor of the active switches, the coupled inductor is used. The converter in [19] is obtained by placing a type of coupled inductor instead of active network converter inductors. One of the most important advantages of this converter is its small volume due to the use of only one core for two coupled inductors. In fact, both inductors are wrapped around a single core. However, the number of diodes in this converter is four more than in a conventional active network converter, which reduces the efficiency of the converter. In order to achieve high voltage gain and reduce voltage and current stress on the active switches, a combination of active network converter, coupled inductor and pump charge has been used in [19]. The efficiency of this converter has increased compared to the flyback boost converter due to the noticeable reduction of voltage and current stress on the active switches and diodes. In [20] to achieve high voltage gain, a hybrid active network converter with switch-inductor / switch-capacitor block is presented. However, the high number of elements used in this converter increases the conduction losses and decreases the overall efficiency of the system.

As can be seen, new switched-capacitor and switched-inductor converters were suggested to present higher DC gains at the lower duty cycles [21-24]. These structures not only can storage the high DC voltages across the capacitors or pass the higher current values through the inductors, but also, they can arrogate the voltages and currents in the power module and mitigate the voltage and current stresses across the power components like transistors and diodes.

This study presents a modified and high DC gain and switched-inductor-based SEPIC buck-boost converter. The number of the components is comparable with the SEPIC converter, and the location of the power components has been changed and rearranged. By this new configuration, around 350VDC and 3A for the load side is considered, and in order to fix the output voltage, a PID-based controller is suggested. All mathematical analysis and simulation results which have been provided by MATLAB/SIMULINK are presented.

2. Operating Principle of the Converter

The proposed converter's circuit diagram is shown in Figure 1. The structure is similar to the SEPIC converter topology and is provided by adding a diode to the circuit. For the time intervals that the power switch is in the OFF state, the second inductance is de-energized over the load. For this reason, the proposed converter is separated from the SEPIC converter. The input inductor (L_1) should be high enough to make the current continuously. The energy storage capacitor (C_1) and the output capacitor (C_0) should also be high enough to keep the output voltage stable. The proposed circuit structure is taken from the study of Fu et al. [25].

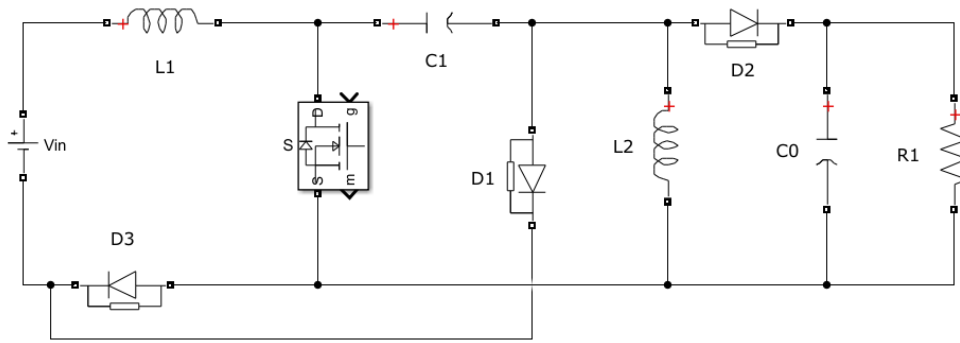


Figure 1. Suggested converter.

While the switch is activated during DT , diodes D_1 and D_2 are reverse biased, and diode D_3 is conducting. The input voltage energy is transmitted to inductance L_1 through the switch and D_3 , and the current of the inductance L_1 increases. The energy across the capacitor C_1 is transmitted to the inductor L_2 through the switch and C_1 , and the current of the inductor L_2 increases. Meanwhile, the output load is supplied through the output capacitor C_0 .

When the switch is deactivated during $(1-D)T$ time interval, diodes D_1 and D_2 are in on-state, and diode D_3 is reverse biased. The energy of the input voltage and inductor L_1 is transmitted to the capacitor C_1 . Hence, the current of inductor L_1 drops. Meanwhile, the energy stored across the inductor L_2 is transmitted through the D_2 diode to supply the output capacitor and output load. Therefore, the current of the inductor L_2 will decrease till the inductor L_2 is discharged. If the energy of the inductor L_2 is finished during the time the switch is open, the converter turns into discontinuous conduction mode, and the diode D_2 is reversed bias. The voltage across the output capacitor C_0 is transferred to the output load. Of course, in the meantime, the input source and inductor L_1 continue to supply the capacitor C_1 .

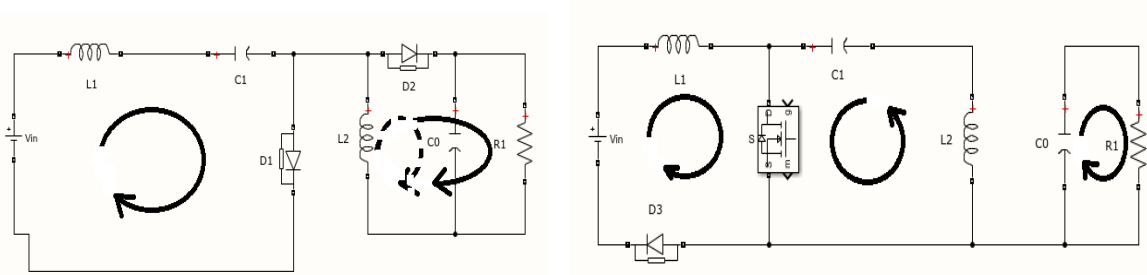


Figure 2. Current paths of the converter when the switch is closed and open. The path indicated by the dashed line disappears when switching from CCM to DCM.

When the switch is closed, the equation for the current flow through the inductors L_1 and L_2 are presented by (1) and (2):

$$L_1 \cdot \frac{di_{L1}}{dt} = V_{in} \tag{1}$$

$$L_2 \cdot \frac{di_{L2}}{dt} = v_{C1} \tag{2}$$

The voltage across the capacitor C_1 is given by (3), and the voltage of the output capacitor is presented by (4). When the switch is deactivated, the formula through the L_1 inductance is given in equation 5 and the current flowing through the L_2 inductance in equation 6. D is the duty ratio of the PWM signal.

$$C_1 \cdot \frac{dv_{C1}}{dt} = -i_{L2} \quad (3)$$

$$C_0 \cdot \frac{dv_1}{dt} = -\frac{v_1}{R_1} \quad (4)$$

$$L_1 \cdot \frac{di_{L1}}{dt} = (V_{in} - V_{C1})(1 - D) \quad (5)$$

$$L_2 \cdot \frac{di_{L2}}{dt} = -v_1 \cdot (1 - D) \quad (6)$$

The voltage across the capacitor C_1 is obtained through equation 7, and the voltage of the output capacitor C_0 is presented in the form of equation 8.

$$C_1 \cdot \frac{dv_{C1}}{dt} = i_{L2} \cdot (1 - D) \quad (7)$$

$$C_0 \cdot \frac{dv_1}{dt} = \left(i_{L2} - \frac{v_1}{R_1} \right) (1 - D) \quad (8)$$

3. Steady-State Analysis of the Suggested Converter

The voltage gain in a converter can be given as the input voltage ratio to the output voltage. All circuit elements used are thought to be ideal. In an ideal system, this ratio is $1/(1-D)$ in the classical boost converter, $-(D/(1-D))$ in the classic buck-boost converter, and CUK converter and $(D/(1-D))$ in the SEPIC converter. In the converter presented in Figure 1, a SEPIC converter scheme was used to get rid of negative polarity, and it was aimed to increase the voltage gain by adding diodes D_1 and D_3 .

In order to obtain the voltage gain, inductor volt second balance is used to get the equations. Which can be seen in equation 9 and 10.

$$\int_0^{DT} V_{in} \cdot dt + \int_{DT}^T (V_{in} - V_{C1}) dt = \int_0^{DT} V_{C1} \cdot dt + \int_{DT}^T (-V_1) dt = 0 \quad (9)$$

$$\frac{V_1}{V_{in}} = \frac{D}{(1 - D)^2} \quad (10)$$

The ratio of the output voltage to the input voltage is given as $(D/(1-D)^2)$ according to the calculation made by Fu et al. [26].

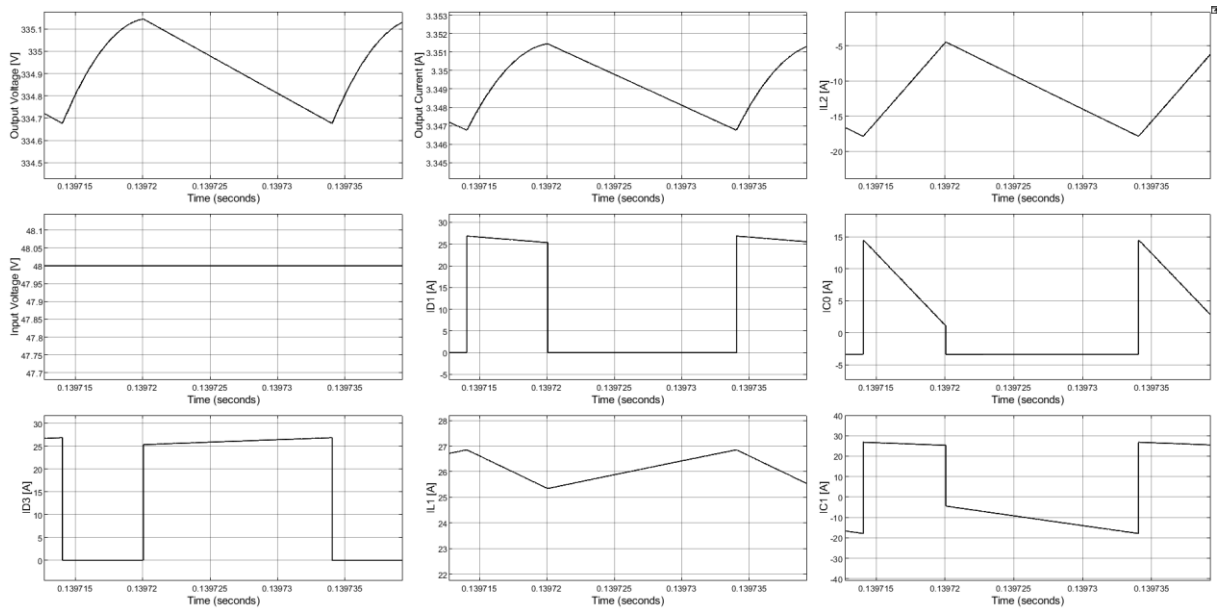


Figure 3. When the converter's duty ratio is 0.7, the output voltage, input voltage, and time-dependent current graphs of the components.

The duty ratio of the converter is set to 0.7. While the input voltage was 48 VDC, the output voltage is obtained equal to 335 VDC. Hence the voltage gain was 7. Figure 3 shows the input and output voltages, current and output current of diode D₃.

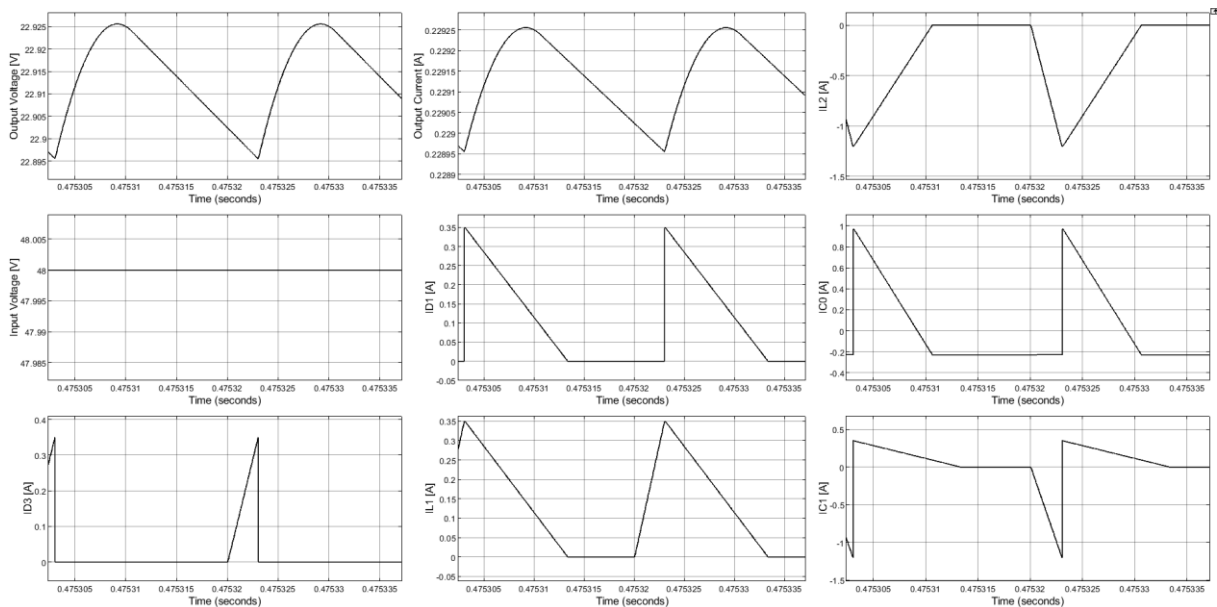


Figure 4. When the duty ratio of the converter is 0.15, the output voltage, input voltage, and time-dependent current graphs of some of the components.

In order to see the graphics of the converter while operating in buck mode, the duty ratio is set as 0.15. While the input voltage was 48 VDC, the output voltage was approximately 23 VDC. In Figure 4, input and output voltages and current values of all circuit elements can be seen.

It has been observed that as the duty ratio decreases, an extra load such as a sudden pulse current occurs, primarily through the D_3 diode.

3.1. Methods for Increasing Voltage Gain

A structure is created by adding additional elements like the capacitor, inductor, and diodes to increase the suggested converter's gain and make a smoother switching. These structures are well-known as the switched capacitor and switch inductor structures.

In this subsection, the proposed structure shown in Figure 5 is placed instead of the input inductance L_1 , and the energy is stored in parallel to the inductors L_1 and L_3 . At the same time, the switch is deactivated during the DT time interval. When the switch is deactivated during $(1-D)T$ time interval, the energy of the inductors L_1 and L_3 is transferred to the capacitor C_1 in series [27].

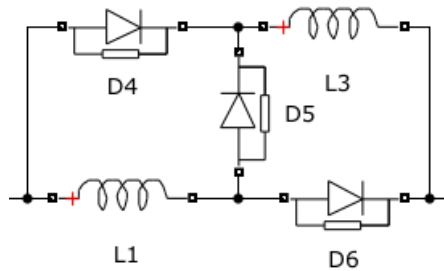


Figure 5. Suggested switched-inductor structure to be added instead of the input inductor L_1 .

When the switch inductor structure was added while the output voltage was 335 VDC, the output voltage increased to 485 VDC. Voltage gain increased from 7 to 10.1.

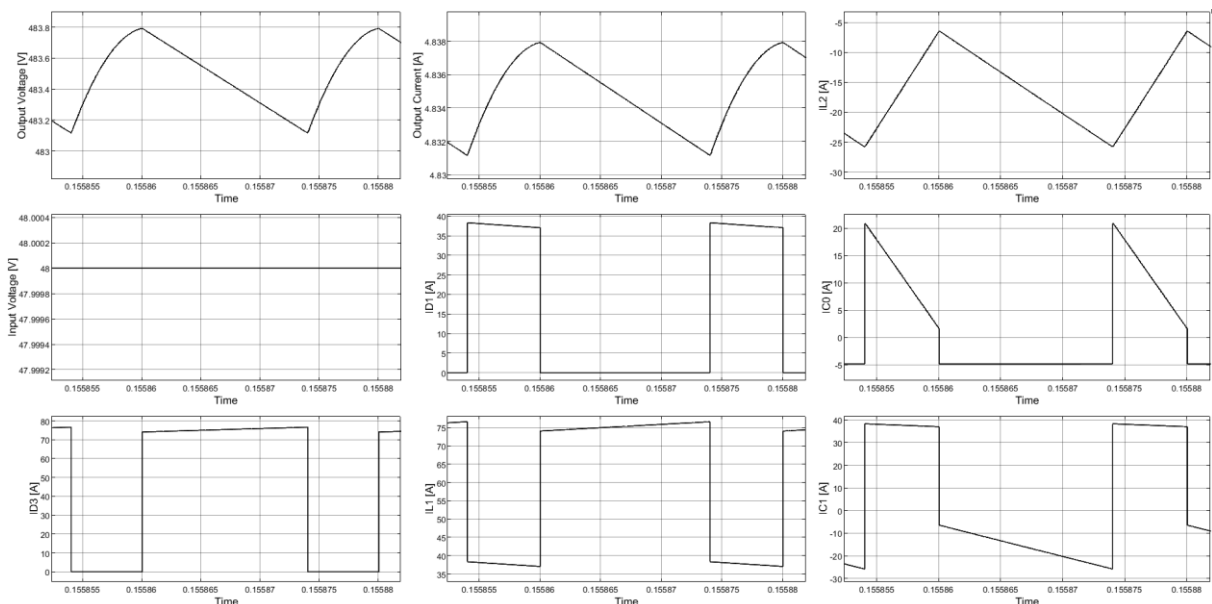


Figure 6. The impact of the proposed switched-inductor topology on the gain and other features of the proposed converter.

The opposite effect is expected when the converter is operating in buck mode. Using the switch capacitor structure, the structure in Figure 7 has been added to the circuit instead of the capacitor C_1 to investigate the buck mode. During the DT time interval, while the switch is closed, the voltage across the C_1 and C_2 capacitors is transmitted to the inductor L_2 in parallel. When the switch is activated during $(1-D)T$, capacitors C_1 and C_2 store the voltage serially [27].

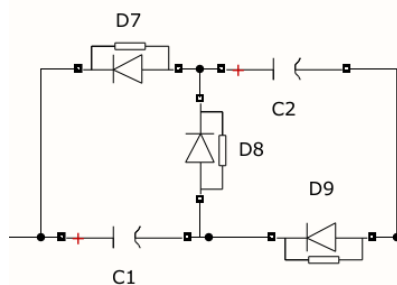


Figure 7. Suggested switched-capacitor structure to be added instead of the capacitor C_1 .

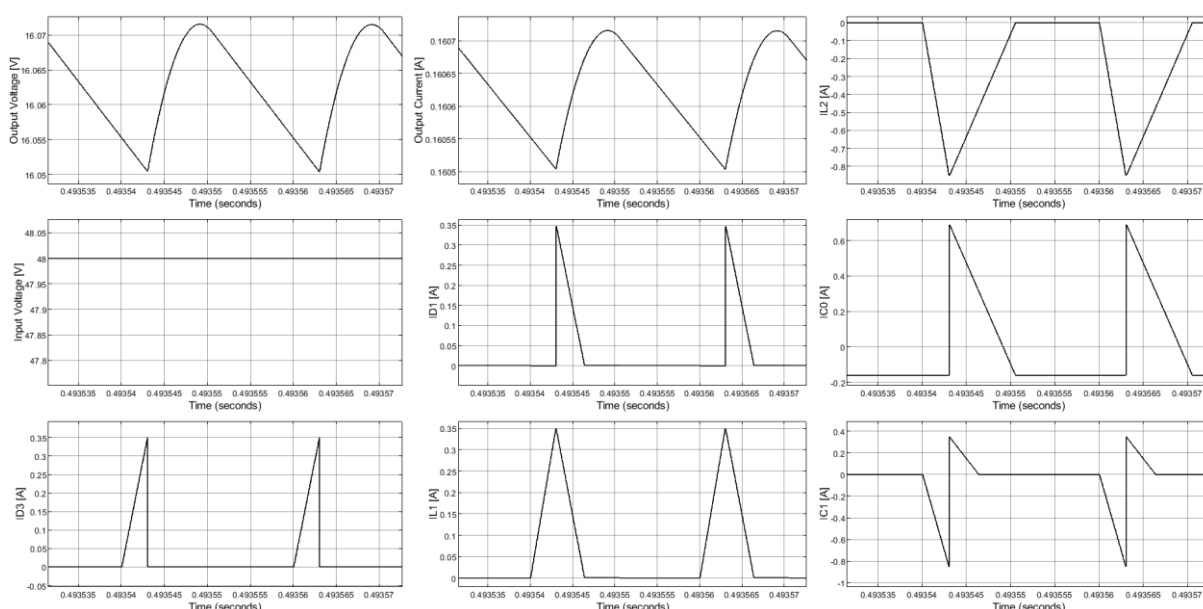


Figure 8. When the duty ratio of the converter is 0.15, the output voltage, input voltage, and time-dependent current graphs of some of the components.

When the switched-capacitor structure is added while the output voltage is 23 VDC, the output voltage is reduced to 16 VDC.

Switched-inductor and switched-capacitor structures are added to the circuit alone. The switched-inductor structure increases the circuit's voltage, while the switched-capacitor structure affects the circuit's voltage in a lower direction. If both sub-circuits are added to the converter, the two sub-circuits will act in the direction of damping each other. Besides, it has been observed that the current of the diode D_3 in the switched-capacitor structure is in the form of a pulse. The low or high duty ratio of the converter operating in both buck and boost modes affects the circuit elements currents and forces the circuit to decrease the converter's efficiency. In addition, the converter circuit's duty ratio is chosen in the range of 0.3-0.6 for the long-term operation of the switches and other circuit elements to provide more efficient operation.

4. Controller Design

In order to fix the output voltage across the specified values of the load, the converter structures should be equipped with a proper controller. This controller works to present different values of the duty cycles for the power switch under different input voltages and output loads. Different controller techniques are presented for converter circuits. Sliding mode controller [28-30], fuzzy logic-based controllers [31-33], FPGA-based controllers [34], and classical PI and PID controllers [35-39] are some of these techniques. Some of these controllers are based on the deep mathematical relations between the components. Some others only check the output voltage and have large damping ratios and high fluctuations at the change moments of the input voltage or the output load. Between these controllers, classical PID controllers have work with high accuracy and minimum damping ratios. The reason is that these converters are operating based on the pure and accurate mathematical analysis of the converter. Therefore, the switch in the converter's duty ratio adjustment by adding a PID (proportional, integral, derivative) controller is considered with the feedback received from the output voltage and comparing with the reference voltage that is equal to the desired voltage of the load. In order to design the controller, a circuit equation is created based on considering the effect of circuit elements on the output voltage. PID parameters are determined using the considered equation [25].

The output signal of the PID controller A is obtained by using the relation of inductor L_2 current with the output voltage.

$$C_0 \cdot \frac{dV_1}{dt} + \frac{V_1}{R_1} = (i_{L2})(1 - D) = A \tag{11}$$

Figure 9 presents the general scheme of a conventional PID-controller. As can be seen, the output voltage of the converter is measured at the specified time intervals and is compared with the desired voltage of the load. Then, the difference of these voltages can be changed the duty ratio of the power switch to seizure the accurate output voltage. Three coefficients for a PID controller are applied can be seen by K_P , K_I , and K_D indexes in this figure. K_P , K_I , and K_D coefficients indicate the proportional, integral and derivative terms. The value of these coefficients should be obtained through an accurate equation between the output voltage and one of the current derivation equations of the inductors or voltage derivations of the capacitors. The simplest equation should be selected for preventing the complexity of the controller mathematical design. Equation (11) is one of these simple equations that presents a relation between the output voltage and current of the inductor L_2 .

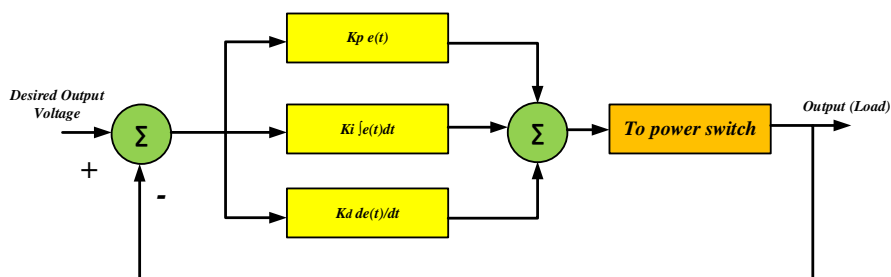


Figure 9. General PID controller with feedback path and coefficients.

Figure 10 presents the model used for the proposed converter in MATLAB/SIMULINK. For obtaining this model, by considering figure 9 and equation 12, the value of the coefficients should be determined.

$$y(t) = K_p e(t) + K_i \int e(t) dt + K_d \frac{de(t)}{e(t)} \tag{12}$$

In this equation, $y(t)$ and $e(t)$ are the output voltage and the error signal can be obtained from the difference of the measured and desired output voltages. By pairing the $y(t)$ with $V_1(t)$ in equation 11 and equalizing with equation 12, the value of the K_p , K_i , and K_D coefficients can be obtained as $K_p = 0.0375$, $K_i = 1.275$ and $K_D = 0.000003$ respectively.

The control circuit is shown in Figures 9 and 10, and the final form of the converter in boost mode is illustrated in Figure 11.

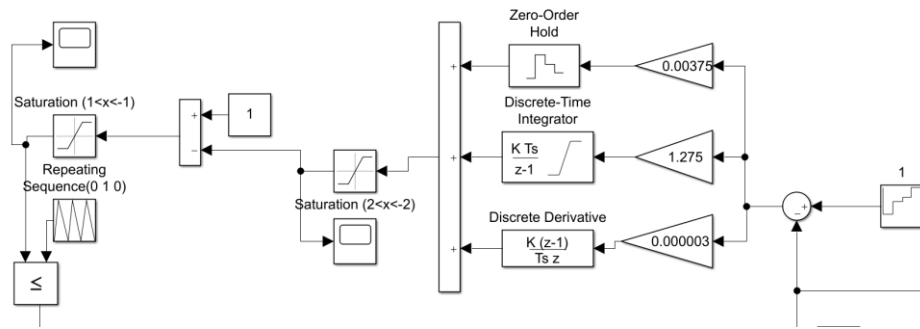


Figure 10. Controller circuit diagram of the converter.

Results were obtained at 4 different voltage levels with the reaction of the designed controller. The switching frequency has been chosen equal to 20 kHz to reduce the switching losses and the losses of the circuit elements. Different input voltages equal to 20, 150, 200, and 300 V are selected for the voltage reference. Figure 11 presents a MATLAB/SIMULINK model including the proposed converter and the controller equipped with a PV panel than can show the performance of the suggested topology for PV applications.

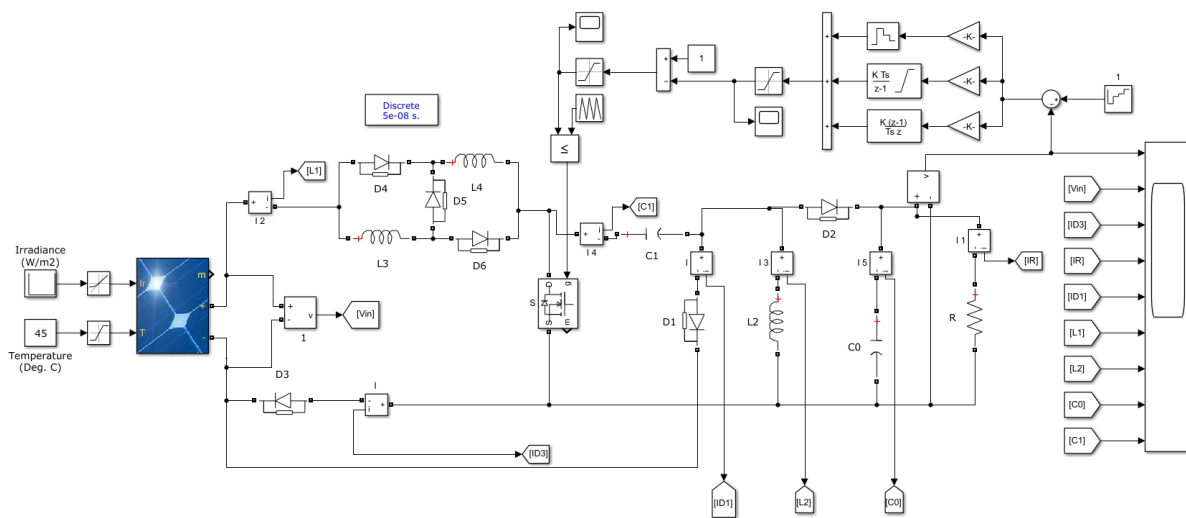


Figure 11. Proposed DC-DC Converter with a designed PID controller.

As can be seen different measurements for currents and voltages can be considered. The specifications of the PV panel can be changed based on the datasheet features of the panel in MATLAB.

Figure 12 shows the results obtained. Only output voltage and current have been added for detailed viewing.

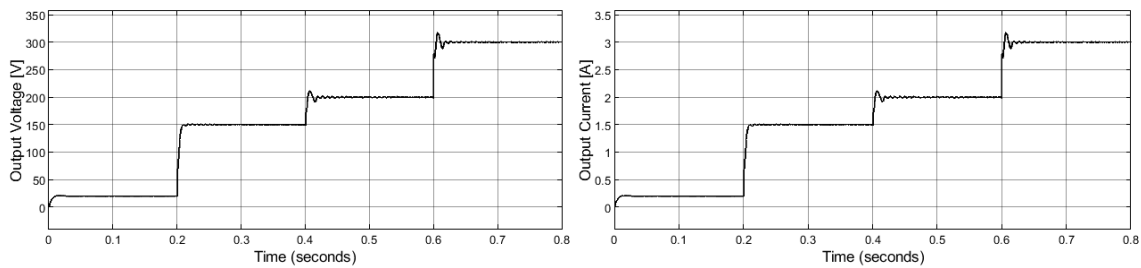


Figure 12. Output voltage and output current values obtained as a result of controller references.

The results in figure 12 show that the controller can accurately track the desired output voltages and the current of the load linearly can change with the output power value. Four 20, 150, 200, and 300 volts as the desired output voltages are selected and figure 12 shows that the tracking of the low voltages is simpler since the difference between the input and output voltages is less. For higher DC voltages a larger duty ratio is needed and this impacts the performance of the controller but with the proposed switch-inductor and capacitor blocks a part of the voltage boosting process is done by these blocks that can help the switch with lower duty cycles. As can be seen from figure 12, the output voltage is tracking the reference voltages and the controller's reaction is considerable. When the reference voltage changes, the controller receives the desired voltage and currents with a short damping time and limited voltage and current fluctuation.

For the simulation process in MATLAB, JIYANGYIN 200W PV panels are used. The test has been done under 45°C. Each panel generates about 200W power and the proposed DC-DC converter is applied to fix the output voltage at the 20, 150, 200, and 300 VDCs.

Figure 13 presents the efficiency of the converter under the proposed PID controller with 1000W output power with the conventional boost converter at the same working conditions and output voltages.

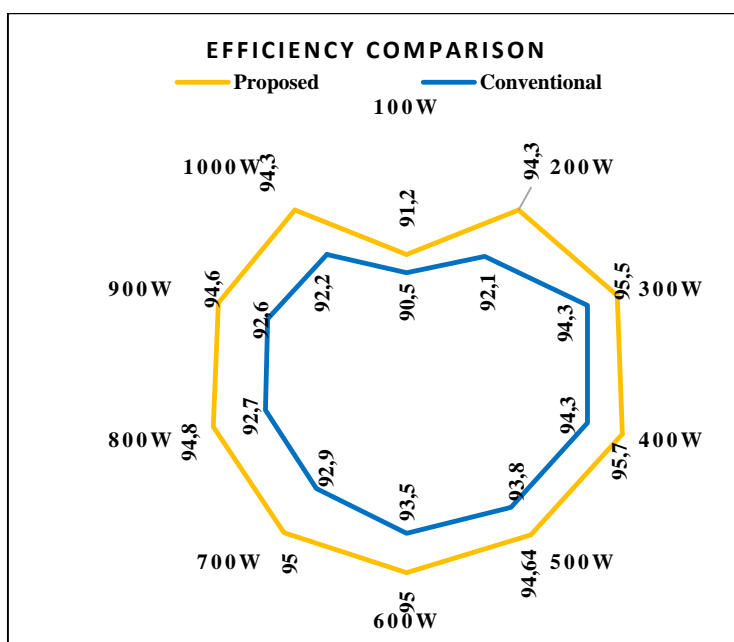


Figure 13. Efficiency comparison for the selected and cascaded converters.

5. Conclusion

An improved SEPIC-based buck-boost DC-DC converter has been provided to operate both as a boost and as a buck topology to be used in solar panel applications. Switched-capacitor and switched-inductor structures that can be used in the circuit were examined. Since for grid applications, a high voltage approached is more important. Therefore, the converter's reaction in boost mode and the switched-inductor structure was considered in more detail. Thanks to this structure's use, the duty ratio was decreased compared to the non-attached version of this structure, and a longer and stable operation of the circuit was planned. A controller has been designed for the circuit. Using the mathematics of this converter circuit, the PID controller was added to the system and operated carefully. The controller's main equation is considered according to the mathematical relations between the output voltage and one of the current equations of the inductors or voltage equations of the capacitors. The selected equation has the minimum complexity and has more suitable for hardware implementations.

References

- [1] Erickson, R. W., & Maksimovic, D. (2007). *Fundamentals of power electronics*. Springer Science & Business Media.
- [2] Ghaderi D, Molaverdi D, Kokabi A, Papari B. A multi-phase impedance source inverter with an improved controller structure. *Electr Eng* 2020;102(2):683–700. <https://doi.org/10.1007/s00202-019-00903-9>.
- [3] Li S, Subramaniam U, Yang G, Ghaderi D, Rajabiyou N. Investigation of the thermal loading and random vibration influences on fatigue life of the solder joints for a metal-oxide-semiconductor-field-effect transistor in a DC-DC power boost converter. *IEEE Access* 2020; 8:64011–9. <https://doi.org/10.1109/ACCESS.2020.2985320>.
- [4] Ghaderi Davood, Padmanaban Sanjeevikumar, Maroti Pandav Kiran, Papari Behnaz, Holm-Nielsen Jens Bo. Design and implementation of an improved sinusoidal controller for a two-phase enhanced impedance source boost inverter. *Comput Electr Eng* 2020;83. <https://doi.org/10.1016/j.compeleceng.2020.106575>.
- [5] Ghaderi D. An FPGA-based switching photovoltaic-connected inverter topology for leakage current suppression in grid-connected utilizations. *Int J Circ Theor Appl* 2020;1–20. <https://doi.org/10.1002/cta.2844>.
- [6] Huang R, Hong F, Ghaderi D. Sliding mode controller-based e-bike charging station for photovoltaic applications. *Int Trans Electr Energy Syst* 2020. <https://doi.org/10.1002/2050-7038.12300>.
- [7] Bayrak G, Ghaderi D. An improved step-up converter with a developed real-time fuzzy-based MPPT controller for PV-based residential applications. *Int Trans Electr Energy Syst*. 2019: e12140. <https://doi.org/10.1002/2050-7038.12140>.
- [8] Ghaderi D, Maroti PK, Sanjeevikumar P, Holm-Nielsen JB, Hossain E, Nayyar A. A modified step-up converter with small signal analysis-based controller for renewable resource applications. *Appl. Sci.* 2020; 10:102.
- [9] Ghaderi D, Bayrak G. A novel step-up power converter configuration for solar energy application. *Elektronika Ir Elektrotechnika* 2019;25(3):50–5. <https://doi.org/10.5755/j01.eie.25.3.23676>.
- [10] Ghaderi D, Celebi M, Minaz MR, Toren M. Efficiency improvement for a DC-DC quadratic power boost converter by applying a switch turn-off lossless snubber structure based on zero voltage switching. *Elektronika Ir Elektrotechnika* 2018;24 (3):15–22. <https://doi.org/10.5755/j01.eie.24.3.20977>
- [11] Ghaderi D, Bayrak G. Performance Assessment of a High-Powered Boost Converter for Photovoltaic Residential Implementations. *Elektronika Ir Elektrotechnika* 2019; 25(6):40–7. <https://doi.org/10.5755/j01.eie.25.6.24825>.

- [12] Qun Qi, Davood Ghaderi, Josep M. Guerrero, Sliding mode controller-based switched-capacitor-based high DC gain and low voltage stress DC-DC boost converter for photovoltaic applications, *International Journal of Electrical Power & Energy Systems*, Volume 125, 2021, 106496, <https://doi.org/10.1016/j.ijepes.2020.106496>.
- [13] H. Liu and F. Li, "A Novel High Step-up Converter With a Quasi-active Switched-Inductor Structure for Renewable Energy Systems," in *IEEE Transactions on Power Electronics*, vol. 31, no. 7, pp. 5030-5039, July 2016, doi: 10.1109/TPEL.2015.2480115.
- [14] V. Balasubramanian, V. S. Nayagam and J. Pradeep, "Alleviate the voltage gain of high step-up DC to DC converter using quasi active switched inductor structure for renewable energy," 2017 International Conference on Computation of Power, Energy Information and Commuincation (ICCPEIC), Melmaruvathur, 2017, pp. 835-841, doi: 10.1109/ICCPEIC.2017.8290482.
- [15] Z. Chen, Y. Chen, C. Jiang, B. Zhang and D. Qiu, "A quasi-Z source network with multiple switch-inductor cells and Cockroft-walton voltage multipliers," *IECON 2017 - 43rd Annual Conference of the IEEE Industrial Electronics Society*, Beijing, 2017, pp. 8009-8014, doi: 10.1109/IECON.2017.8217405.
- [16] M. O. Badawy, Y. Sozer and J. A. De Abreu-Garcia, "A Novel Control for a Cascaded Buck–Boost PFC Converter Operating in Discontinuous Capacitor Voltage Mode," in *IEEE Transactions on Industrial Electronics*, vol. 63, no. 7, pp. 4198-4210, July 2016, doi: 10.1109/TIE.2016.2539247.
- [17] Q. Lei, F. Z. Peng and S. Yang, "Discontinuous operation modes of current-fed Quasi-Z-Source inverter," 2011 Twenty-Sixth Annual IEEE Applied Power Electronics Conference and Exposition (APEC), Fort Worth, TX, 2011, pp. 437-441, doi: 10.1109/APEC.2011.5744633.
- [18] Y. Tang, D. Fu, T. Wang and Z. Xu, "Analysis of Active-Network Converter With Coupled Inductors," in *IEEE Transactions on Power Electronics*, vol. 30, no. 9, pp. 4874-4882, Sept. 2015, doi: 10.1109/TPEL.2014.2363662.
- [19] Y. Tang, D. Fu, J. Kan and T. Wang, "Dual Switches DC/DC Converter With Three-Winding-Coupled Inductor and Charge Pump," in *IEEE Transactions on Power Electronics*, vol. 31, no. 1, pp. 461-469, Jan. 2016, doi: 10.1109/TPEL.2015.2410803.
- [20] B. Axelrod, Y. Berkovich and A. Ioinovici, "Switched-Capacitor/Switched-Inductor Structures for Getting Transformerless Hybrid DC–DC PWM Converters," in *IEEE Transactions on Circuits and Systems I: Regular Papers*, vol. 55, no. 2, pp. 687-696, March 2008, doi: 10.1109/TCSI.2008.916403.
- [21] O. Abdel-Rahim and H. Wang, "A new high gain DC-DC converter with model-predictive-control based MPPT technique for photovoltaic systems," in *CPSS Transactions on Power Electronics and Applications*, vol. 5, no. 2, pp. 191-200, June 2020, doi: 10.24295/CPSSTPEA.2020.00016.
- [22] O. Abdel-Rahim, Z. M. Ali and S. Kamel, "Switched inductor switched capacitor based active network inverter for photovoltaic applications," 2018 International Conference on Innovative Trends in Computer Engineering (ITCE), Aswan, 2018, pp. 410-412, doi: 10.1109/ITCE.2018.8316659.
- [23] R. Cakmak, I. H. Altas and A. M. Sharaf, "Modeling of FLC-Incremental based MPPT using DC-DC boost converter for standalone PV system," 2012 International Symposium on Innovations in Intelligent Systems and Applications, Trabzon, 2012, pp. 1-5, doi: 10.1109/INISTA.2012.6246932.
- [24] Karthikeyan, V., Sundaramoorthy, K., Kumar, G. G., & Babaei, E. (2019). Regenerative switched-inductor/capacitor type DC–DC converter with large voltage gain for PV applications. *IET Power Electronics*, 13(1), 68-77.
- [25] Fey, A. N., Romaneli, E. F. R., Fernandes, L. G., & Gules, R. (2018, November). A Switched-Capacitor Double Boost Converter for a Photovoltaic Application. In 2018 13th IEEE International Conference on Industry Applications (INDUSCON) (pp. 126-130). IEEE.
- [26] Fu, J., Zhang, B., Qiu, D., & Xiao, W. (2014, August). A novel single-switch cascaded DC-DC converter of boost and buck-boost converters. In 2014 16th European Conference on Power Electronics and Applications (pp. 1-9). IEEE.

- [27] Axelrod, B., Berkovich, Y., & Ioinovici, A. (2008). Switched-capacitor/switched-inductor structures for getting transformerless hybrid DC-DC PWM converters. *IEEE Transactions on Circuits and Systems I: Regular Papers*, 55(2), 687-696.
- [28] S. H. Chincholkar, W. Jiang, and C. Chan, "An Improved PWM-Based Sliding-Mode Controller for a DC-DC Cascade Boost Converter," in *IEEE Transactions on Circuits and Systems II: Express Briefs*, vol. 65, no. 11, pp. 1639-1643, Nov. 2018, doi: 10.1109/TCSII.2017.2754292.
- [29] J. Wu and Y. Lu, "Adaptive Backstepping Sliding Mode Control for Boost Converter With Constant Power Load," in *IEEE Access*, vol. 7, pp. 50797-50807, 2019, doi: 10.1109/ACCESS.2019.2910936.
- [30] S. H. Chincholkar, W. Jiang and C. Chan, "A Normalized Output Error-Based Sliding-Mode Controller for the DC-DC Cascade Boost Converter," in *IEEE Transactions on Circuits and Systems II: Express Briefs*, vol. 67, no. 1, pp. 92-96, Jan. 2020, doi: 10.1109/TCSII.2019.2899388.
- [31] P. K. Ray, S. R. Das, and A. Mohanty, "Fuzzy-Controller-Designed-PV-Based Custom Power Device for Power Quality Enhancement," *IEEE Transactions on Energy Conversion*, vol. 34, no. 1, pp. 405-414, March 2019, doi: 10.1109/TEC.2018.2880593.
- [32] S. K. Gadari, P. Kumar, K. Mishra, A. R. Bhowmik and A. Kumar Chakraborty, "Detailed analysis of Fuzzy Logic Controller for Second-order DC-DC Converters," 2019 8th International Conference on Power Systems (ICPS), Jaipur, India, 2019, pp. 1-6, doi: 10.1109/ICPS48983.2019.9067607.
- [33] S. Maity et al., "Performance Analysis of Fuzzy Logic Controlled DC-DC Converters," 2019 International Conference on Communication and Signal Processing (ICCSP), Chennai, India, 2019, pp. 0165-0171, doi: 10.1109/ICCSP.2019.8698113.
- [34] H. Bai, C. Liu, S. Zhuo, R. Ma, D. Paire, and F. Gao, "FPGA-Based Device-Level Electro-Thermal Modeling of Floating Interleaved Boost Converter for Fuel Cell Hardware-in-the-Loop Applications," in *IEEE Transactions on Industry Applications*, vol. 55, no. 5, pp. 5300-5310, Sept.-Oct. 2019, doi: 10.1109/TIA.2019.2918048.
- [35] D. Ghaderi and M. Çelebi, "Implementation of load sharing with fast voltage regulation in parallel connected cascaded power boost converters based on droop coefficients refreshing method," 2017 9th International Conference on Computational Intelligence and Communication Networks (CICN), Girne, 2017, pp. 195-199, doi: 10.1109/CICN.2017.8319384.
- [36] D. Ghaderi, "A PID-Fuzzy Based Controller for Three-Phase Solar Network," 2019 11th International Conference on Electrical and Electronics Engineering (ELECO), Bursa, Turkey, 2019, pp. 323-328, doi: 10.23919/ELECO47770.2019.8990482.
- [37] D. Ghaderi, "A Multi-Level DC-DC Converter Configuration for PV Applications," 2019 11th International Conference on Electrical and Electronics Engineering (ELECO), Bursa, Turkey, 2019, pp. 225-229, doi: 10.23919/ELECO47770.2019.8990532.
- [38] Ghaderi Davood, Çelebi Mehmet, Implementation of PI Controlled Cascaded Boost Power Converters in Parallel Connection with High Efficiency, *Journal of Electrical Systems*; Paris Vol. 13, Iss. 2, (2017): 307-321.
- [39] K. K. Nimisha and R. Senthilkumar, "A Survey On Optimal Tuning Of PID Controller For Buck-Boost converter Using Cuckoo-Search Algorithm," 2018 International Conference on Control, Power, Communication and Computing Technologies (ICCPCT), Kannur, 2018, pp. 216-221, doi: 10.1109/ICPCT.2018.8574321.

An Action Management System Design and Case Study on Its Usage for Cyber Fraud Prevention and Risk Analysis

Abdulkadir Battal ¹ , Ruya Samli ^{1*} 

^{1*} Department of Computer Engineering, Istanbul University-Cerrahpasa, Istanbul, Turkey.

Cite this paper as:

Battal, A., Samli, R. (2021). *An Action Management System Design and Case Study on Its Usage for Cyber Fraud Prevention and Risk Analysis*. Journal of Innovative Science and Engineering. 5(2): 143-161

*Corresponding author: Ruya Samli
E-mail: ruyasamli@iuc.edu.tr

Received Date: 28/12/2020
Accepted Date: 23/05/2021
© Copyright 2021 by
Bursa Technical University. Available
online at <http://jise.btu.edu.tr/>



The works published in Journal of Innovative Science and Engineering (JISE) are licensed under a Creative Commons Attribution-NonCommercial 4.0 International License.

Abstract

Today, various types of devices are used to be connected to Internet at every moment of the life. This variety of devices present both benefits and problems to individuals and companies. One of the more important problems in cyber world is “fraud detection”. It is known that, malicious uses in the cyber world are increasing rapidly, fraudsters who seek openness in systems cause material and moral damages to both individuals and companies. In the relevant literature, there are many studies on the detection and prevention of cyber frauds in many sectors such as finance, telecommunication and online shopping. This study aims to develop an action management system to detect cyber frauds and follow the actions of the cases with automatic workflows so as to protect the users according to their next actions. It also reveals the results of this action management system’s usage in a case study of a telecommunication company in Turkey.

Keywords: Action management system, risk analysis, cyber fraud

1. Introduction

In today's digital world, information technologies are used to provide many personal and corporate transactions. While transactions over the Internet provide many advantages to both individuals and corporations such as speed, time-saving, labour-saving and convenience, the security of these transactions is becoming a serious issue. In the cyber world, for the safe completion of transactions; the users must ensure that the information is transmitted to the other party without any corruption (integrity), the information is not received by another person (confidentiality) and the individual/company that received the information is the one to whom the information is intended to be sent (authentication). Each of these topics gains importance day by day in cyber security world. The topic handled in this study is "confidentiality". Today, as the type, the amount and the importance of the information shared over the Internet increase, the possibility of the information being received by any unauthorized persons also increases. Cyber-attacks or/and cyber wars intrude from the systems of individuals, institutions and even countries and receive their information. As this situation causes high material and moral damages, large scale studies are being conducted for analyzing attack risks and detecting/preventing attacks. It is of great importance that a cyber-attack on an institution can be determined in advance and as a result, be prevented. However, it can be possible only with an accurate risk analysis. This study aims to develop an action management system to prevent cyber fraud which can be accepted as a form of cyber-attack and also, perform risk analysis. The action management system is a structure that ensures the correct and safe processing of actions that need to be taken automatically for workflows. If the actions in the workflows are handled correctly and safely, then cyber-crimes will decrease significantly and possible attacks will be able to be prevented.

The rest of this study is organized as follows: In Section 2, a wide range of literature review is carried out. In Section 3, the technological structures of the application developed in this study are explained. In Section 4, the developed application is explained by examples, and also the results of a case study of this implementation in a telecommunication company of Turkey are given. The study is concluded in Section 5.

2. Related Works

2.1. Studies About Action Management Systems

Especially companies that provide services to a large number of customers use systems that take automatic actions in certain situations in order to prevent assigning all the work to the employees. By automating some of the actions, more work can be accomplished in a shorter time frame. Particularly, action systems that is related with "fraud and risk management" are becoming more common every day. These systems are generally configured with a marker and do not allow the action units to be used separately. The information of the action is uploaded to the system and the action is taken automatically after the process definitions. Information on how the processes are defined or which parts of the processes are available cannot be accessed. Furthermore, in systems of the prior art, structured and sequential actions cannot be provided, since the user's interaction with the system is kept to a minimum value. There are some patents on this subject in the literature. The patent [1] discloses an action method and apparatus for determining the dynamic flow in distributed systems. The dynamic flow detection apparatus enables dynamic determination of flow through the action chain in event processing performed in the distributed system. The fact that actions are general and independent enables event processing to take place or to be changed flexibly. The patent [2] discloses a method and system for setting up,

processing and implementing scenarios in event-based information systems. The present invention allows the actions to be reused in specified scenarios, to collect action and action chains throughout the scenario, and to minimize the operations in each defined scenario. The workflow management system mentioned in a patent given by [3] provides computer-aided, graphical tools for defining and managing complex processes in terms of workflow. The patent [4] discloses a workflow management system that automates the definition and application of a process that can be performed according to defined rules. The system is used to ensure that all individual activities are received in defined sequence, form and time. The system is based on three bases (coordination unit, organization unit and messaging unit). In [5], a selective action management system across a computer system was presented. In this action management system, actions can be selectively retrieved, fixed and reconfigured. In [6], the patent mentions an action management system that is responsible for managing and supporting the work of various tasks in production. The system uses process information defining the flow of many jobs in a task executed by at least one person and product information comprising the content of a product produced in each of the many jobs. It also includes a controller that controls the system to control the relationship between product information and most of the tasks, the input and output information, and the relationship that includes a product generated in each task immediately before each task, and a memory that stores and holds each of the work and the associated product information.

2.2. Studies About Cyber Fraud

Since investigating cyber fraud is a very popular and wide concept, many studies on this subject have been carried out in the related literature. Some of these studies have developed a new system for detecting cyber fraud in a private company or institution, some have investigated the reasons and some have researched on how to detect cyber fraud. In the study [7], it is aimed to use an anomaly detection algorithm performed using data mining for fraud detection in some transactions performed over the Internet in real-time. In this study, credit card fraud has been handled specifically between anomalies and cyber frauds. The aforementioned anomaly detection algorithm is based on Artificial Neural Networks (ANN) and is designed by using supervised learning. The study [8] attempted to identify cyber frauds on a global digital network and stated that cyber frauds are riskier than many other threats and must be identified and prevented surely. In [9], it is presented a framework designed to build Internet banking security based on a multi-layered ANN. This system, which can detect anomaly detection, intrusion detection and cyber fraud, has made significant gains by identifying these threats which are particularly harmful in financial terms. The study [10], which is conducted on 22 banks in total, identified deficits caused by lack of information and carelessness, identified cyber fraud transactions performed by using these deficits and took necessary measures. In [11], a cyber-fraud detection system using ANN was developed. In [12], cyber frauds in the banking sector were tried to be determined by the behavior of the customers and the transactions they performed. In this study, a combination of data mining, artificial intelligence and classification methods has been used and thus, frauds have been identified. The study [13] aimed to detect cyber frauds in online finance systems using blockchain technology. The study given by [14] designed a system that uses the Hidden Markov Model (HMM) to detect online frauds. In the study [15], cyber frauds about smart grid energy were determined by using ANN. This study presents a new application based on machine learning to determine energy consumption. The study [16] developed a system that uses Bidirectional Associative Memory (BAM) to detect cyber fraud in mobile phones. The main advantage of the system is the ability to detect not only cyber frauds, but also real-time frauds. In [17], cyber frauds were identified by using self-organizing maps.

There are also some survey studies about cyber fraud in the literature. The study [18] surveyed several techniques for detecting credit card frauds. In this study, some techniques such as ANN, artificial intelligence, Bayesian, data mining, k-nearest neighborhood, decision tree, fuzzy logic, Support Vector Machine (SVM), machine learning and genetic algorithm are examined. The study [19] examined the studies on the detection of cyber frauds in the field of e-commerce. The study [20] is one of the largest studies on cyber fraud detection which have focused on how to detect cyber fraud in many areas such as e-commerce systems, health systems, credit cards, and so on.

There are also several patent designs related to cyber fraud detection. The patents given by [21-23] have tried to detect frauds in health systems. The systems designed in these patents try to detect anomalies in health and analyze to distinguish frauds between these anomalies. The patent given by [24] designed a system for detecting frauds in interactive link analysis and the patent [25] developed a complete system of a device and software for detecting cyber frauds.

3. Material and Methods

Fraud detection systems consist of four main steps: data collection, detection, examination and action. In this study, an action management system that simulates all these steps was designed. In this system, the actions defined by the user throughout the smallest building blocks are recorded in the system and depending on the action building blocks; it is ensured that it is operated safely and sequentially according to the rules previously determined by the user.

3.1. Methods and Technologies

This section describes the methods and the technologies used for the designed action management system. These methods and technologies are as follows: Spring framework, Hibernate framework, Java messaging service, Quartz framework, Ehcache framework, microservice architecture and database.

Spring is an open source application development framework for Java and can be considered as “framework of frameworks” because it supports the use of frameworks such as Hibernate and Quartz. Hibernate is an object/relational mapping library designed for software developers. By providing the relationship with the database according to the object-oriented models, it simplifies the operations performed on the database and also strengthens the established structure. Java Messaging Service (JMS) is a synchronous or asynchronous programming interface that enables messaging between Application Programming Interface (API) software. In software projects, there is an increase in the dimension of the code when new functionality features are added. After a while, it becomes difficult to dominate the project because of this increase. In order to combat such problems in a monolithic project, abstractions and modules are created in the code as much as possible. Micro-service is the name given to this type of small and co-operating services. Quartz is an open source business planning system that can be used for small or large enterprise systems. Basically, the structure proceeds in two stages. Firstly, the active job must be determined. Secondly, the next job is determined. Figure 1 shows the Quartz framework structure.

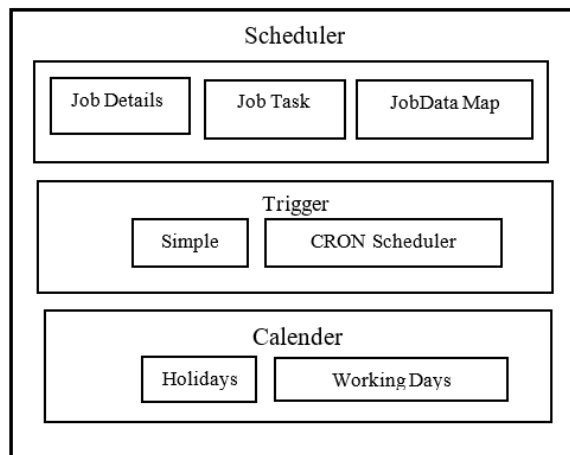


Figure 1. Quartz framework structure

The Ehcache framework is an open source caching mechanism used to improve system performance, reduce database load, and simplify scalability. Ehcache is a very powerful framework, and it has become one of the most widely used Java-based caching mechanisms for distributed caching and for the use of disk memory in cases of insufficient RAM. In Figure 2, Ehcache framework structure is shown.

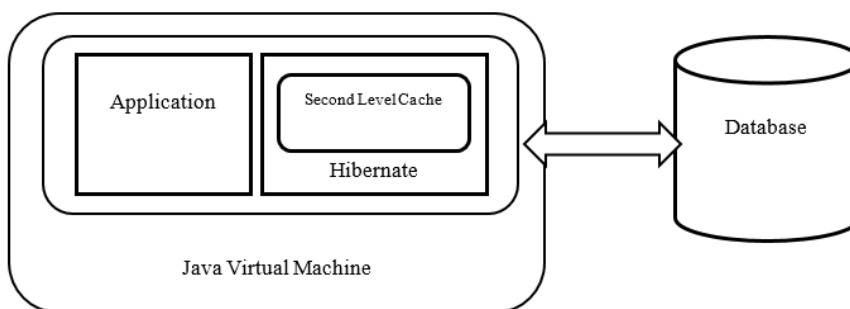


Figure 2. Ehcache framework structure

The application developed during this study has no database dependency. Thanks to the frameworks used, it can work on all of the preferred databases. In this example, the application runs on the Oracle database. Designed with information security and performance in mind, the data in this system can be divided into 4 groups according to the information security and performance. Figure 3 shows the configuration database model of the application.

- Action configuration data: Action data designed by users on the management screens.
- Profile data of the customer: Personal and profile data of the customer.
- Customer-transaction-event data: Customer-owned; motion and event data.
- Action data: The records of the actions taken to the customer.

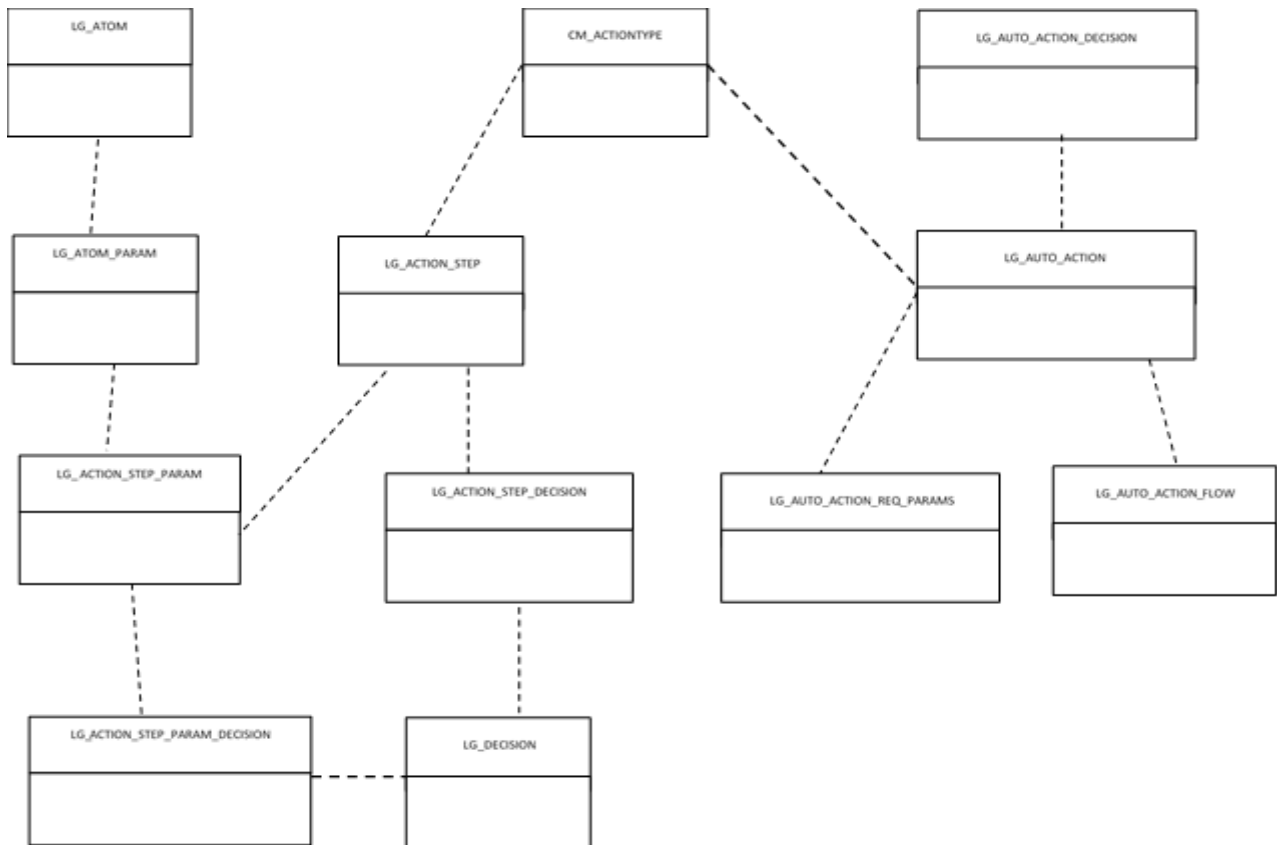


Figure 3. The configuration database model of the application

The tables in this database are described below.

LG_ATOM: It holds the information of atoms which are the basic building block of the action system. The fields in this table are **ATOM_ID** (NUMBER (10)), **NAME** (VARCHAR2 (100 Byte)), **DESCRIPTION** (VARCHAR2 (500 Byte)), **CLASS_NAME** (VARCHAR2 (500 Byte)).

CM_ACTIONTYPE: It holds the information about action types. The fields in this table are **ACTION_CODE** (NUMBER), **ACTION_TYPE** (VARCHAR2 (50 Char)), **MAIN_XML_TEMPLATE** (XMLTYPE), **REF_PARAM_COUNT** (NUMBER), **ENTITY_PARAM_COUNT** (NUMBER), **CHILD_XML_TEMPLATE** (XMLTYPE).

LG_ATOM_PARAM: It holds the parameters of atoms, which are the basic building blocks of the action system. The fields in this table are **ATOM_PARAM_ID** (NUMBER (10)), **ATOM_ID** (NUMBER (10)), **PARAM_NAME** (VARCHAR2 (200 Byte)), **REQUIRED** (NUMBER (1)).

LG_ACTION_STEP: It holds information about the conditions under which the flow will continue. The fields in this table are **ACTION_STEP_ID** (NUMBER (10)), **CM_ACTION_TYPE_ID** (NUMBER (10)), **ATOM_ID** (NUMBER (10)), **NAME** (VARCHAR2 (100 Byte)), **DESCRIPTION** (VARCHAR2 (500 Byte)), **ORDER_NO** (NUMBER (5)), **EXIT_ON_ERROR** (NUMBER (1)), **IS_ROLLBACK_ACTIVE** (NUMBER (1)).

LG_ACTION_STEP_PARAM: It holds the method of calculating the parameters for each step of the action. The fields in this table are **ACTION_STEP_PARAM_ID** (NUMBER (10)), **ACTION_STEP_ID** (NUMBER (10)), **ACTION_PARAM_ID** (NUMBER (10)), **PARAM_SOURCE_ID** (NUMBER (10)), **ORDER_NO** (NUMBER (10)).

LG_ACTION_STEP_DECISION: It holds the decision control conditions for each step of the action. The fields in this table are ID (NUMBER (10)), ACTION_STEP_ID (NUMBER (10)), DECISION_ID (NUMBER (10)), VALUE (VARCHAR2 (1000 Byte)), COMPARISON_TYPE (VARCHAR2 (100 Byte)), EXIT_FROM_ACTION (NUMBER (1)).

LG_ACTION_STEP_PARAM_DECISION: It holds the operating conditions of the parameters for each step of the action. The fields in this table are ID (NUMBER (10)), ACTION_STEP_PARAM_ID (NUMBER (10)), DECISION_ID (NUMBER (10)), VALUE (VARCHAR2 (1000 Byte)), COMPARISON_TYPE (VARCHAR2 (100 Byte)), EXIT_FROM_ACTION (NUMBER (1)).

LG_DECISION: It holds the decision structures of the action system. The fields in this table are DECISION_ID (NUMBER (10)), NAME (VARCHAR2 (500 Byte)), CLASS_NAME (VARCHAR2 (500 Byte)), GUI_SQL_TEXT (CLOB), PARAM_ID (NUMBER (10)), PARAM_SOURCE_ID (NUMBER (10)).

LG_AUTO_ACTION_DECISION: It holds the definitions of decisions for sequential action definitions of the action system. The fields in this table are ID (NUMBER (10)), AUTO_ACTION_ID (NUMBER (10)), PARAM_SOURCE_ID (NUMBER (10)), STATUS (NUMBER (1)), CREATE_DATE (DATE), ORDER_NO (NUMBER (4)), FAIL_AUTO_ACTION_ID (NUMBER (10)), FAIL_MISSION_RM_SRC_ID (NUMBER (10)).

LG_AUTO_ACTION: It holds the sequential action of the action system. The fields in this table are AUTO_ACTION_ID (NUMBER (10)), NAME (VARCHAR2 (100 Byte)), DESCRIPTION (VARCHAR2 (500 Byte)), STATUS (NUMBER (1)), CM_ACTION_TYPE_ID (NUMBER (10)), EVENT_CODE (NUMBER (10)), REASON_CODE (NUMBER (10)), DEFAULT_RUNDATE_IN_MINUTES (NUMBER (10)), RETRY_IN_MINUTES (NUMBER (10)), RETRY_MAX_COUNT (NUMBER (10)), CREATSE_DATE (DATE), DEFAULT_RUNDATE_RULES (VARCHAR2 (100 Byte)), GROUP_NAME (VARCHAR2 (40 Byte)), WAITING_ACTION (NUMBER (5)).

LG_AUTO_ACTION_REQ_PARAMS: It holds the parameter values for sequential action definitions of the action system. The fields in this table are ID (NUMBER (10)), AUTO_ACTION_ID (NUMBER (10)), REF_OR_ENTITY (VARCHAR2 (1 Byte)), NT_PARAM_CODE (NUMBER (10)), PARAM_SOURCE_CODE (NUMBER (10)), STATUS (NUMBER (1)), CREATE_DATE (DATE).

LG_AUTO_ACTION_FLOW: It holds the flow structure for sequential action definitions of the action system. The fields in this table are ID (NUMBER (10)), AUTO_ACTION_ID (NUMBER (10)), PARAM_SOURCE_CODE (NUMBER (10)), NEXT_AUTO_ACTION_ID (NUMBER (10)), ORDER_NO (NUMBER (10)), STATUS (NUMBER (1)), CREATE_DATE (DATE).

3.2 Proposed System

This section describes the design of the application performed in this study. For this purpose, the concepts of the atom, parameter, action, sequential action and decision-control building blocks are explained. Figure 4 shows the proposed system design.

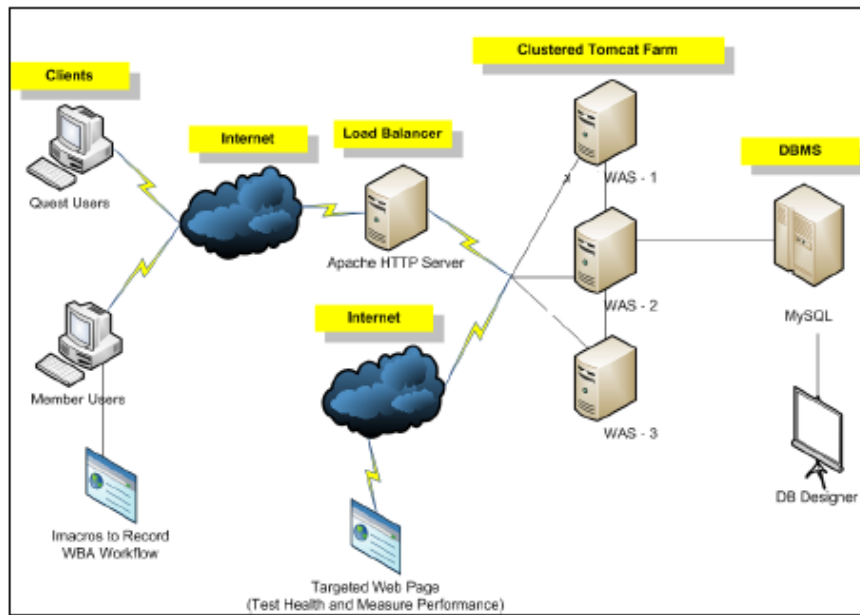


Figure 4. Proposed system design

3.2.1. Atom

Atom is the smallest building block of the designed action management system and is the name of each code snippet that provides the specified interface design. It is designed to perform a certain simple operation. Its task is to perform singular operations. In order to give the system a new simple process, it is necessary to develop it according to the rules and define it to the system. This situation allows the application to have an expandable design. When a new atom is added to the action system, it can be used as an action step to create an action definition. There is three basic information about atoms: performing basic operations, withdrawing the basic operation and keeping the information whether the basic operation is suitable for the withdrawal. Apart from these, there are various atomic processes specific to the application. Examples of atomic transactions are: money withdrawal, invoice opening, list addition, list removal, sequential action request generation.

3.2.2. Parameter

Atoms need some information while they are working. The parameter structure is the structure that allows this information to be automatically retrieved from external systems. This structure allows to read any parameter value with a specified design and provides flexibility during the action by reading the desired type of values from internal or external systems. Using these calculated values, the action is taken for users. The parameter structure of the action system is also designed to expand dynamically. Using the specified design, customized parameter reading services can be added to the action management system. For example, in one embodiment, current debt amount of the subscriber and data subscriber's data service status on-off information can be considered as parameters.

3.2.3. Action

Action is formed by combining one or more action steps. The action steps hold information about the sequence in which they will run, how to proceed if there is an error at which step, and whether there is a process that requires rollback. System administrators design their actions from the action configuration unit and make them requestable from the action collection unit.

3.24. Ordered Action

Ordered Action is the structure that enables the creation of workflows in the action management system. Actions are designed to be self-feeding and can trigger a different action. This triggering occurs through scheduled tasks. A request is left to the queue to run at any time. When the time comes, the conditions of the sequential action are controlled, and a new action is run. Sequential action consists of three foundations. These foundations can be expressed as:

- decision parameters for taking action,
- parameter values required for action
- another action as a scheduled task after the action is taken.

3.25. Decision – Control Building Blocks

The flexible decision-control building blocks provide the control mechanism of the action management system. With the improvements made according to the rules, new decision structures can be added to the action management system. It provides instant access to data from the internal system or external system to change the flow at the time of action and to select the parameters. The general control structures provide the decisions that affect the flow in the action management system by comparing the values with the specified values in the system after reading the values from the desired external systems. Decision-control building blocks are used in two different structures:

- **Parameter Control Structures:** They allow the user to select the parameters of the action step. They provide the parameters under which the system will be retrieved. For example, different conditions may be added to determine the invoice amount when opening a payment invoice. Different amounts of rules are provided to work according to these conditions.
- **Action Step Control Structures:** They allow the user to decide whether operations can be executed during action steps. For example, for a subscriber who does not want a Short Message Service (SMS), the SMS information step may not need to be run.

4. Experimental Study

In this study, an action management system has been designed for the prevention of cyber fraud and risk analysis by using Java programming language, and it was used in a telecommunication company in Turkey. This application, which is designed in accordance with the micro-service architecture and called Lego, consists of a combination of different units operating independently from one another. In this way, application interruptions are kept to a minimum and load distribution is ensured. In this embodiment, the units described below and described in the subsections are included.

In Figure 5, these units were shown.

- Action Configuration Unit
- Action Collection Unit
- Action Management Unit
- Action Processing Unit

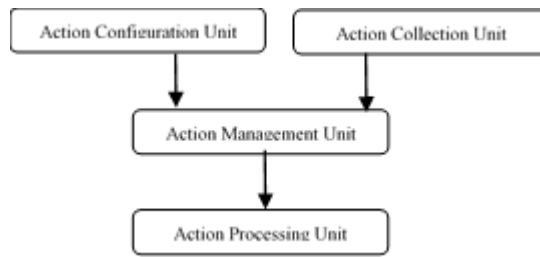


Figure 5. Action units

4.1. Action Configuration Unit

In the study, first of all, Lego Action Configuration Unit was developed using Java programming language. This unit enables the actions to be configured by authorized users from the Action Configuration Unit screens and to be defined from the atoms that are the smallest unit that make up the action. The action consists of at least one structured atom. The structured state of the atoms is called the "Action Step". The unit consisting of atom, input parameters, input parameter controls, atom controls is called action step.

An action can consist of one or more action steps. An action step refers to the smallest unit of work called the atom. For each action step, the required parameter definitions are configured. More than one source can be specified for a parameter. In this case, the priority order of the parameters is determined. In addition, control steps for reading a parameter value are defined. If it passes the control steps, the relevant parameter source is used. If it cannot pass the control step, the next parameter source is passed. Control steps are defined for the action step. Control steps are used to decide whether the action step will run or not. They can be defined in general if necessary, in case of not passing the control defined in this way, the action will be terminated. Each of the action steps is configured for transaction integrity. An action step keeps the information that in case of an error, the next step will be passed, the action will be completed at this step, or the previous steps will be undone. Table 1 shows an example of configuration screen.

Table 1. An example of configuration screen

Step	Order	Name	Exit CnError	Parameters								
				Order	Code Name	Req.	Source	NTParam	Default	Param Decisions		
610	1	Reactivation	√	No records found.								
620	2	Remove Blacklist	X	Order	Code Name	Req.	Source	NTParam	Default	Param Decisions		
				1	ASE_PARAM	true	Ase Param	-	2	Value	Decision	Type
				No records found.								
630	3	Remove FboList	X	Order	Code Name	Req.	Source	NTParam	Default	Param Decisions		
				No records found.								
211	4	Reactivation	X	Order	Code Name	Req.	Source	NTParam	Default	Param Decisions		
				1	YTS_FRAUD	false	Update YTS Fraud	-	1	Value	Decision	Type
				No records found.								
640	6	Auto action	X	Order	Code Name	Req.	Source	NTParam	Default	Param Decisions		
				1	AUTO_ACTION_DEF_ID	false	Update YTS Fraud	-	1622	Value	Decision	Type
				No records found.								
650	7	VAS	X	Order	Code Name	Req.	Source	NTParam	Default	Param Decisions		
				1	SDP_TEMP_BLOCK_FLAG	true	false	-	false	Value	Decision	Type
				No records found.								

As an example, an action consisting of six steps has been created. If the first action step receives an error, the action process will be completed here and will be deemed as incorrect. Since the "exitOnError" feature is not active in the other steps, it can be called optional steps. Again, three decision control structures were added for the first step and the "Exit" feature was defined as active for these steps. In this case, if any decision control is negative, the action process will be terminated and there will be no transition to other steps. In case of positive results from all three controls, the action step

will work. As can be seen on the second step, an atom parameter has been defined and its value is given a fixed value of two. No decision control structure has been added on the parameter.

4.2. Action Collection Unit

In this study, Action Collection Unit was designed secondly. This unit receives the information of the actions to be taken via Representational state transfer (REST) service, which is in communication with the external systems and saves it to the database system. In addition, it is responsible for carrying out the necessary authorization and security controls regarding the actions to be taken. It transmits to the Action Management Unit for simultaneous or asynchronous action processing on demand. Figure 6 shows examples of customer requests and responses in this unit.

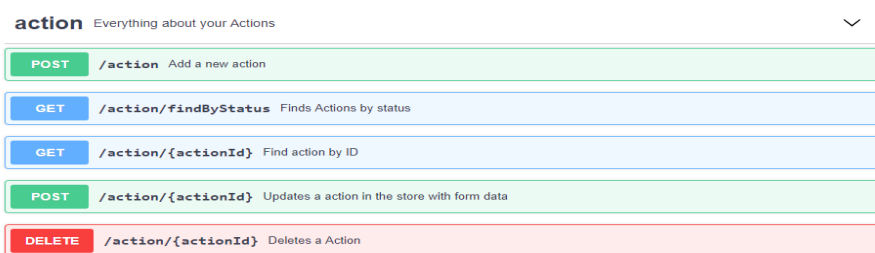


Figure 6. Request and response examples

As shown in Figure 6, the action collection service offers five different operations which are described below.

- **New Action Request:** It enables the action request from external systems to be recorded in the action management system. Authorization checks and time information of the relevant system are determined.
- **Finding Action Request by Status:** Action listing service is offered to external systems. It gives the action list according to date, action status.
- **Find Action with Reference Number:** Another action listing service offered to external systems. It gives the action list according to the reference number.
- **Action Request Update:** It performs the update of action requests from external systems.
- **Action Request Delete:** It performs action cancellation requests from external systems.

An example of action request information is given in Figure 7. As shown in the example, action request data consists of customer information and action information. The applications that make action request indicate which action to take with code. Here, the user is told which action to take and the parameters of the action are transmitted as a list from the key-value structure.

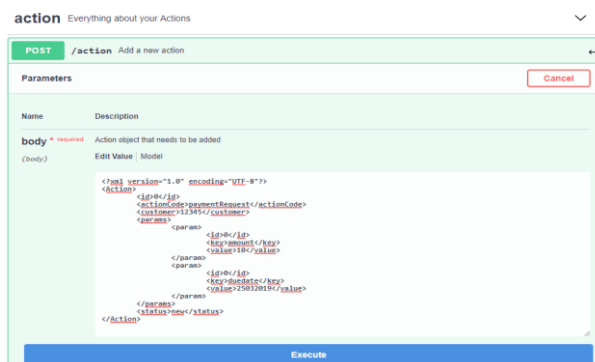


Figure 7. An example action request data

4.3. Action Management Unit

In this study, Action Management Unit was designed as the third. This unit ensures the correct and safe reception of the defined actions and communicates with the Action Collection Unit, the Action Configuration Unit, the Action Processing Unit and the database. The way this unit works consists of the following steps:

- It finds the desired action from the database with the action information collection unit.
- It transmits the small action particles recorded together with the action to the Action Processing Unit for sequential operation in order to fully perform the action.
- It is connected to the Action Processing Unit by taking action particles, conditions and parameters.
- It transmits the action steps to the Action Processing Unit according to the sequence at the specified time.
- The condition connected to the action particles is retrieved from the Action Processing Unit either successfully or unsuccessfully.
- It takes the action results of the action particles from the Action Processing Unit as successful or unsuccessful and records the last status of the action by updating the database.
- Based on the definition of the action particles and the predetermined conditions, it decides on the failure of the action performed by the Action Processing Unit to quit the action and no further processing. Figure 8 is a flow chart of the Action Management Unit.

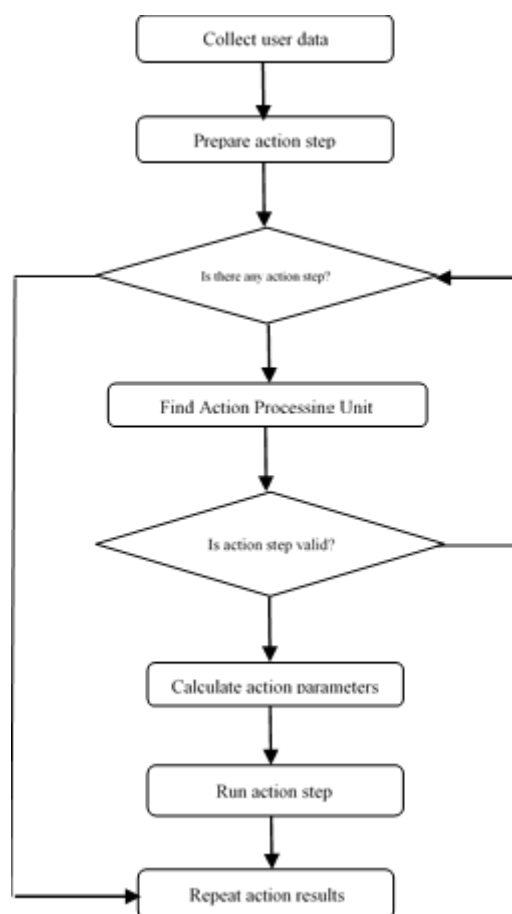


Figure 8. Action Management Unit. Flowchart

The Action Management Unit is responsible for process integrity management at all times. If a step is completed successfully, it completes the relevant records and transaction integrity of the action step; otherwise, it performs process integrity management according to the settings of the action step. At this point, the user decides what to do when he/she gets an error in the step. When an error is received, if there is an adjustment to skip the step, it records the corresponding step incorrectly, undoes the operations of the step and sends a message to the Action Processing Unit for the next step to run. If there is an adjustment to undo all action when it receives an error, it finds the previous running steps and performs the undo procedures for each of these steps. One of the most important parts of the action management system is the decision control structures. These structures, which determine how the action flow occurs, also decide which parameter calculation method to use. Table 2 shows the definitions of an exemplary action step decision control structure.

Table 2. Action step decision control definition

Value	Decision	Exit	Type
1	Reason	√	eq
240	Event	X	eq
1	CustomerType	X	eq
101	CustomerType	X	eq
30	Event	X	eq
OK	Control	√	eq
1	SubscriberType	X	eq

The functional relationships between the selected decision control service and the defined values are listed below.

- **equal to:** In order to accept the result as positive, the value defined in the action step must be equal to the value in the decision-control service.
- **greaterThan:** In order to accept the result as positive, the value defined in the action step must be greater than the value available in the relevant decision-control service.
- **smallerThan:** In order to accept the result as positive, the value defined in the action step must be smaller than the value available in the relevant decision-control service.
- **inList:** In order to accept the result as positive, the value defined in the action step must be equal to one of the values in the relevant decision-control service.

Figure 9 shows an example of a parameter calculation request information.

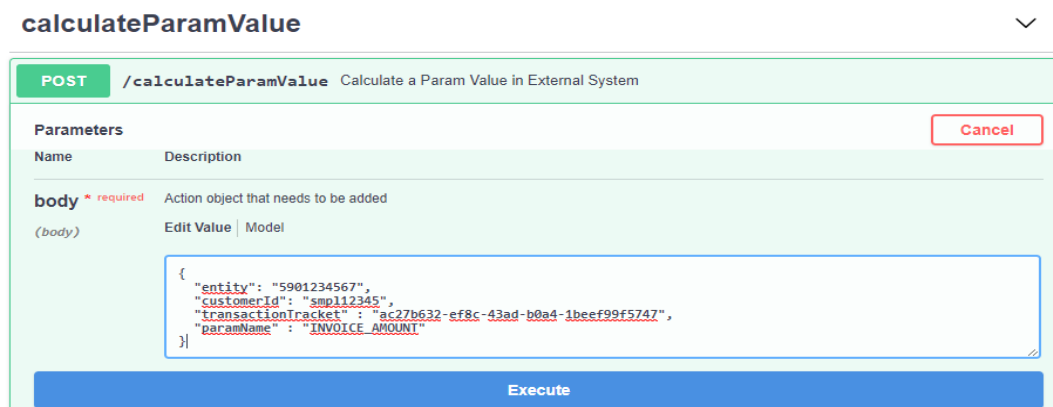


Figure 9. An example of a parameter calculation request information

While the action management system executes the action flow, it manages the flow according to different system variables. In this application, the action management system has gained the ability to manage the flow by reading values over different systems. Thus, faster integration of the action management system in all systems and an increase in development speed has been achieved. For this, a common parametric data reading service structure has been established. It integrates with external systems with a specified REST service interface. Here, responsibility is given to external systems. They are expected to offer services that support a common messaging type. It is ensured that the action management system takes the actions with the correct values by offering the REST services in accordance with the sample in Figure 9 for many different external systems. It is ensured that the latest status of user data in different systems is easily retrieved. Thus, actions are processed more reliably and verified with up-to-date data.

4.4. Action Processing Unit

In this study, Lego Action Processing Unit was developed using Java programming language. The Action Processing Unit in the action management system is in communication with the management unit. The Action Processing Unit manages the processing of the atoms that make up the action so that they can perform the action steps that come to it from the management unit.

The Action Processing Unit manages the calculation of the parameter values of the action step. Thus, it enables the action step to be processed according to the selected parameter values. Parameter definitions of an example action step are shown in Table 3.

Table 3. Action step parameter definition

Order	Code Name	Req.	Source	SQL	NTParam	Default	Param Decisions		
							Value	Decision	Type
1	ADVANCE_AMOUNT	False	70 AMOUNT_REQUEST		70-E		123	Event	eq
							45	Event	eq
							34	Event	eq
							Value	Decision	Type
2	ADVANCE_AMOUNT	False	72 CALCUNBAMT		72-E		49	Event	eq
							Value	Decision	Type
							No records found.		
1	ADVANCE_DUEDATE	False	17 DUEDATE	Service 36	17-E		Value	Decision	Type
3	ADVANCE_AMOUNT	False	70 AMOUNT_REQUEST		70-E	14	Value	Decision	Type
							No records found.		
							No records found.		

The Action Processing Unit will calculate the value of the parameters related to the definitions here. If there is a service parameter definition as a priority, parameter information will be calculated from this service. Then, if there is a variable reading definition for which action is requested, these values are prioritized. If these two last values are undefined, the fixed value definition will be considered. As seen in Table 3, the invoice amount information has been repeated three times. In this case, the calculation of parameter values is processed by the Action Processing Unit in a way that the definition sequence number is taken into account. Again, as seen in Table 3, parameter decision controls are seen. There are three decision control definitions in the first row for the invoice amount parameter. In the second row, there is one decision control definition. If a positive result cannot be obtained from these two control sets, the invoice amount parameter in the third row will be used as an alternative fixed value.

The Action Processing Unit is also responsible for the registration, time and process integrity management of the atoms being operated. The transaction results are returned to the Action Management Unit as successful or unsuccessful. Depending on the definition of the action steps and the pre-determined conditions, if the result of the operation performed

by the Action Processing Unit fails, a message is notified to the management unit in order to exit the action and to revoke all transactions related to the particles that were previously run. Figure 10 shows the flowchart of the Action Processing Unit.

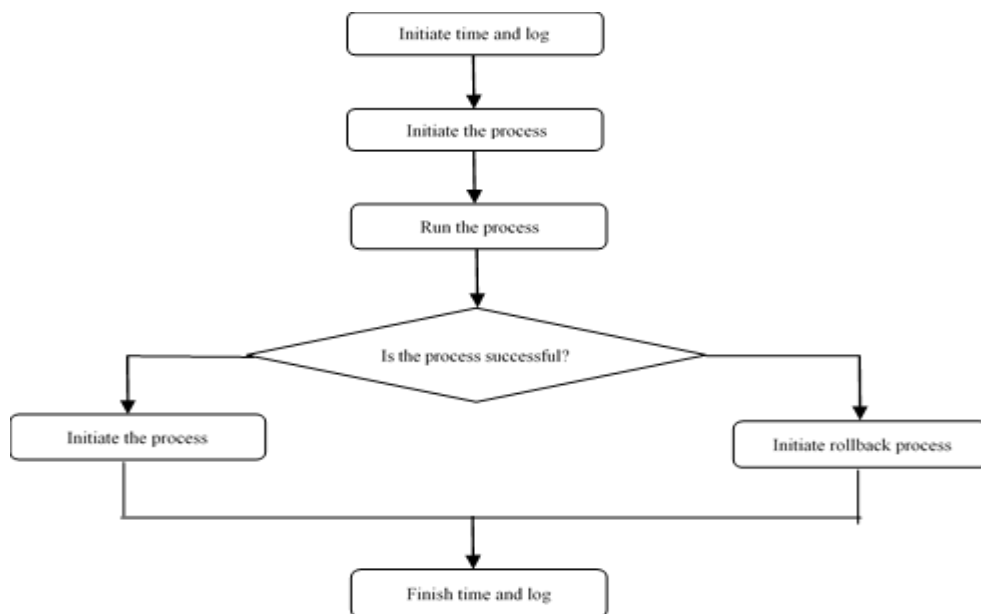


Figure 10. Action processing unit flowchart

Adding New Atom to the Action Processing Unit: Action management systems should ensure that action is taken on all systems with fast integrations in a structure with complex systems. In this application, new atoms that operate on different systems were developed for the action management system, enabling the action management system to manage risky situations in all systems. By connecting to external systems with REST services, which are mostly provided, software development of atoms specific to the system is provided with the messaging types specific to that system. However, it is aimed to ensure faster integration of the action management system in all systems and to increase the speed of development. For this situation, a common atom processing service structure has been established. It can be integrated into external systems with a specified REST service interface. Here, responsibility is given to external systems. They are expected to offer services that support a common messaging type. Thus, the Action Management Unit knows only the Uniform Resource Locator (URL) information of the relevant service, thanks to a common atom development. This service provides actions to be taken in external systems with the requests to be sent to the URL address. Figure 11 shows a sample of the request of the relevant service. Figure 12 shows Action Management System sample application flow.

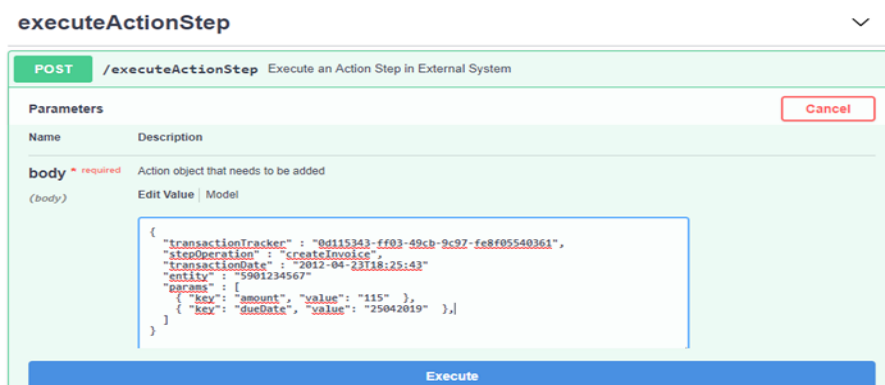


Figure 11. A sample of the request of the relevant service

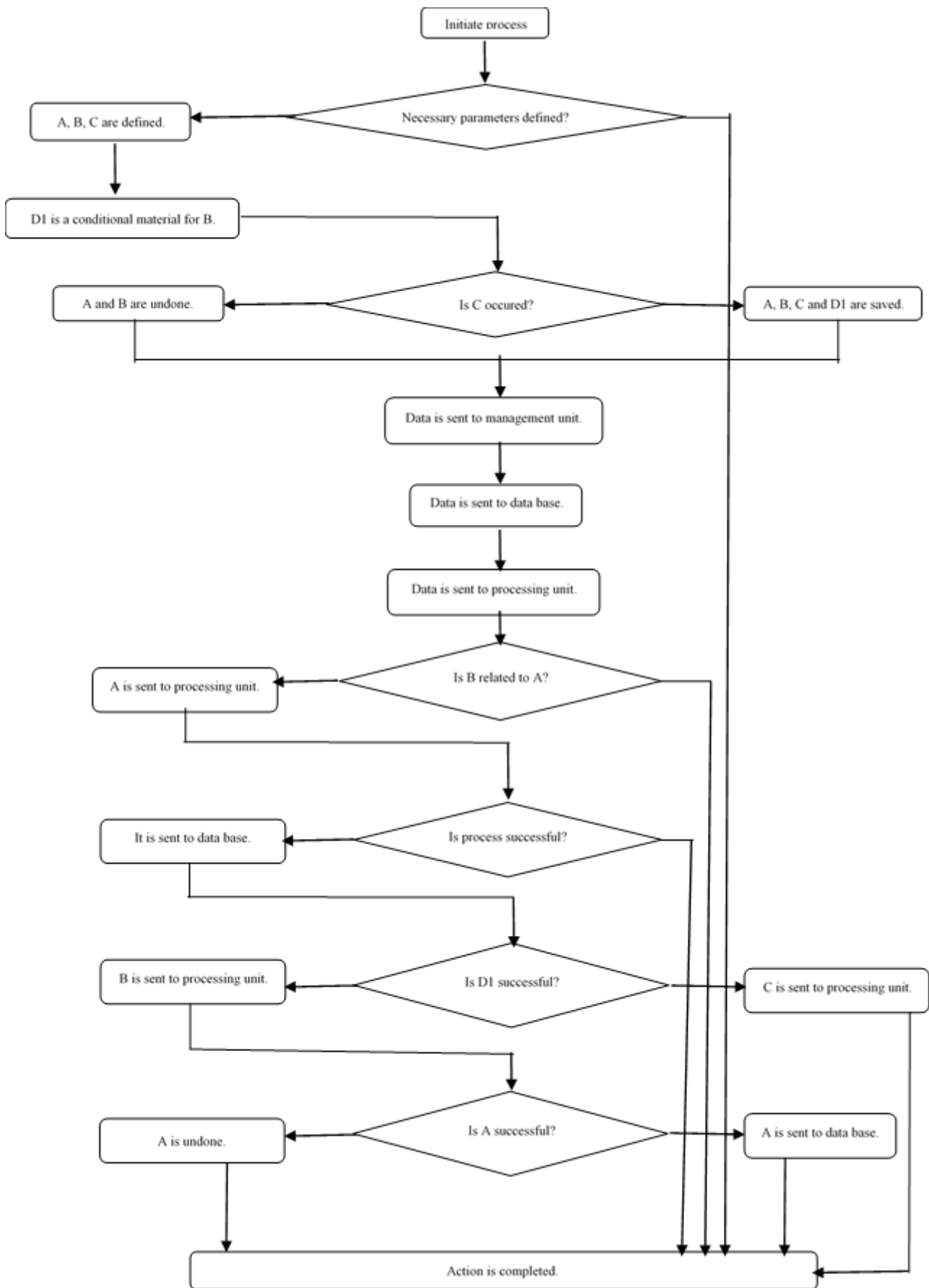


Figure 12. Action Management System sample application flow

4.5. Experimental Results

After the design of the action management system has been completed, case study on its usage for cyber fraud prevention and risk analysis is done with the data of a telecommunication company in Turkey as a case study. The proposed action system was used in 2014 for this case study. Action values obtained before and after the use of this action system are presented in Table 4 as monthly data for 2014 and 2015. After this date, any data cannot be obtained from the company. These data were used to be an example of the usage of proposed action management system. The explanations of the actions in the table are as follows:

- **Action A - Investigation:** The action of suspicious transactions belonging to the subscriber.
- **Action B - Service opening:** The action taken for a subscriber service via SMS, Internet and so on.
- **Action C - Call center:** The action for the information and additional actions made by reaching the subscriber through the call center.
- **Action D - Information:** The action for transactions made to the subscriber via SMS, e-mail, and so on.
- **Action E - Trip:** The action for activation of the search of the line again.
- **Action F - Shutdown:** The action for suspending the search of the line.

Table 4. Action numbers in 2014 and 2015

YEAR-MONTH	ACTION TYPES						TOTAL
	Action A	Action B	Action C	Action D	Action E	Action F	
2014-01	26K	24K	36K	76K	24K	31K	217K
2014-02	23K	36K	35K	75K	24K	26K	219K
2014-03	22K	31K	35K	96K	32K	33K	249K
2014-04	24K	24K	45K	96K	30K	53K	272K
2014-05	21K	21K	34K	81K	33K	44K	234K
2014-06	28K	23K	41K	96K	32K	42K	262K
2014-07	22K	29K	37K	84K	38K	50K	260K
2014-08	38K	23K	34K	89K	51K	71K	306K
2014-09	56K	40K	48K	178K	75K	113K	510K
2014-10	47K	38K	38K	201K	59K	56K	439K
2014-11	46K	33K	46K	270K	54K	66K	515K
2014-12	54K	38K	50K	262K	59K	88K	551K
2015-01	50K	33K	41K	230K	54K	80K	480K
2015-02	48K	34K	32K	218K	48K	69K	449K
2015-03	63K	35K	72K	202K	45K	61K	478K
2015-04	53K	41K	67K	178K	47K	65K	451K
2015-05	50K	28K	58K	192K	39K	50K	417K
2015-06	46K	28K	63K	169K	41K	54K	401K
2015-07	49K	30K	68K	219K	42K	63K	471K
2015-08	45K	29K	74K	207K	48K	82K	485K
2015-09	56K	24K	95K	209K	53K	72K	509K
2015-10	54K	26K	98K	207K	60K	87K	532K
2015-11	66K	28K	86K	193K	54K	73K	500K
2015-12	53K	31K	81K	213K	65K	84K	527K

The results show that, after using the proposed Action Management System, the number and the dimension of all actions (Action A, Action B, Action C, Action D, Action E and Action F) individually and the total number actions captured are increasing except for a few exceptional situations.

5. Conclusion

In this study, an action management system has been developed to ensure that the actions required to be taken automatically in order to protect users from risks in the cyber world are processed correctly and safely. This system allows actions to be defined independently and processed in a user-specific manner, and undertakes all process management tasks. It also provides fast asynchronous return as well as asynchronous operation options for long-term operations and allows the creation of a workflow, allowing sequential operations to be performed reliably in sequence. The action management system provides fast and accurate actions thanks to its flexible and modular configuration. This study is conducted in a telecommunications company in Turkey, it examines the action values prior to and after the use of the system, and the proposed action values are shown to increase with the help of an action management system. Thanks to the system, which does not wait for end-user approval, the following benefits have been observed because reliable actions are taken around specified rules:

- decision-making times are shortened,
- transaction waiting queues are shortened,
- the decision-making process is automated,
- resource utilization is optimized,
- operational costs are reduced,
- human resources are used correctly,
- productivity is increased,
- changes in the action process take place quickly,
- processes are adapted to changing cases quickly,
- human errors are mostly eliminated,
- cases are assigned to the right people when necessary.

References

- [1] Fukuta, S.F.L. and Nishigaya, T.F.N. (2000). Method and apparatus for determining dynamic flow in a distributed system, EP1120710A2 numbered patent.
- [2] Alshab, M.A., Bales, P.J., Covington, R.D., Theophilus, J.D. and Trotter, L.M. (2006). Method and system for building, processing, and maintaining scenarios in event-driven information systems, WO2007035452A1 numbered patent.
- [3] Berg, W.C., McCallum, D.J. and Newman, R.W. (1995). Method and system for managing workflow, US5999911A numbered patent.
- [4] Randell, J. (1996). Workflow real time intervention, US5826020A numbered patent.
- [5] Shapiro, M., O'Brien, J.W., Matheson, C.E., Rodriguez, P.R. and Costa, M. (2003). System-wide selective action management, US7290002B2 numbered patent.

- [6] Kawai, M., Rimoldi, A. and Bassi, G. (2001). Action management support system, US20030233162A1 numbered patent.
- [7] Akhilomen, J. (2013). Data Mining Application for Cyber Credit-Card Fraud Detection System, Industrial Conference on Data Mining, Advances in Data Mining. Applications and Theoretical Aspects.
- [8] Mirea, V., Blăjan, A. and Ionescu, L. (2011). Fraud, Corruption And Cyber Crime In A Global Digital Network, *Economics, Management, and Financial Markets*, 6(2): 373-380.
- [9] Bignell, K.B. (2006). Authentication in an Internet Banking Environment; Towards Developing a Strategy for Fraud Detection, International Conference on Internet Surveillance and Protection.
- [10] Dzumira, S. (2014). Electronic Fraud (Cyber Fraud) Risk In The Banking Industry, Zimbabwe, *Risk Governance & Control: Financial Markets & Institutions*, 4(2): 16-26.
- [11] Arya, A.S., Ravi, V., Tejasviram, V., Sengupta, N. and Kasabov, N. (2016). Cyber fraud detection using evolving spiking neural network, International Conference on Industrial and Information Systems.
- [12] Singh, P. and Singh, M. (2015). Fraud Detection by Monitoring Customer Behavior and Activities, *International Journal of Computer Applications*, 111(11): 23-32.
- [13] Cai, Y. and Zhu, D. (2016). Fraud detections for online businesses: a perspective from blockchain technology, *Financial Innovation*, 2.
- [14] Gupta, P. and Mundra, A. (2015). Online in-auction fraud detection using online hybrid model, International Conference on Computing, Communication & Automation.
- [15] Ford, V., Siraj, A. and Eberle, W. (2014). Smart grid energy fraud detection using artificial neural networks, *IEEE Symposium on Computational Intelligence Applications in Smart Grid*.
- [16] Krenker, A., Volk, M., Sedlar, U., Bešter, J. and Kos, A. (2009). Bidirectional Artificial Neural Networks for Mobile-Phone Fraud Detection, *ETRI Journal*, 31(1): 92-94.
- [17] Olszewski, D. (2014). Fraud detection using self-organizing map visualizing the user profiles, *Knowledge-Based Systems*, 70: 324-334.
- [18] Sethi, N., Gera, A. (2014). A Revived Survey of Various Credit Card Fraud Detection Techniques, *International Journal of Computer Science and Mobile Computing*, 3(4): 780-791.
- [19] Rana, P.J. and Baria, J. (2015). A Survey on Fraud Detection Techniques in Ecommerce, *International Journal of Computer Applications*, 113(14): 5-7.
- [20] Abdallah, A., Maarof, M.A. and Zainal, A. (2016). Fraud detection system: A survey, *Journal of Network and Computer Applications*, 68: 90-113.
- [21] Arkel, J.H.V., Wagner, J.J., Schweyen, C.L., Mahone, S.M., Tada, D.D., Curtis, T.J. and Hagins, S. (2012). Predictive modeling processes for healthcare fraud detection, US20130006668A1 numbered patent.
- [22] Arkel, J.H.V., Wagner, J.J., Schweyen, C.L., Mahone, S.M., Tada, D.D., Curtis, T.J. and Hagins, S. (2012). Near real-time healthcare fraud detection, US20130006655A1 numbered patent.
- [23] Tyler, M., Basant, N., Robin, P. and Rahman, S. (2010). Healthcare insurance claim fraud detection using datasets derived from multiple insurers, US8214232B2 numbered patent.
- [24] Crawford, S.L., Erickson, C., Miagkikh, V., Steele, M., Thorsen, M. and Tolmanov, S. (2008). Systems and methods for fraud detection via interactive link analysis, S20090044279A1 numbered patent.
- [25] Turgeman, A., Kedem, O. and Rivner, U. (2015). Method, device, and system of generating fraud-alerts for cyber-attacks, US9552470B2 numbered patent.

Ultra Small Fluorine Carbon Nanoclusters by Density Functional Theory

Yelda Kadioglu^{1,2} 

¹ Department of Physics, Faculty of Science, Aydın Adnan Menderes University, Aydın, Turkey

² Department of Physics, Faculty of Natural and Mathematical Sciences, University of Maryland Baltimore Country, Baltimore, USA

Cite this paper as:

Kadioglu, Y. (2021). *Ultra Small Fluorine Carbon Nanoclusters by Density Functional Theory*. Journal of Innovative Science and Engineering.5(2):162-172

*Corresponding author: Yelda Kadioglu
E-mail: yeldaakadioglu@gmail.com

Received Date:18/03/2021

Accepted Date:04/06/2021

© Copyright 2021 by

Bursa Technical University. Available
online at <http://jise.btu.edu.tr/>



The works published in Journal of Innovative Science and Engineering (JISE) are licensed under a Creative Commons Attribution-NonCommercial 4.0 International License.

Abstract

Density functional theory (DFT) calculations were performed in order to provide theoretical knowledge about fluorine-carbon alloy nanoclusters in this study. While fluorine atoms do not show a stable nanocluster formalism, carbon atom addition initiates the formation of F_xC_y nanoclusters by a strong F-C bonding mechanism. Single fluorine systems were the most favorable nanoclusters in F_xC_y alloys. FC₂, FC₃, FC₄ nanoclusters were found to be minimum energy structures for three, four and five atoms respectively. The cohesive energy values of nanoclusters increase with the increasing number of carbon atoms in nanoclusters. Shape dependent magnetic moment was found in particular nanoclusters. The highest occupied molecular orbital (HOMO) and the lowest unoccupied molecular orbital (LUMO) energy gap (HLG) values of each stable cluster were also presented which provide information about chemical reactivity. The findings of this study can be a basis for fluorine-carbon alloy applications in nanotechnology.

Keywords: Nanocluster, Fluorine-carbon alloy, Density functional theory.

1. Introduction

Nanoclusters are of significant interest in recent years due to being an intermediate model between atoms and bulk structures. Their formation process helps us to understand the physics under the nature of crystallization and transition from nanocluster to bulk state. They also play a role especially in the design and production of new materials in nanotechnology. Therefore, investigations on nanoclusters are important in a wide range of areas for next-generation technology.

Nanoclusters can be composed of a few to a hundred atoms and possess different behaviours from their bulk counterparts due to quantum confinement effects. For example, gold has been known as one of the least reactive metals in the bulk form, however, it shows catalytic properties in nanosized [1].

It is known that the chemical, optical, magnetic etc. properties of nanoclusters can be controlled by their geometric structure sensitively [2]. The size, shape and compositions of nanoclusters are crucial for understanding the mechanism of the relationship between their geometric structure and electronic properties especially.

Carbon-bound fluorine atoms are unique in organic chemistry. Because of the high industrial demand for carbon and fluorine contained organic molecules, C-F bond formation has become active research field [3]. Due to the major successes of fluorinated compounds in medicinal chemistry [4], they are more attractive recently. Similarly, fluorinated compounds are also frequently synthesized in modern medicinal chemistry and have led to a large number of highly effective drugs [5].

Graphite fluoride composed of carbon and fluorine atoms is a well-known covalent derivative of graphite with interesting electrochemical and electronic properties and potential applications in hydrogen storage. It has been synthesized [6,7] and can be used as a wide bandgap two-dimensional (2D) material in electro-optical applications [8].

The F-F bond is known as one of the weakest of all covalent bonds [9]. However, F-C is one of the strongest bonds in organic chemistry and this makes carbon substitution attractive to obtain stable nanoclusters for fluorine. The main purpose of this study is to obtain strongly bonded nanoclusters by adding C atoms to weakly bonded fluorine nanoclusters. Therefore the nanoclusters of fluorine and carbon (F_xC_y) were investigated in this study systematically to make stronger clusters. There is no study about small fluorine-carbon nanoclusters so far. By this motivation, the structural characterizations of fluorine-carbon nanoclusters were investigated in this study. While pure fluorine clusters do not show nanocluster formalism, carbon atom addition to these systems systematically, increase cohesive energy values and initiates the formation of nanoclusters. The results of this study can be useful for the design and functionalization of fluorine-carbon alloys in nanotechnology.

2. Materials and Methods

All DFT calculations were carried out by using the SIESTA package which uses a numerical atomic orbital basis set [10]. The Perdew-Burke-Ernzerhof (PBE) exchange-correlation functionals were used within generalized gradient approximation (GGA) [11]. The calculations have been performed at Gamma point. Mesh cut off has been taken as 300 Ry. The tolerance value in the maximum difference between input and output density matrix has been used of 10⁻⁵. Spin polarization was taken into account in all calculations.

Cohesive energy (E_{coh}) of the clusters were calculated by the formula below [12].

$$E_{coh} = \frac{(x \times E_F) + (y \times E_C) - E_{cluster}}{x + y}$$

where $E_{cluster}$ is the total energy of isolated nanocluster, E_F and E_C are the energy of free fluorine and free carbon atoms respectively. The parameters x and y are the numbers of F and C atoms in the cell.

3. Results and Discussion

The possible shape and compositions of fluorine-carbon nanoclusters (F_xC_y , $x+y=5$) up to five atoms are shown in Figure 1, Figure 2 and Figure 3. The geometric structures of clusters were obtained after the optimization process and the most stable (minimum energy) structures of each cluster system are shown in yellow shaded areas. Each red letter on the top side of figures corresponds to the different cluster shapes below and each number denotes a compound containing a different number of F or C atoms and permutations of one F or C atom. Therefore each cluster name is symbolized by three-component. The first number is the number of atoms in nanocluster, the subsequent letter is the shape of nanocluster and the last number is composition of the nanocluster. For example, 3a1 is the nanocluster in the first row in the leftmost column in Figure 1.

Cohesive energy (E_{coh}) is a quantity of the energy required to separate constituent atoms apart from each other and shows how these atoms bond together strongly. Hence the calculated E_{coh} values per atom were written on the figures for each nanocluster system.

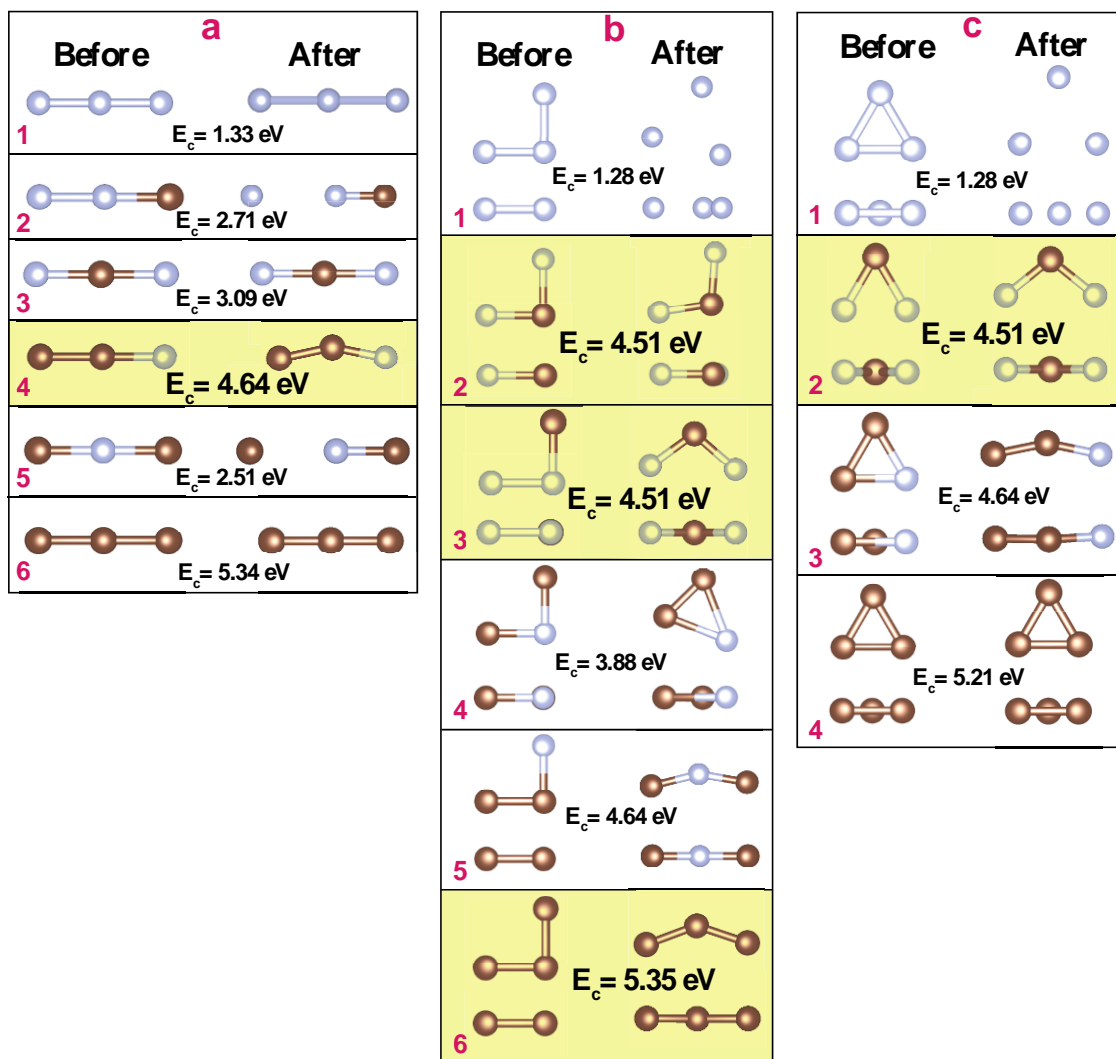


Figure 1. The optimized structures of three atom nanoclusters before and after relaxation process. The grey and brown coloured atoms represent fluorine and carbon atoms respectively. Each column shows different cluster shapes. Both of top and view side of each cluster were shown. Cohesive energy values were also presented. The most stable nanoclusters with the highest cohesive energy values in each number of carbon atoms were shown in yellow shaded areas.

Fluorine nanoclusters are shown in the first rows of figures. The F-F bond length for dimer was found as 1.41 Å which is an excellent consistency with the literature [9]. However, fluorine atoms do not exhibit a stable clustering as can be seen from the figures. F-F bond length was calculated as 1.63 Å in 3a1 nanoclusters (Figure 1). Except for this three atom clustering, other forms of fluorine atoms show either dimer forms such as F₂ molecule or aggeration of unconnected atoms. However, it can be seen that clustering process starts with the C atom addition to the system. As a result of this situation, E_{coh} values of systems increase significantly when the C atoms add into the system. The F-F distance on triangle clusters is 1.87 Å because of the repulsive interaction inherent in the so-called lone-pair bond weakening effect [13,14,15]. Adding carbon atoms increases the cohesive energy to more than three times for 3b and 3c systems. The minimum energy cluster for one carbon and two fluorine atoms system is L-shaped (3b2,3b3 and 3c2). The cohesive energy for them is 4.51 eV/atom and the bond length of F-C atoms on these nonmagnetic clusters is 1.33 Å. Two carbon and one fluorine system cluster (3a4) shape is the most stable one among three atom clusters of F_xC_y system with 4.64 eV/atom E_{coh} value. It has a 175° angle with 1.28 Å of both C-C and C-F bond lengths. The magnetic moment value of

this cluster is $1.0 \mu_B$. Nonmagnetic three atom bare carbon cluster is shown as 3b6 cluster and it has a 141° angle with a 1.31 \AA bond length between C atoms.

Four atom F_xC_y clusters are presented in Figure 2. The F clusters given in linear (4a1) and rectangular (4b1) form initially have transformed into F_2 molecules. 4c1 and 4d1 tetragonal forms have an F-F distance of about $1.86\text{-}1.89 \text{ \AA}$, showing no chemical bond between them. The addition of one C atom to the linear system shows the formation of F-C dimer and F_2 molecules separately in the 4a2 system. In 4b2 and 4c2 systems, we can see a CF_2 nanocluster and one free F atom as a final position. One C atom in 4d2 system shows a stable nanocluster with a high E_{coh} value in three dimensions. The 1.33 \AA bond length of F-C atoms and $1.0 \mu_B$ magnetic moment value in this cluster have also been calculated. The most stable nanocluster among F_2C_2 systems is a 4d3 structure in linear form with a 5.13 eV/atom E_{coh} value. It is a nonmagnetic cluster with 1.29 \AA F-C and 1.21 \AA C-C bond lengths. 4d4 and 4d5 structures have the same final configuration therefore they have same E_{coh} value of 5.43 eV/atom . The magnetic moment value of this cluster is $1.0 \mu_B$. C-C bonds are about $1.38\text{-}1.41 \text{ \AA}$ and F-C bond length is 1.29 \AA . The four atom C cluster (4a7) is the most stable structure among rectangular and three-dimensional shapes. It has a linear form and $2.0 \mu_B$ magnetic moment value. Its E_{coh} value is 5.64 eV/atom and C-C bond lengths are between $1.31\text{-}1.33 \text{ \AA}$.

There are many compositions of five atoms F_xC_y clusters as can be seen in Figure 3. Carbon clusters prefer linear shape for five atoms with an E_{coh} value of 6.17 eV/atom . It is the highest E_{coh} value among the systems considered in this study and show zero magnetization. The fully bonded state of the atoms in linear shape has not been formed except for the 5a16 composition. Carbon clusters with one carbon four fluorines atoms are the most stable in the shape of 5e2 structure which is called carbon tetrafluoride or tetrafluoromethane molecule in literature and it is nonmagnetic. The most stable two carbons three fluorines systems are seen as 5b7 and 5b8 clusters which are in the same shape with $1.0 \mu_B$ magnetic moment value. 5e8 is the most stable shape for three carbons two fluorines systems and it is nonmagnetic. 5b13 result in linear shape and it is the most stable structure for four carbons and one fluorine atom with a $1.0 \mu_B$ magnetic moment value.

Among the alloy nanoclusters, those with minimum energy were obtained as FC_2 for three atoms, FC_3 for four atoms and FC_4 for five atoms. It is obvious that single fluorine systems are the most favorable nanoclusters for F_xC_y alloys.

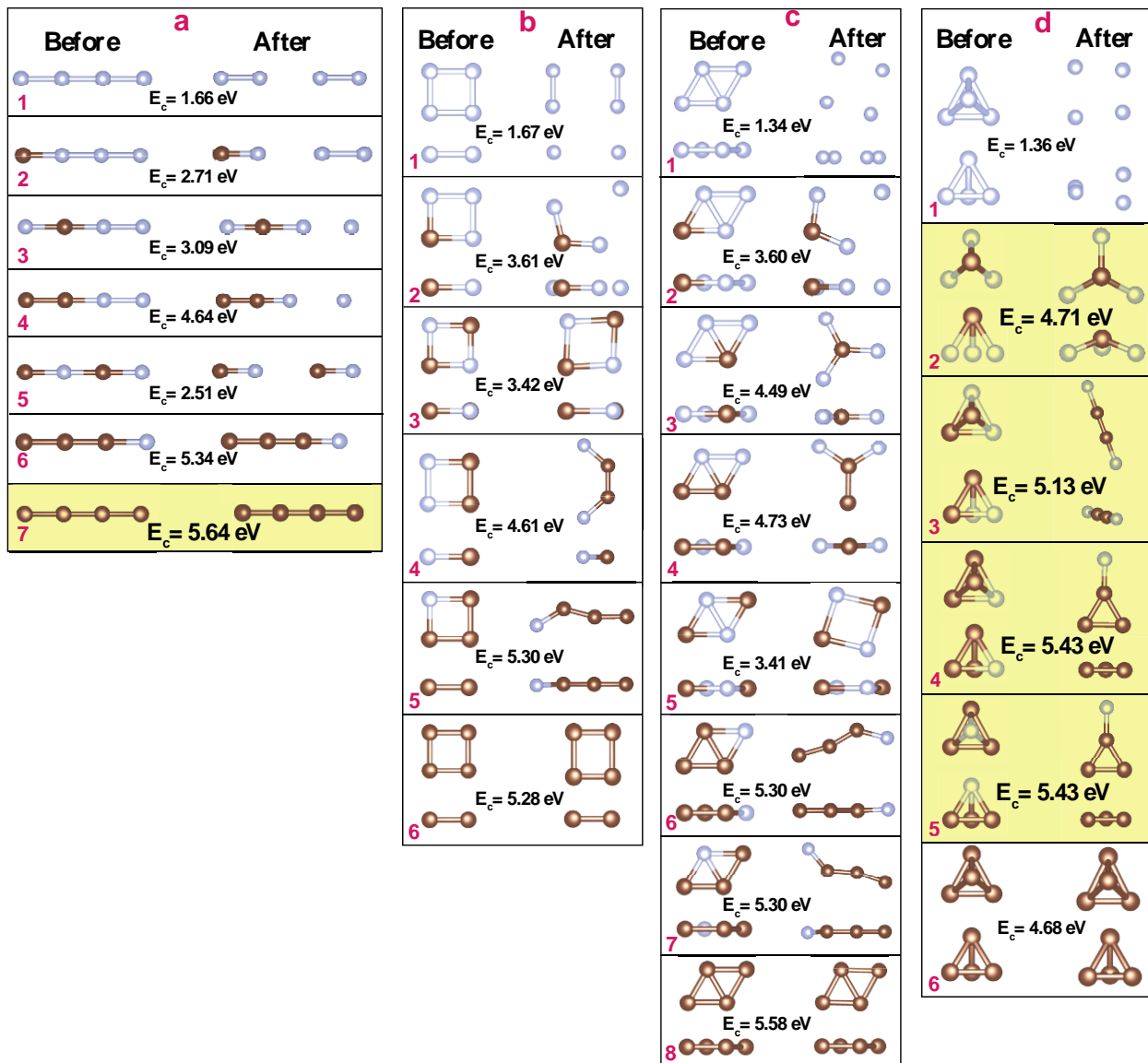


Figure 2. The optimized structures of four atom nanoclusters before and after the relaxation process. The grey and brown coloured atoms represent fluorine and carbon atoms respectively. Each column shows different cluster shapes. Both of top and view side of each cluster were shown. Cohesive energy values were also presented. The most stable nanoclusters with the highest cohesive energy values in each number of carbon atoms were shown in yellow shaded areas.

It is interesting to find nanoclusters in same compositions which have different magnetic moment value. 3a3 and 3b2 structures have one C and two F atoms and 3c2 as well. But 3a3 structure has a $2 \mu_B$ magnetic moment value while 3b2 and 3c2 are nonmagnetic. Here the orientation of the F atoms is the determining factor. Similarly, 4c4 and 4d3 structures are nonmagnetic while the other same composition clusters have $2 \mu_B$ magnetic moments. Shape dependent magnetic moment has been found in F_xC_y clusters but further step on this subject is beyond the scope of this study.

The difference between of the highest occupied molecular orbital (HOMO) and the lowest unoccupied molecular orbital (LUMO) is known as the HOMO-LUMO gap (HLG). High HLG is an indicator of high chemical stability. In other words, high HLG is an unfavorable energetic process in terms of electrons due to action from lower HOMO to higher LUMO, therefore high HLG represents low chemical reactivity.

HLG values of the most stable clusters are shown in Figure 4. Since 3b2, 3b3 and 3c2 clusters have the same structure after the optimization process, only the HLG value of the 3b2 cluster representing them was calculated. This also applies to 4d4 and 4d5 structures and similarly to 5b7 and 5b8 structures. 3a4 structure shows a minimum HLG value among the three atoms clusters, while the highest HLG value belongs to the 3b2 structure with the value of 3.29 eV. Three atoms carbon clusters show a relatively high HLG value of 2.48 eV. 4d3 nanocluster has the highest HLG value among the alloy clusters. The minimum HLG value among all stable nanoclusters in this study was calculated for 5b13 nanocluster with the value of 0.49 eV. However, the most chemically stable nanocluster with the highest HLG value is the F₄C (5e2) structure (tetrafluoromethane). It is known as an extremely stable gas [16] and this is consistent with having the highest HLG value of 13.34 eV in this study.

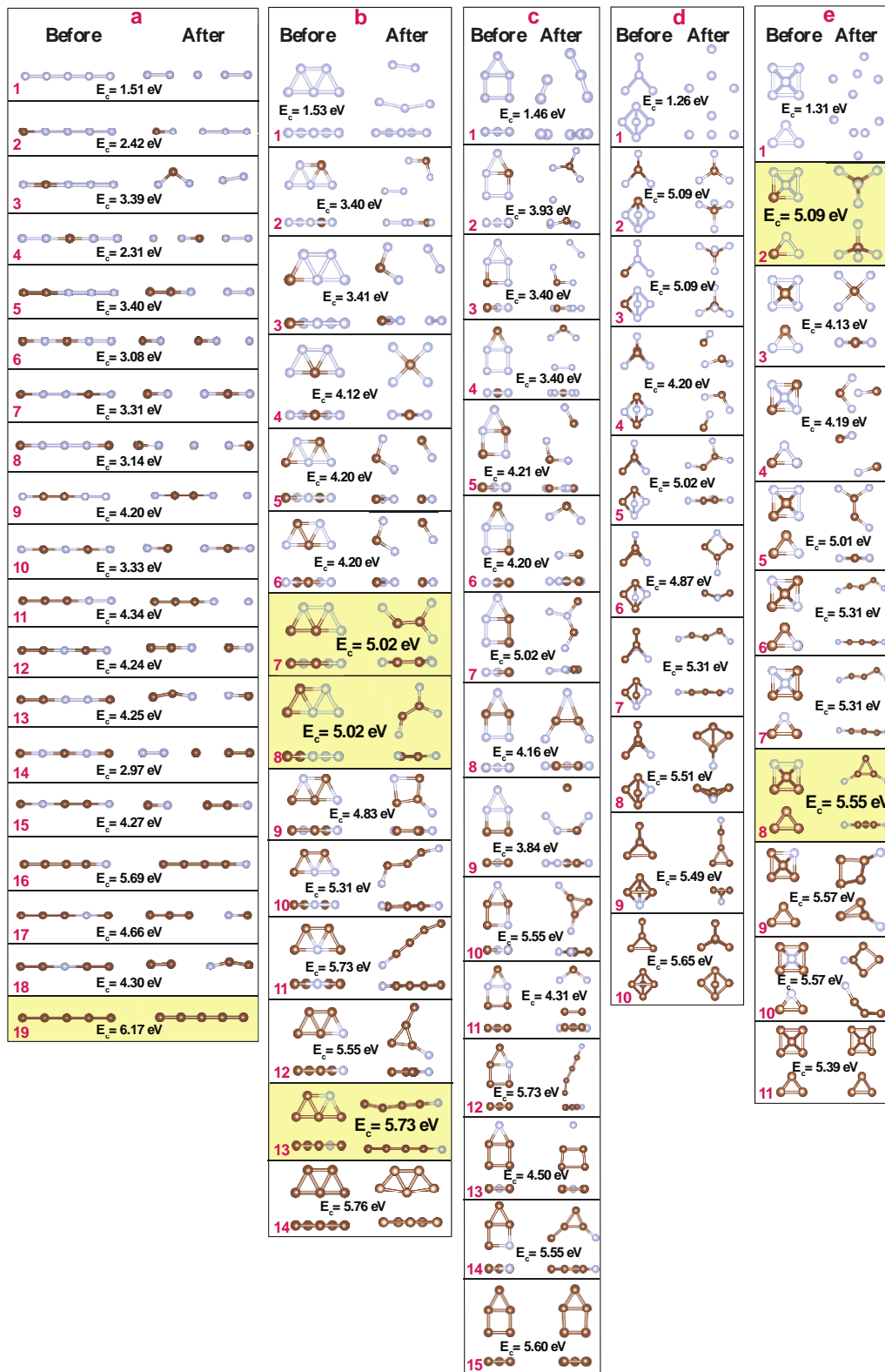


Figure 3. The optimized structures of five atom nanoclusters before and after the relaxation process. The grey and brown coloured atoms represent fluorine and carbon atoms respectively. Each column shows different cluster shapes. Both of top and view side of each cluster were shown. Cohesive energy values were also presented. The most stable nanoclusters with the highest cohesive energy values in each number of carbon atoms were shown in yellow shaded areas.

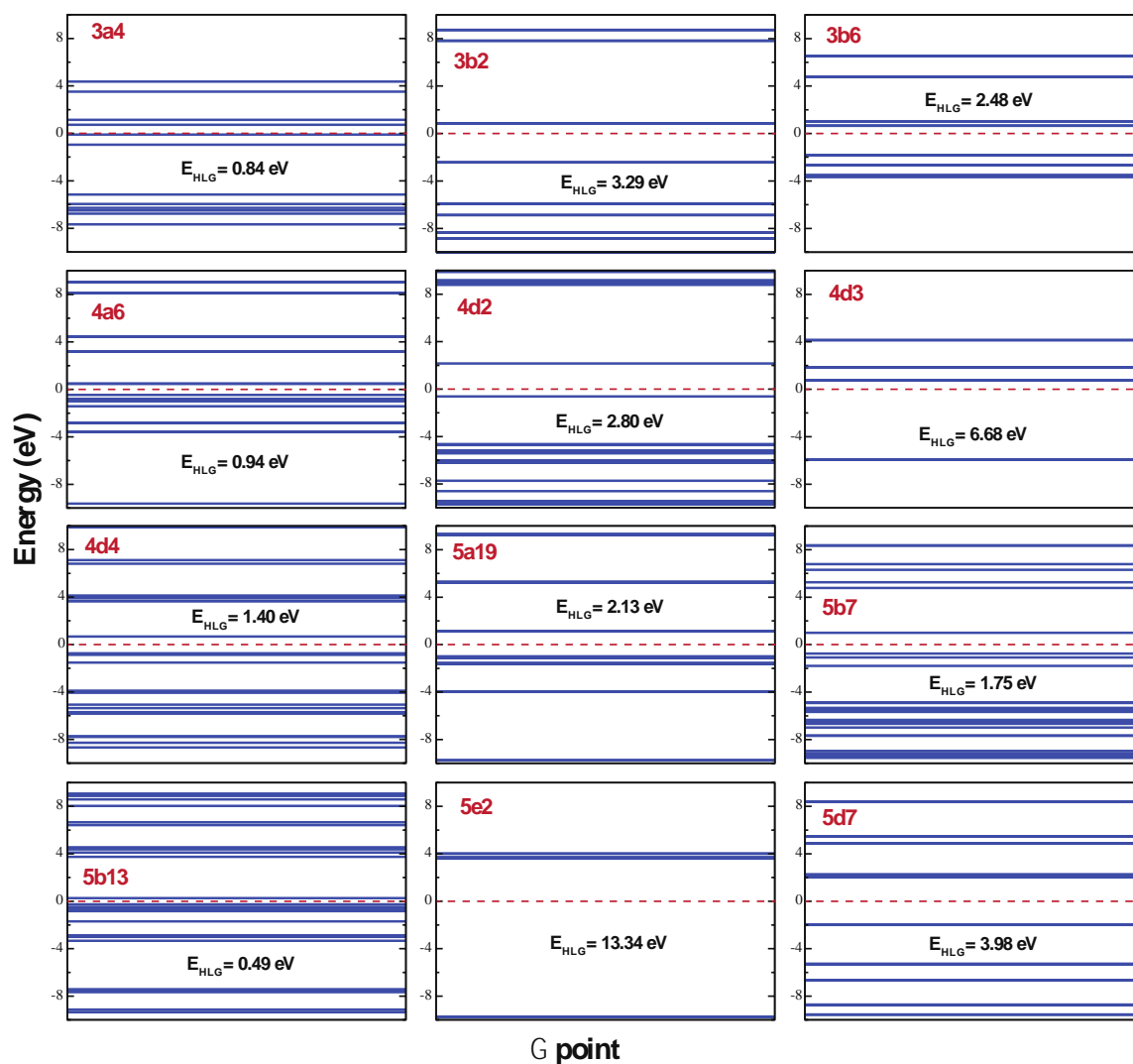


Figure 4. HOMO LUMO energy gap (E_{HLG}) graphs of each stable nanocluster. Fermi level was set to zero levels and shown by the red dashed line.

4. Conclusion

In conclusion, the structural formalism of fluorine-carbon alloy nanoclusters was investigated in this study. Fluorine atoms did not show a stable nanocluster configuration. However, carbon atoms affected the formation of fluorine-carbon nanoclusters by strong F-C bonding and formed stable and strongly bonded F_xC_y clusters. The cohesive energy values of nanoclusters increased with an increasing number of carbon atoms. The minimum energy compositions were obtained for FC_2 (3 atoms), FC_3 (4 atoms), FC_4 (5 atoms) clusters except for carbon clusters. Hence single fluorine systems were the most favorable nanoclusters for F_xC_y alloys. There were the same composition nanoclusters which had different magnetic moment values leading shape-dependent magnetic moment. The highest occupied molecular orbital (HOMO) and the lowest unoccupied molecular orbital (LUMO) energy gap (HLG) values were also presented. According to these values, the F_4C molecule which is called tetrafluoromethane showed the highest HLG value indicating lowest chemical activity among the nanoclusters in this study. These results can provide an insight into applications on nanotechnology and the studies on organic chemistry.

Acknowledgement



The computational resources were provided by Scientific and Technological Research Council of Turkey (TUBITAK) ULAKBIM, High Performance and Grid Computing Center (TR-Grid e-Infrastructure).

References

- [1] Haruta, M., Kobayashi, T., Sano, H., Yamada, N. (1987). Novel Gold Catalysts for the Oxidation of Carbon Monoxide at a Temperature far Below 0°C. *Chemistry Letters* 16: 405-408.
- [2] Laxmikanth Rao, J., Krishna Chaitanya, G., Basavaraja, S., Bhanuprakash, K., Venkataramana, A. (2007). Density-functional study of Au-Cu binary clusters of small size (n=6): Effect of structure on electronic properties. *Journal of Molecular Structure THEOCHEM* 803(1-3): 89-93.
- [3] Sabater, S., Mata, J.A., Peris, E. (2013). Hydrodefluorination of carbon-fluorine bonds by the synergistic action of a ruthenium-palladium catalyst. *Nature Communications* 4: 2553.
- [4] Purser, S., Moore, P.R., Swallow, S., Gouverneur, V. (2008). Fluorine in medicinal chemistry. *Chemical Society Reviews* 37: 320-330.
- [5] Böhm, H.J., Banner, D., Bendels, S., Kansy, M., Kuhn, B., Müller, K., Obst-Sander, U., Stahl, M. (2004). Fluorine in Medicinal Chemistry. *ChemBioChem* 5: 637-643.
- [6] Withers, F., Dubois, M., Savchenko, A.K. (2010). Electron properties of fluorinated single-layer graphene transistors. *Physical Review B* 82: 073403.
- [7] Zboril, R., Karlicky, F., Bourlinos, A.B., Steriotis, T.A., Stubos, A.K., Georgakilas, V., Safarova, K., ancik, D., Trapalis, C., Otyepka, M. (2010). Graphene Fluoride: A Stable Stoichiometric Graphene Derivative and its Chemical Conversion to Graphene. *Small* 6(24) 2885-2891.
- [8] Cheng, S.-H., Zou, K., Okino, F., Gutierrez, H. R., Gupta, A., Shen, N., Eklund, P. C., Sofo, J. O., Zhu, J. (2010). Reversible fluorination of graphene: Evidence of a two-dimensional wide bandgap semiconductor. *Physical Review B* 81: 205435.
- [9] Forslund, L.E., Kaltsoyannis, N. (2003). Why is the F2 bond so weak? A bond energy decomposition analysis. *New Journal of Chemistry* 27: 1108-1114.
- [10] Soler, J. M., Artacho, E., Gale, J. D., Garcia, A., Junquera, J., Ordejon, P., Sanchez-Portal, D. (2002). The SIESTA method for ab initio order-n materials simulation. *Journal of Physics Condensed Matter* 14 (11):2745-2779.
- [11] Perdew, J. P., Burke, K., Ernzerhof, M. (1996). Generalized Gradient Approximation Made Simple. *Physical Review Letters* 77: 3865.
- [12] Morita, A. (1958). Theory of Cohesive Energies and Energy-Band Structures of Diamond-Type Valence Crystals: The Method of SLCO, II. *Progress of Theoretical Physics* 19 (5): 534-540.
- [13] Schwartz, W. H. E., Valtazanos, P., Ruedenberg, K. (1985). Electron difference densities and chemical bonding. *Theoretica Chimica Acta* 68: 471-506.
- [14] Sanderson R. (1983). Polar Covalence. Academic Press, New York, USA. pp. 20-34. ISBN: 9780323159029.

- [15] Ponec, R., Cooper, D. L. (2007). Anatomy of Bond Formation. Domain-Averaged Fermi Holes as a Tool for the Study of the Nature of the Chemical Bonding in Li₂, Li₄, and F₂. *The Journal Physical Chemistry A* 111: 11294-11301.
- [16] Weston-Jr, R. E. (1996). Possible greenhouse effects of tetrafluoromethane and carbon dioxide emitted from aluminum production. *Atmospheric Environment* 30(16): 2901-2910.

Keyword-based Sentiment Analysis of Covid-19 Related Tweets

Mustafa Ozgür Cingiz^{1*}  Ece Celiktaş² 

^{1,2} Department of Computer Engineering, Bursa Technical University, 16310 Bursa, TURKEY

Abstract

With the emergence of Web 2.0, internet users share their feelings, thoughts and ideas with other people using social networks. Understanding people's thought analysis is important for examining marketing and user feedback in social networks. For this reason, sentiment analysis on social networks with machine learning algorithms is a popular field of study. Our study is based on the sentiment analysis of people against the new coronavirus, which affects the world. People can have different moods due to pandemia. The governance of mental issues must be observed to manage the pandemic time period more successfully. In this article, we retrieved 387,953 tweets due to the ten most frequently used COVID-19 related keywords. The most frequently used keywords about COVID-19 which enable to obtain and assess the reaction of Twitter users are investigated. Even if COVID-19 is a health issue and tweets about COVID-19 is expected to contain negative content, we found positive, negative and neutral tweets to analyze texts using sentiment analysis and machine learning approaches. We applied four classifiers like logistic regression, multinomial naive Bayes, support vector machines and decision tree. These classifiers are well studied and utilized in many studies which we mentioned in our study. The performance of the support vector machine, decision tree and logistic regression classifiers are close to each other. The lowest F-score is obtained from multinomial naive Bayes classifier. The classification results for each negative, neutral and positive class were compared separately in our study.

Keywords: Social Networks, Microblogs, Sentiment Analysis, Covid-19, Classification.

Cite this paper as:

Cingiz, O. M. and Celiktaş, E. (2021). *Keyword-based Sentiment Analysis of Covid-19 Related Tweets*. Journal of Innovative Science and Engineering.5(2):173-182

*Corresponding author: Mustafa Ozgür Cingiz
E-mail: mustafa.cingiz@btu.edu.tr

Received Date:11/05/2021
Accepted Date:09/10/2021
© Copyright 2021 by
Bursa Technical University. Available
online at <http://jise.btu.edu.tr/>



The works published in Journal of Innovative Science and Engineering (JISE) are licensed under a Creative Commons Attribution-NonCommercial 4.0 International License.

1. Introduction

Twitter has become a social networking platform where people can instantly share their thoughts. People can share many situations they have experienced and encountered in their lives, or their thoughts on a subject, positively, negatively or objectively. Twitter has been doing a lot of research for guidance. Users are offered the opportunity to share emotions, thoughts and ideas (Tweet) limited to 280 characters on Twitter. The Twitter API allows us to analyze the responses of a particular community on the topic it addresses. Sentiment analysis has gained great importance in recent years due to market research and commercial use. The usage of machine learning algorithms enables researchers to model the opinions of users.

COVID-19 has been declared a global pandemic in the world and continues its effect. Twitter users ignore the importance of COVID-19 in the early stage even though general thoughts of users in Twitter reflect anxiety. In this study, English tweets containing COVID-19 content on the Twitter platform were handled and analyzed. During the pandemic process, the tweets shared by Twitter users on the issue and reacted to were collected and their opinions were analyzed.

There were many studies have been published about sentiment analysis using Twitter data, inferred or public datasets. Barkur [1] examined tweets of Indians during the first days of pandemia. The study intends to understand the mental health of people via examining tweets which are classified as positive, negative via word-cloud analysis. Chakraborty [2] used corona, covid, sarscov2, covid19 and coronavirus keywords to infer COVID-19 related tweets. They used different classifiers to make machine learning models and logistic regression and the tf-IDF model outperformed in the study. Alamoodi [3] surveyed lexicon, machine learning and hybrid techniques about sentiment analysis for COVID-19. Rustam [4] also utilized five different classifiers and tf-IDF, a bag of words patterns in the sentiment analysis of COVID-19 tweets. Sentiment analysis is also popular in different study areas. Ayan investigated whether the content is Islamophobic by analyzing the sentiment of tweets over social networks using the machine learning method using a distributed computing infrastructure [5]. By using naïve Bayes and support vector machines machine learning algorithms by İlhan, sentiment analysis was performed on Twitter data where users shared their status updates on Twitter [6]. Akin presented a sentiment analysis model using a dictionary-based analysis of positive and negative emotions [7]. Uslu applied the Dictionary-based support vector machines, naïve Bayes, logistic regression and decision tree approaches on the Turkish dataset in order to examine the emotions on user comments on movie websites [8]. Neethu and Rajasree aimed to analyze sentiment with the machine learning method. In their study, naïve Bayes, support vector machines have compared the successful performances of classifiers using collective learning approaches [9]. Saha aimed to analyze the product quality of companies. They classified the tweets with positive and negative content about the products using naïve Bayes and support vector machines [10]. Gautam [11] discussed a machine learning algorithm with semantic analysis for classifying the sentence and product reviews based on Twitter data. Wongkar [12] investigated the sentiment analysis of the public towards the Republic of Indonesia's presidential candidates. They compared SVM and KNN algorithms in their study. Mandloi [13] utilized different machine learning techniques of data analysis of twitter that are discussed naïve Bayes, SVM and maximum entropy method in their study. El Rahman [14] analyzed opinions on several social media sites. In their study, they compared machine learning methods such as naïve Bayes classification method, support vector machine and maximum entropy classification methods. Al Shammari [15] investigated the

problem of real-time Twitter sentiment analysis which relies on providing a graphical representation of tweets categories (positive, negative, and neutral) opinions to help such as companies and agencies to focus on users' opinions of their products.

We created our own dataset for this study, by collecting tweets from Twitter users between March and May 2020. The time interval of tweet retrieval is important due to the pandemic period which indicates the beginning of the pandemia. The obtained tweets were taken from the first times of the coronavirus pandemic, so it allowed us to analyze the first feelings and thoughts of people about the pandemic. The similar studies utilized fewer keywords to retrieve tweets about COVID-19 but we determined keywords due to their usage and hashtag analysis. COVID-19 related tweets are collected by ten frequent keywords. We present materials and methods in the second part, results and discussion in the third part and conclusion in the last part of our study.

2. Materials and Methods

In our study, 10 subject tags were used to obtain tweets from Twitter, these keywords are: #Corona, #Covid, #Covid19, #CoronaVirus, #Wuhan, #Covid2019, #Corona, #CoronaVirusUpdate, Covid-19, Covid-2019. Twitter Stream API provides the opportunity to instantly collect tweets. Tweepy library dataset containing user tweets associated with COVID-19 was created [16]. NLTK library was used in Python software to perform pre-processing steps [17]. Positive, negative or neutral (not expressing opinion) information, which is the sentiment information of the contents, was obtained using the TextBlob library [18].

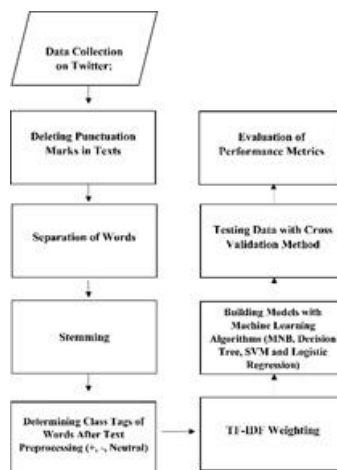


Figure 1. The Proposed System Model

In the classification and evaluation, machine learning algorithms were applied using the Sklearn library [19]. In this study, the steps of the proposed system model are shown in Figure 1 and details of the steps are given as subsections in the second part of the study.

2.1. Data Sets

387,953 tweets were retrieved as the dataset. The fetching date of these tweets is between March 2020 and May 2020. A total of 3 class labels, positive, negative and neutral were used in the dataset. It consists of a total of 387,953 data; 155,305 tweets in the positive class, 60,610 tweets in the negative class and 172,038 tweets in the neutral class. The dataset sample is presented in in Table 1.

Table 1. Samples and Classes from the Data Set

	Text(tweet)	Sentiment Class
1.	@qureshik74: My brave nephew stated his duty in the #Corona ward at Benazir Bhutto Hospital	Positive
2.	@ITSJEREMYSCOTT Irresponsible behavior will make you pay heavy... you destroyed others too #Corona	Negative
3.	One thing everyone talking about is #Covid_19	Neutral

2.2. Data Pre-processing

It is aimed to reveal the features of the text by cleaning it in the text pre-processing stage. These steps are as follows; Conversion of capital letters to lowercase letters, removal of punctuation marks and ineffective words, deletion of excess spaces and, finally, the process of retrieval of stems of words. Examples of the data set where text pre-processing steps are applied are shown in Table 2.

Table 2. Samples from the Pre-processed Data Set

	Text(tweet)
1.	['brave','nephew','stated','duty','corona','ward','benazir','bhutto','hospital']
2.	['irresponsible','behavior','make','pay','heavy','destroyed','others','corona']
3.	['one','thing','everyone','talking','covid']

2.3. Determining Class Labels

In this section, the classification of the pre-processed texts was carried out with TextBlob. Textblob is an NLP library based on Python language that is used for text processing. The inferred tweets of our study are labelled as positive, negative or neutral, based on sentiment analysis via Textblob. Table 3 shows some examples from the dataset that are labelled with sentiment analysis tags of Textblob.

Table 3. Dataset samples for classification

	Text(tweet)	Sentiment class
1.	['brave','nephew','stated','duty','corona','ward','benazir','bhutto','hospital']	Positive
2.	['irresponsible','behavior','make','pay','heavy','destroyed','others','corona']	Negative
3.	['one','thing','everyone','talking','covid']	Neutral

2.4. Term Weighting TF-IDF

Text documents are represented as vectors in the vector space model. Each dimension of the vector corresponds to words in the word space model. If a term is included in the text, its weight in the vector cannot be zero. There are many methods of expressing the weight of terms in the text. In this study, the frequently used TF-IDF (TF, term frequency-IDF, reverse document frequency) weighting method was utilized. TF is the frequency of a term in the document and indicates how many times the word occurs in the document.

The mathematical expression of the term frequency (TF) is given in equation (1). $f_d(t)$ represents the number of occurrences of term t in document d the maximum number of term occurrence is used for normalization of term frequency.

$$tf(t, d) = \frac{f_d(t)}{\max_{\omega \in d} f_d(\omega)} \quad (1)$$

Reverse document frequency (IDF) shows how often the word occurs in all documents. The mathematical expression of the inverse document calculation is given in equation (2). $|D|$ show number of documents and divisor part indicates the number of documents that term t occur.

$$idf(t, D) = \ln\left(\frac{|D|}{|\{d \in D: t \in d\}|}\right) \quad (2)$$

In TF-IDF weighting, it is obtained from the product of TF and IDF values, and the corresponding mathematical expression is given in equation (3).

$$tf \cdot idf(t, d, D) = tf(t, d) \cdot idf(t, D) \quad (3)$$

A word has strong weight when it has high term frequency and low reverse document frequency according to Equation 3.

2.5. Classification

Multinomial Naïve Bayes, decision tree, support vector machines (SVM), logistic regression classification algorithms are applied on the retrieved dataset using the scikit-learn Python library. The classic Naïve Bayes classifier is a machine learning model. The classifier is based on the Bayes theorem. In this study, multinomial Naïve Bayes, which is a Naïve Bayes classifier type, was used. Multinomial Naïve Bayes is used especially for document classification problems. The logistic regression method is a method that provides flexibility in the classification of multivariate data. It performs classification operations by determining the probability value that predicts the logistic regression dependent variable and supports vector machine classifier basically performs classification using boundary data close to the decision-making

axes. Decision boundaries, also known as the hyperplane, are determined. Support vector machines linear kernel function is used in our study. This method provides better scaling for datasets with a large number of samples. A decision tree classifier is a classification method that creates a tree structure model consisting of decision nodes and leaf nodes according to feature and target. The decision tree algorithm divides the data set into small pieces. A decision node can contain one or more branches. The first node is called a root node. A decision tree can consist of both categorical and numerical data. In this study, the parameter of the decision tree classifier was chosen as entropy. Linear SVC was used when calculating the support vector machine classifier.

2.5.1 Performance Metrics

The performance of the classifiers was evaluated by using the 10-fold cross-validation method and the k value is determined 10 in our study. Accuracy, precision, recall and F1-score criteria were used as classification performance evaluation metrics. True positive (TP) indicates a classifier predicts the positive class label of the instance correctly. If a classifier determines a positive class for a negative class instance then it is represented as false positive (FP) in the confusion matrix. If a classifier determines a negative class for a positive class instance then it is represented as a false negative (FN). The last metric of the confusion matrix is true negative (TN) which occurs when a classifier specifies a negative class label for an actual negative class instance.

Accuracy: This statistic is the correct prediction rate. The accurate prediction rate is divided by the total number of test observations of the test observations whose labels are correctly predicted. The mathematical expression of the accuracy is given in Equation 4.

$$\frac{TP+TN}{TP+TN+FP+FN} \quad (4)$$

Recall: It is how accurately we estimate from all positive classes. The mathematical expression of the recall is given in Equation 5. The recall represents how accurately a classifier specifies actual positive classes of instances. Its calculation is given in Equation 5.

$$\frac{TP}{TP+FN} \quad (5)$$

Precision: Precision represents how accurately a classifier specifies the ratio of positive labelled instances, which are found as correctly, to all positive predicted labelled instances. Its calculation is given in Equation 6.

$$\frac{TP}{TP+FP} \quad (6)$$

F1-Score: It is the harmonic mean of the Precision and Recall values. The mathematical expression of the F1-Score is given in equation (7).

$$\frac{2 \times \text{Recall} \times \text{Precision}}{\text{Recall} + \text{Precision}} \quad (7)$$

ROC (Receiver Operating Characteristic) Curve: ROC curve is a plot whose x-axis presents a false positive rate and the y-axis displays true positive rates. The false-positive rate indicates $FP/(FP+TN)$ and the true positive rate shows recall value. The area under the ROC curve approximates to one means obtaining better classification results.

3. Results and Discussion

The true positive(TP), true negative(TN), false positive(FP), and false-negative (FN) values obtained for each classifier algorithm in this study are shown in Table 4.

Table 4. TP, TN, FP and FN values for each classifier

Classifier	Class	TP	TN	FP	FN
Multinomial Naive Bayes	Negative	822	32740	5192	5
	Neutral	15215	19869	1698	1946
	Positive	15218	17318	462	5873
Decision Tree	Negative	5469	32316	540	571
	Neutral	17167	21418	207	131
	Positive	14787	22705	629	567
SVM	Negative	5779	32565	253	209
	Neutral	17045	21473	105	173
	Positive	15388	23046	184	260
Logistic Regression	Negative	5447	32525	569	254
	Neutral	17051	21024	561	151
	Positive	15083	22886	448	380

The median values of TP, TN, FP and FN of 10-fold cross-validation are given in Table 4. Four classifiers performance results can be measured in each class. Multinomial naive Bayes classifier presents lowest TP values in negative tweets. It predicts negative tweets as positive due to TP and FP values of multinomial naive Bayes. TP values of SVM on negative and positive classes is higher than TP values of other classifiers. FN values of the Decision tree is also higher than FN values of SVM and logistic regression. The highest FN values are also obtained from multinomial naive Bayes. The lowest FP and FN values are obtained using SVM. We created a supplementary file that contains all TP, FP, FN and TN values for all classifiers on three classes using 10-fold cross-validation.

All TP, FN, FP, and FN values are summed to calculate more robust classification performance metrics. Accuracy, precision, recall and F- score values are presented in Table 5.

Table 5. Performance Metrics of Classifiers

	Accuracy	Precision	Recall	F1-Score
Multinomial Naive Bayes	0.80	0.87	0.66	0.65
Logistic Regression	0.96	0.95	0.95	0.96
Support Vector Machine	0.98	0.98	0.97	0.97
Decision Tree	0.96	0.95	0.95	0.95

Performance metrics were calculated with the four machine learning algorithm methods used in this study. The success performances of the machine learning algorithms obtained are given in Table 5. According to the model evaluation, F1-Score values were obtained as 0.65 for multinomial naive Bayes, 0.95 for the decision tree, 0.97 for support vector machines and 0.96 for logistic regression classifiers respectively. The performance score of the support vector machine, decision tree and logistic regression is similar.

The figure 2 shows the area under the curve (AUC) of the receiver operating characteristic (ROC) curve analysis of the 4 classification methods. The area under the ROC curve displays similar results which is presented in Table 2. The largest ROC curve area is obtained using support vector machines.

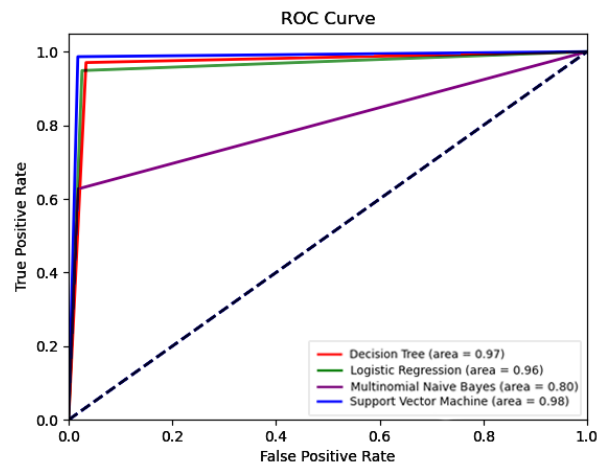


Figure 2. ROC Curves of Four Classification Methods

When the study is compared with similar studies, it is observed that the results obtained are consistent with the literature. According to the obtained results in the study, the algorithm with the best success was obtained by using support vector machines with a 0.97 F1-Score value. In the sentiment analysis study conducted by İlhan et al. [6], the highest success performance was obtained with support vector machines. Likewise, another study [20] achieved the highest success performance by using the support vectors algorithm in their sentiment analysis study.

In addition, as a result of the analysis, the multinomial naive Bayes classifier achieved a lower result than other machine learning algorithms with a successful performance of 0.65 F1-Score. Kaynar [21] and Çoban [22] showed in their studies that the multinomial naive Bayes classifier works with lower performance than other classification algorithms. Considering the obtained results, it was observed that the success rate achieved by the multinomial naive Bayes classifier is approximate with our study.

4. Conclusion

Sentiment analysis is basically a text analysis and aims to determine the class that the given text wants to express emotions as positive, negative and neutral. It is a popular method today and can be used for research in many areas. Generally, it is used to analyze the opinions of the companies about the service they provide or by getting feedback from

the customers who use the products of the brands. In addition, sentiment analysis aims to find out what people think about a specific issue.

In this study, it is aimed to classify people's thoughts about COVID-19 as positive, negative, neither positive nor negative (neutral) by taking the tweets randomly shared by users about COVID-19 on the social media platform Twitter.

The difference of this study from other similar studies in the literature is that we collected our dataset due to ten different keywords. These keywords are determined by the frequency of terms in hashtags and the content of tweets. In addition, tweets of our study are collected at the first phase of pandemia. In the retrieval period, there are lots of different opinions and feelings about COVID-19. The tweets we obtained were taken from the first time of the coronavirus pandemic, so it allowed us to analyze the first feelings and thoughts of people about the pandemic. In pandemia, text mining techniques are applied to tweets to evaluate the opinions of people. The hybrid approaches that utilized TF-IDF weighting, tag clouds, word2vec and various machine learning algorithms are used in literature. The performance results of our study are higher or close to the results of similar studies whose accuracy values are between 0.6 and 0.95 in three label classification [2,4].

Using machine learning algorithms on the dataset obtained from Twitter, it was investigated which algorithm would classify more successfully. As a result, all machine learning algorithms have been compared. It has been observed that the support vector machines algorithm has a high success performance in classification with a success rate of 0.97. The performances results will be improved via obtaining millions of tweets about COVID-19 and classifying them with deep learning algorithms in the future.

References

- [1] Barkur, G. and Vibha, G. B. K. (2020). Sentiment analysis of nationwide lockdown due to COVID 19 outbreak: Evidence from India. *Asian journal of psychiatry*, 51, 102089.
- [2] Chakraborty, K., Bhatia, S., Bhattacharyya, S., Platos, J., Bag, R. and Hassanien, A. E. (2020). Sentiment Analysis of COVID-19 tweets by Deep Learning Classifiers—A study to show how popularity is affecting accuracy in social media. *Applied Soft Computing*, 97, 106754.
- [3] Alamoodi, A, et al. (2020). Sentiment analysis and its applications in fighting COVID-19 and infectious diseases: A systematic review. *Expert systems with applications*, 114155.
- [4] Rustam, F., Khalid, M., Aslam, W., Rupapara, V., Mehmood, A. and Choi, G. S. (2021). A performance comparison of supervised machine learning models for Covid-19 tweets sentiment analysis. *Plos one*, 16(2), e0245909.
- [5] Ayan, B., Kuyumcu, B., Ciylan, B. (2019) Detection of Islamophobic Tweets on Twitter Using Sentiment Analysis, *Gazi University Journal of Science Part C*, 7(2), pp 495-502.
- [6] İlhan, N., Sağaltıcı D. (2020) Sentiment Analysis in Twitter, *Harran University Journal of Engineering*, 5(2), pp. 146-156, doi: 10.46578/humder.772929
- [7] Akın, B. ve Şimşek, T. (2018) Adaptive Learning Lexicon Based Sentiment Analysis Proposal, *Information Technologies Journal*, 11(3), doi: 10.17671/gazibtd.342419

- [8] Uslu, A., Tekin, S. ve AYTEKIN, T. (2019) Sentiment Analysis In Turkish Film Comments, IEEE 27th Signal Processing and Communications (SIU), doi: 10.1109/SIU.2019.8806355
- [9] Neethu, M.S., Rajasree, R. (2013) Sentiment Analysis in Twitter Using Machine Learning Techniques, 2013 Fourth International Conference on Computing, Communications and Networking Technologies (ICCCNT), doi: 10.1109/ICCCNT.2013.6726818
- [10] Saha, S., Yadav, J. ve Ranjan, P. (2017) Proposed Approach for Sarcasm Detection in Twitter, Indian Journal of Science and Technology, 10(25), pp. 1-8.
- [11] Gautam, G., & Yadav, D. (2014). Sentiment analysis of twitter data using machine learning approaches and semantic analysis. 2014 Seventh International Conference on Contemporary Computing (IC3). doi:10.1109/ic3.2014.6897213
- [12] Wongkar, M., & Angdresay, A. (2019). Sentiment Analysis Using Naïve Bayes Algorithm of The Data Crawler: Twitter. 2019 Fourth International Conference on Informatics and Computing (ICIC). doi:10.1109/icic47613.2019.8985884
- [13] Mandloi, L., & Patel, R. (2020). Twitter Sentiments Analysis Using Machine Learning Methods. 2020 International Conference for Emerging Technology (INCET). doi:10.1109/incet49848.2020.9154183
- [14] El Rahman, S. A., AlOtaibi, F. A., & AlShehri, W. A. (2019). Sentiment Analysis of Twitter Data. 2019 International Conference on Computer and Information Sciences (ICCIS). doi:10.1109/iccisci.2019.8716464
- [15] Al Shammari, A. S. (2018). Real-time Twitter Sentiment Analysis using 3-way classifier. 2018 21st Saudi Computer Society National Computer Conference (NCC). doi:10.1109/ngc.2018.8593205
- [16] Documentation–tweepy, Tweepy. "3.5. 0 documentation." (2020).
- [17] Loper, E., & Bird, S. (2002) NLTK: the natural language toolkit. arXiv preprint cs/0205028.
- [18] Loria, S., Keen, P., Honnibal, M., Yankovsky, R., Karesh, D., & Dempsey, E. (2014). Textblob: simplified text processing. Secondary TextBlob: simplified text processing, 3.
- [19] Pedregosa, Fabian, et al. (2011) Scikit-learn: Machine learning in Python. Journal of machine Learning research 12, 2825-2830.
- [20] Çelik, Ö, Osmanoğlu, U, Çanakçı, B. (2020). Sentiment Analysis from Social Media Comments, Mühendislik Bilimleri ve Tasarım Dergisi, 8 (2), 366-374. DOI: 10.21923/jesd.546224
- [21] Kaynar, O, Görmez, Y., Yıldız, M. ve Albayrak, A. (2016) Sentiment Analysis with Machine Learning Techniques, Processing Symposium (IDAP'16), pp. 17-18.
- [22] Çoban, Ö., Ozyer, B. ve Ozyer, G. (2015) Sentiment Analysis for Turkish Twitter Feeds, 3th Signal Processing and Communications Applications Conference (SIU), pp. 2388-2391.